

UNIVERSITAT POLITÈCNICA DE VALÈNCIA



UNIVERSITAT
POLITÈCNICA
DE VALÈNCIA

Tactile and Touchless Sensors Printed on Flexible
Textile Substrates for Gesture Recognition

Ph. D. Thesis / Tesis Doctoral

by

Josué Ferri Pascual

Advisors:

Raúl Llinares Llopis
Eduardo García Breijo

Tesis presentada para la obtención del grado de Doctor por la Universitat Politècnica de València

Thesis presented to obtain the PhD from the Universitat Politècnica de València

Valencia, July 2020

A mi familia

Agradecimientos

En primer lugar, mis más sinceros agradecimientos a mis directores de tesis, y amigos, Eduardo y Raúl, por la confianza puesta en mí para el desarrollo del presente trabajo de investigación a lo largo de estos últimos años, y quienes me empujaron para dar este paso en mi carrera profesional. Agradezco todo vuestro tiempo dedicado, trabajando conjuntamente codo con codo, y la pasión por la investigación que me habéis transmitido. Sabéis que sois piezas claves en el éxito de este proyecto. Ha sido todo un privilegio que nuestras vidas de algún modo se cruzaran. Contar con vosotros durante todo este tiempo ha sido todo un placer.

También quiero dar un cariñoso agradecimiento a todo el equipo de Textiles Inteligentes y Soluciones de las Tecnologías de Información y Comunicaciones, quienes en su mayor y menor medida han colaborado de alguna forma para alcanzar los objetivos de esta tesis, Ana, Elena, Gabi, Jorge, José María y Juan. Y en particular a mi responsable y amigo Jorge por haber confiado en mí y en esta línea de investigación de impresión electrónica. Gracias por haber luchado y defendido inversiones, colaboraciones y proyectos para facilitar el trabajo aquí condensado. Agradezco al Instituto de Investigación Textil AITEX y a su Dirección por facilitar y apoyar tanto la realización de actividades formativas como el desarrollo de esta investigación.

Un agradecimiento especial a mi mujer y a mis hijas Carla y Mireia por su paciencia y apoyo diarios. Quiero agradecer también a toda mi familia, a mis padres y hermana por su apoyo, que me han permitido seguir siempre adelante durante todas las etapas de mi vida.

Resumen

La presente tesis doctoral tiene como objetivo fundamental el desarrollo de nuevos sensores y actuadores empleando la tecnología electrónica impresa, también conocida como *Printed Electronics*. Para ello, se emplean materiales poliméricos conductores, semiconductores y dieléctricos sobre sustratos flexibles y/o elásticos. Por medio de diseños y procesos de aplicación adecuados, es posible fabricar sensores capaces de interactuar con el entorno. De este modo, se pueden incorporar a los sustratos, como puedan ser tejidos textiles, funcionalidades específicas de medición del entorno y de respuesta ante cambios de este. Adicionalmente, es necesario incluir sistemas electrónicos, capaces de realizar el procesamiento de los datos obtenidos, así como de su registro. En el desarrollo de estos sensores y actuadores se combinan las propiedades físicas de los diferentes materiales de forma precisa. Para ello, se diseñan estructuras multicapa donde las propiedades de unos materiales interaccionan con las de los demás. El resultado es un sensor capaz de captar variaciones físicas del entorno, y convertirlas en señales que pueden ser procesadas y transformadas finalmente en datos.

Por una parte, se ha desarrollado un sensor táctil impreso sobre sustrato textil para reconocimiento de gestos en 2D. Este sensor se compone de una matriz formada por pequeños sensores capacitivos basados en estructura de tipo condensador. Estos se han diseñado de forma que, si un dedo u otro objeto con propiedades capacitivas se aproxima suficientemente, su comportamiento varía, pudiendo ser medido. Los pequeños sensores están ordenados en dicha matriz como en una cuadrícula. Cada sensor tiene una posición que viene determinada por una fila y por una columna. Periódicamente se mide la capacidad de cada pequeño sensor con el fin de evaluar si ha sufrido variaciones significativas. Para ello es necesario convertir la capacidad del sensor en un valor que posteriormente es procesado digitalmente. Cuando un usuario aproxima un dedo, la capacidad del sensor se ve aumentada. De este modo, cualquier variación en la capacidad de uno de los sensores puede ser detectada y medida. Estas medidas son procesadas de forma conjunta pudiendo determinar la posición y el movimiento del dedo sobre la superficie de la matriz de sensores. Varios diseños y prototipos se han desarrollado con el desafío de ser impresos sobre sustrato textil.

Por otro lado, con el fin de mejorar la efectividad en el uso de los sensores táctiles 2D desarrollados, se ha estudiado el modo de incorporar un sistema actuador. De esta forma, el usuario recibe una retroalimentación indicando que la orden o acción ha sido reconocida. Para ello, se ha complementado la matriz de sensores capacitivos con una pantalla electroluminiscente también impresa. El resultado final ofrece una solución

que combina un sensor táctil 2D con un actuador electroluminiscente realizado mediante impresión electrónica sobre sustrato textil. Así, el usuario recibe una señal lumínica en respuesta a un gesto, confirmándole que dicho gesto ha sido reconocido.

Posteriormente, se ha llevado a cabo el desarrollo de un sensor de gestos 3D empleando una combinación de sensores impresos también sobre sustrato textil. En este tipo de sensor 3D, se envía una señal que genera un campo eléctrico sobre los sensores impresos. Esto se lleva a cabo mediante un electrodo de transmisión situado muy cerca de ellos. El campo generado es recibido por los sensores y convertido a señales eléctricas. Para ello, los sensores se basan en electrodos que actúan de receptores. Si una persona coloca su mano dentro del área de emisión, se crea una perturbación de las líneas de los campos eléctricos. Esto es debido a la desviación de las líneas de campo a tierra utilizando la conductividad intrínseca del cuerpo humano. Esta perturbación cambia/afecta a las señales recibidas por los electrodos. Las variaciones captadas por todos los electrodos son procesadas de forma conjunta pudiendo determinar la posición y el movimiento de la mano sobre la superficie del sensor. Varios diseños y prototipos se han desarrollado con el reto de ser impresos sobre sustrato textil. Este tipo de sensor permite detectar la posición de la mano o el dedo, sin necesidad de contacto directo. En comparación con los sensores 2D, esto supone una ventaja que posibilita otro tipo de aplicaciones, como pueda ser que el sensor tenga que estar oculto bajo una espuma o tejido muy grueso. Durante el desarrollo del sensor 3D, se evaluó su uso en varios tejidos combinando diferentes tintas conductoras. Además, también se evaluaron diferentes posibilidades de impresión, con la finalidad de optimizar su proceso de fabricación.

Finalmente, se ha llevado a cabo el desarrollo de un sensor de gestos 3D mejorado. Al igual que el desarrollo anterior, permite la detección de gestos sin necesidad de contacto, pero incrementando la distancia de alcance. Además de la tecnología de impresión electrónica, se ha evaluado el empleo de otras dos tecnologías de fabricación textil. Por una parte, se han realizado los prototipos empleado hilos conductores y maquinaria de bordado industrial. Y, por otra parte, se ha evaluado el uso de tejidos conductores empleando equipamiento de corte de tejido automatizado y laminado de tejido por calor. Los prototipos fueron validados con respecto a la detección de gestos con resultados positivos. Respecto a las técnicas de fabricación empleadas, se realizaron estudios comparativos de respuesta frente a la humedad, variaciones de temperatura y lavados.

Resum

La present tesi doctoral té com a objectiu fonamental el desenvolupament de nous sensors i actuadors fent servir la tecnologia de electrònica impresa, també coneguda com *Printed Electronics*. Es va fer us de materials polimèrics conductors, semiconductors i dielèctrics sobre substrats flexibles i/o elàstics. Per mitjà de dissenys i processos d'aplicació adequats, és possible fabricar sensors capaços d'interactuar amb l'entorn. D'aquesta manera, es poden incorporar als substrats, com ara teixits tèxtils, funcionalitats específiques de mesurament de l'entorn i de resposta davant canvis d'aquest. Addicionalment, és necessari incloure sistemes electrònics, capaços de realitzar el processament de les dades obtingudes, així com del seu registre. En el desenvolupament d'aquests sensors i actuadors es combinen les propietats físiques dels diferents materials de forma precisa. Cal dissenyar estructures multicapa on les propietats d'uns materials interaccionen amb les de la resta. manera El resultat es un sensor capaç de captar variacions físiques de l'entorn, i convertir-les en senyals que poden ser processades i convertides en dades.

D'una banda, s'ha desenvolupat un sensor tàctil imprès sobre substrat tèxtil per a reconeixement de gestos en 2D. Aquest sensor es compon d'una matriu formada amb petits sensors capacitius basats en una estructura de tipus condensador. Aquests s'han dissenyat de manera que, si un dit o un altre objecte amb propietats capacitives s'aproxima prou, el seu comportament varia, podent ser mesurat. Els petits sensors estan ordenats en aquesta matriu com en una quadrícula. Cada sensor té una posició que ve determinada per una fila i per una columna. Periòdicament es mesura la capacitat de cada petit sensor per tal d'avaluar si ha sofert variacions significatives. Per a això cal convertir la capacitat del sensor a un valor que posteriorment és processat digitalment. Quan un usuari s'aproxima un dit la capacitat del sensor es veurà augmentada. D'aquesta manera, qualsevol variació en la capacitat d'un dels sensors pot ser detectada y mesurada. Aquestes mesures són processades de manera conjunta per determinar la posició i el moviment del dit sobre la superfície de la matriu de sensors. Diversos dissenys i prototips s'han desenvolupat amb el desafiament de ser impresos sobre substrat tèxtil.

D'altra banda, per tal de millorar l'efectivitat en l'ús dels sensors tàctils 2D desenvolupats, s'ha estudiat la manera d'incorporar un sistema actuator. D'aquesta forma, l'usuari rep una retroalimentació indicant que l'ordre o acció ha estat reconeguda. Per a això, s'ha complementat la matriu de sensors capacitius amb una pantalla electroluminescent també impresa. El resultat final ofereix una solució que combina un sensor tàctil 2D amb un actuator electroluminescent realitzat mitjançant impressió electrònica sobre

substrat tèxtil. Així, l'usuari rep un senyal lumínica en resposta a un gest, confirmant-li que dit gest ha estat reconegut.

Posteriorment, s'ha dut a terme el desenvolupament d'un sensor de gestos 3D emprant una combinació d'un mínim de sensors impresos també sobre substrat tèxtil. En aquest tipus de sensor 3D, s'envia un senyal que genera un camp elèctric sobre els sensors impresos. Això es porta a terme mitjançant un elèctrode de transmissió situat molt a proper a ells. El camp generat és rebut pels sensors i convertit a senyals elèctrics. Per això, els sensors es basen en elèctrodes que actuen de receptors. Si una persona col·loca la seva mà dins de l'àrea d'emissió, es crea una pertorbació de les línies dels camps elèctrics. Això és a causa de la desviació de les línies de camp a terra utilitzant la conductivitat intrínseca de el cos humà. Aquesta pertorbació afecta als senyals rebudes pels elèctrodes. Les variacions captades per tots els elèctrodes són processades de manera conjunta per determinar la posició i el moviment de la mà sobre la superfície del sensor. Diversos dissenys i prototips s'han desenvolupat amb el desafiament de ser impresos sobre substrat tèxtil. Aquest tipus de sensor permet detectar la posició de la mà o el dit, però sense necessitat de contacte directe. En comparació amb els sensors 2D, açò suposa un avantatge que possibilita un altre tipus d'aplicacions, on els sensors anteriors poguessin tenir alguna limitació, com pugui ser que el sensor hagi d'estar amagat sota una escuma o teixit molt gruixut. Durant el desenvolupament del sensor 3D, es va avaluar el seu ús en diversos teixits combinant diferents tintes conductores. A més, també es va avaluar diferents possibilitats d'impressió amb la finalitat d'optimitzar el seu procés de fabricació.

Finalment, s'ha dut a terme el desenvolupament d'un sensor de gestos 3D millorat. A l'igual que el desenvolupament anterior, permet la detecció de gestos sense necessitat de contacte, però incrementant la distància d'abast. A més a més de la tecnologia d'impressió electrònica, s'ha avaluat emprar altres dues tecnologies de fabricació tèxtil. D'una banda, s'han realitzat els prototips emprant fils conductors i maquinària de bordat industrial. I, d'altra banda, s'ha avaluat l'ús de teixits conductors emprant equipament de tall de teixit automatitzat i laminat de teixit per calor. Els prototips van ser validats pel que fa a la detecció de gestos amb resultats positius. Respecte a les tècniques de fabricació emprades, s'han realitzat estudis comparatius de resposta enfront de la humitat, variacions de temperatura i rentats.

Abstract

The main objective of this thesis is the development of new sensors and actuators using Printed Electronics technology. For this, conductive, semiconductor and dielectric polymeric materials are used on flexible and/or elastic substrates. By means of suitable designs and application processes, it is possible to manufacture sensors capable of interacting with the environment. In this way, specific sensing functionalities can be incorporated into the substrates, such as textile fabrics. Additionally, it is necessary to include electronic systems capable of processing the data obtained, as well as its registration. In the development of these sensors and actuators, the physical properties of the different materials are precisely combined. For this, multilayer structures are designed where the properties of some materials interact with those of others. The result is a sensor capable of capturing physical variations of the environment, and convert them into signals that can be processed, and finally transformed into data.

On the one hand, a tactile sensor printed on textile substrate for 2D gesture recognition was developed. This sensor consists of a matrix composed of small capacitive sensors based on a capacitor type structure. These sensors were designed in such a way that, if a finger or other object with capacitive properties, gets close enough, its behaviour varies, and it can be measured. The small sensors are arranged in this matrix as in a grid. Each sensor has a position that is determined by a row and a column. The capacity of each small sensor is periodically measured in order to assess whether significant variations have been produced. For this, it is necessary to convert the sensor capacity into a value that is subsequently digitally processed. When a user approaches a finger, the capacity of the sensor is increased. In this way, any variation in the capacity of one of the sensors can be detected and measured. These measurements are processed together and the position and movement of the finger on the surface of the sensor array can be determined. Various designs and prototypes have been developed with the objective of being printed on textile substrate.

On the other hand, to improve the effectiveness in the use of the developed 2D touch sensors, the way of incorporating an actuator system was studied. Thereby, the user receives feedback that the order or action was recognized. To achieve this, the capacitive sensor grid was complemented with an electroluminescent screen printed as well. The final prototype offers a solution that combines a 2D tactile sensor with an electroluminescent actuator on a printed textile substrate. Thus, the user receives a light signal in response to a gesture, confirming that the gesture has been recognized.

Next, the development of a 3D gesture sensor was carried out using a combination of sensors also printed on textile substrate. In this type of 3D sensor, a signal is sent generating an electric field on the sensors. This is done using a transmission electrode located very close to them. The generated field is received by the reception sensors and converted to electrical signals. For this, the sensors are based on electrodes that act as receivers. If a person places their hands within the emission area, a disturbance of the electric field lines is created. This is due to the deviation of the lines to ground using the intrinsic conductivity of the human body. This disturbance affects the signals received by the electrodes. Variations captured by all electrodes are processed together and can determine the position and movement of the hand on the sensor surface. Various designs and prototypes have been developed with the challenge of being printed on textile substrate. This type of sensor allows the position of the hand or finger to be detected, without the need of direct contact. In comparison to 2D sensors, this is an advantage that allows them to be used in other types of applications. The fact that the sensor must be hidden under very thick foam or fabric gives them more possibilities. During the development of the 3D sensor, its use in various tissues was evaluated by combining different conductive inks. In addition, different printing possibilities were also evaluated to optimize the manufacturing process.

Finally, the development of an improved 3D gesture sensor was carried out. As in the previous development, the sensor allows contactless gesture detection, but increasing the detection range. In addition to printed electronic technology, two other textile manufacturing technologies were evaluated. On the one hand, prototypes were made using conductive threads and industrial embroidery machine. On the other hand, the use of conductive fabrics was evaluated using automated fabric cutting equipment and heat fabric lamination. The prototypes were validated with respect to gesture detection with positive results. Regarding the manufacturing techniques used, comparative studies of response to humidity, temperature variations and washes were carried out.

Table of Contents

RESUMEN.....	I
RESUM	III
ABSTRACT	V
TABLE OF CONTENTS.....	VII
FIGURE LIST.....	XI
TABLE LIST.....	XVII
ACRONYMS.....	XIX
1. INTRODUCTION.....	1
1.1. STATE OF THE ART	2
1.1.1. <i>Smart Textiles</i>	2
1.1.2. <i>Components of Smart Textiles</i>	2
1.1.3. <i>Sensor Types</i>	3
1.1.4. <i>Sensing Technologies</i>	3
1.1.5. <i>Manufacturing Processes</i>	7
1.1.6. <i>Controller</i>	8
1.2. MOTIVATION AND SCOPE.....	9
1.3. OBJECTIVES.....	10
1.4. CONTEXT	11
1.4.1. <i>SmartLife</i>	11
1.4.2. <i>Screentex</i>	12
1.4.3. <i>Flexitex</i>	13
1.5. THESIS OVERVIEW.....	14
1.6. SCIENTIFIC PUBLICATIONS	15
1.7. ACADEMIC CONTRIBUTIONS	16
<i>International Journals:</i>	16
<i>International Conferences:</i>	16
1.8. RIGHTS.....	17
2. 2D TOUCHPAD SENSOR PRINTED ON TEXTILE SUBSTRATE	27
2.1. INTRODUCTION	28
2.2. DESIGN AND WORKING PRINCIPLE.....	29

2.2.1.	<i>Sensor Pattern</i>	30
2.2.2.	<i>Textile Touchpad Design</i>	31
2.2.3.	<i>Design of Electronic System</i>	33
2.3.	MATERIALS AND METHODS	33
2.3.1.	<i>Sensor Development</i>	33
2.4.	RESULTS.....	38
2.4.1.	<i>Physical Parameters</i>	38
2.4.2.	<i>Electrical Parameters</i>	38
2.4.3.	<i>4.3. Design Using Different Types of Fabrics</i>	40
2.4.4.	<i>Design Reducing the Size</i>	40
2.4.5.	<i>Operation</i>	41
2.5.	CONCLUSIONS	42
3.	A 2D TOUCH TEXTILE SENSOR WITH AN ELECTROLUMINESCENT DISPLAY	47
3.1.	INTRODUCTION	48
3.2.	MATERIALS AND METHODS	49
3.2.1.	<i>Device Architecture Development</i>	49
3.2.2.	<i>Electronic Systems Development</i>	53
3.3.	RESULTS AND DISCUSSION	54
3.3.1.	<i>Physical Parameters</i>	54
3.3.2.	<i>Electroluminescent Display Results</i>	57
3.3.3.	<i>2D Touchpad Results</i>	59
3.3.4.	<i>Final Design</i>	60
3.4.	CONCLUSIONS	61
4.	A TEXTILE 3D GESTURE RECOGNITION TEXTILE SENSOR	67
4.1.	INTRODUCTION	68
4.2.	DESIGN AND WORKING PRINCIPLE	70
4.2.1.	<i>Working Principle</i>	70
4.2.2.	<i>Microchip Sensor Design</i>	74
4.2.3.	<i>Textile 3D Gesture Sensor Design</i>	80
4.3.	MATERIALS AND METHODS	84
4.3.1.	<i>Materials</i>	84
4.3.2.	<i>Sensor Development</i>	86
4.3.3.	<i>Measurements</i>	87
4.4.	RESULTS AND DISCUSSION	87
4.5.	CONCLUSIONS	101
5.	A BOOSTED TEXTILE 3D GESTURE RECOGNITION TEXTILE SENSOR	107
5.1.	INTRODUCTION	108
5.2.	MATERIALS AND METHODS	109
5.2.1.	<i>Electronic Design</i>	110

5.2.2.	<i>Materials</i>	113
5.2.3.	<i>Manufacturing</i>	114
5.2.4.	<i>Sensor Development</i>	116
5.2.5.	<i>Measurement</i>	118
5.3.	RESULTS AND DISCUSSION	118
5.4.	CONCLUSION.....	128
6.	CONCLUSIONS	133
6.1.	CONCLUSIONS	134
6.2.	FUTURE RESEARCH LINES.....	136

Figure List

Figure 1. Textile electrodes to be used as ECG and EMG sensors. Source: AITEX.	3
Figure 2. Resistive sensor structure for touch applications. Source: Screenshot Project from AITEX.	4
Figure 3. Conductive plates printed on fabric working as electrodes. Source: Screenshot Project from AITEX.....	4
Figure 4. Surface capacitive sensor. Source: Own elaboration.	5
Figure 5. Projected capacitive sensor. Source: Flexitex Project from AITEX.....	6
Figure 6. Self-capacitance sensor. Source: Own elaboration based on Walker, G. et al. [91].	6
Figure 7. Mutual-capacitance sensor. Source: Own elaboration based on Walker, G. et al. [91].....	7
Figure 8. 3D gesture sensor. Source: Own elaboration based on Microchip design recommendations.	7
Figure 9. Printing technologies: inkjet, screen and flexography. Source: Flexitex Project from AITEX.....	8
Figure 10. Source: Smartlife Project from AITEX.	12
Figure 11. Thesis diagram.....	15
Figure 12. (a) Diamond pattern; and (b) 2D array sensors in the case of single layer or two layers.	30
Figure 13. Two Layers Design (TLD): (a) Vertical or X layer; (b) dielectric layer; (c) Horizontal or Y layer; and (d) the complete design.	32
Figure 14. One Layer Design (OLD): (a) conductive layer for connection tracks; (b) dielectric layer with via-holes; (c) X-Y layer; and (d) the complete design.	33
Figure 15. Pinholes in the dielectric layer; and (b) detail of pinhole.	34
Figure 16. (a) First conductive layer, above for TLD and below for OLD; (b) dielectric layer; (c) second conductive layer; and (d) complete Design.	36
Figure 17. (a) Two-layer design; and (b) one-layer design magnification views.....	38

Figure 18. (a) Capacitance distribution on OLD; and (b) capacitance distribution on TLD.	39
Figure 19. Two-layer design: (a) “released” signal; and (b) “pressed” signal.....	39
Figure 20. One-layer design: (a) “released” signal; and (b) “pressed” signal.	40
Figure 21. Capacitances and failures for each type of fabric and design.....	40
Figure 22. Touchpads with the same design but different size.	41
Figure 23. (a) Performance test on a curved surface touching two different points; and (b) performance test touching on the same point but on a flat and a curved surface, obtaining the same result.	41
Figure 24. ELD + 2D touchpad architecture: All the design on one side of the textile (a); Using the textile itself as a separating element, on one side the ELD and on the other one the 2D touchpad sensor (b). ELD: electroluminescent display.....	50
Figure 25. ELD Design: Conductive silver electrode (a); dielectric layer (b); Phosphor layer (c); and clear conductor (d).	51
Figure 26. Different types of fabrics used as substrates.	51
Figure 27. 2D Touchpad Design: Vertical or X layer (a); dielectric layer (b); and Horizontal or Y layer (c).	53
Figure 28. Electronic System Block Diagram (a); real electronic system applied to a mouse control in a mobile phone (b).	53
Figure 29. Electroluminescent Display layers profilometry (a). 2D Touchpad layers profilometry, in this case fabrics A and B are studied in order to value the insulator layer (b).	55
Figure 30. Cotton fibers without PEDOT: PSS (a) and after the screen printing of PEDOT: PSS (b).....	56
Figure 31. SEM micrograph showing device cross-section. Fabric_A (a) and Fabric_C (b). In a box, in the bottom right corner of each figure, the virgin fabric is shown...	57
Figure 32. Chromaticity diagram according to the CIE 1931 standard.	58
Figure 33. Train of pulses sent by the Touch Controller. Normal signal (a) and disturbed signal (b).....	60
Figure 34. ELD + 2D touchpad architecture with ITO EMI shield. ELD: electroluminescent display; ITO: indium tin oxide; EMI: electromagnetic interferences.	60
Figure 35. 2D touchpad with ELD on and off (a). Redesign in order to turn on only the zone that has been touched (b). The design has been manufactured with Fabric_A...	61
Figure 36. Field lines generated by the transmission Tx electrode. The reception Rx electrodes are located inside of the generated field. On the left side of the Figure, the field lines are shown when they are not modified by any conductor object.	

	On the right side of the Figure, a hand is causing a modification of the field lines, leading to a variation in the signal received by the Rx electrodes. Source: Microchip Technology Inc.	71
Figure 37.	Gestures recognized by the internal algorithm of MGC3130: approach detection, position tracking in 3D, sensor touch (touch, multitouch, tap, and double tap), flick gestures, circle gestures, and airwheel. Source: Microchip Technology Inc.	71
Figure 38.	Standard sensor used by Microchip. It consists of a first layer where four Rx electrodes are located on each of the cardinal points as well as a central Rx electrode. This layer is separated from the bottom layer that contains the Tx electrode by a dielectric. The ground plane layer is optional and would be located below the Tx electrode layer. The sensitive area is just delimited by the four perimeter Rx sensors. Source: Microchip Technology Inc.	72
Figure 39.	MGC3130 Block Diagram, composed of an analog front-end module that allows to generate the transmission Tx signal and receive the signals from the 5 Rx electrodes. The signals, properly processed, are transferred to the Signal Processing Unit that, together with the GestIC library, processes and converts them into the different programmed gestures. Lastly, there is a communication block with a host. Source: Microchip Technology Inc.	73
Figure 40.	Equivalent simplified circuit of the combination sensor-MGC3130. Source: Microchip Technology Inc.	74
Figure 41.	Basic scheme of the gesture sensor recommended by Microchip. Source: Microchip Technology Inc.	75
Figure 42.	Variation of signal deviation received by Rx in function of the distance of the hand to the sensor and of the Rx electrode width.	76
Figure 43.	An op-amp buffer must be inserted between the Tx pin and the Tx electrode in case C_{TxGND} is greater than 1 nF. Source: Microchip Technology Inc.	77
Figure 44.	Basic design parameters recommended by Microchip. Source: Microchip Technology Inc.	77
Figure 45.	General characteristics of the 95×60 sensor from Microchip. Source: Microchip Technology Inc.	78
Figure 46.	Crosscut of the PCB of the 95×60 sensor; dimensions and number of layers. Source: Microchip Technology Inc.	78
Figure 47.	(a) Waveform of the transmission signal, (b) the received Rx signal with no object modifying the field lines, (c) the received Rx signal with an object modifying the field lines.	80
Figure 48.	3DS-1 design with four layers: (a) ground plane layer, (b) transmission Tx electrode, (c) dielectric layer between Rx and Tx layers and vias, (d) Rx electrode layer.	81

Figure 49. Cross-section of the 3DS-1 sensor. In addition to the 4 layers shown in Figure 48 the textile substrate between the ground plane layer and the Tx electrode layer can be observed.	82
Figure 50. 3DS-2 design with four layers. Ground plane layer (a). Dielectric layer between Tx and ground layer (b). Transmission Tx layer (c). Rx layer (d).	82
Figure 51. Cross-section of the 3DS-2 sensor. In addition to the 4 layers shown in Figure 50, the textile substrate between the Rx layer and the Tx electrode layer can be observed.	83
Figure 52. 3DS-1 Design with two construction structures: (a) the textile substrate acting as a dielectric between the Tx electrode and the ground plane (sensor name 3DS_1a) and (b) the textile substrate acting as a mere base (sensor name 3DS_1b).	88
Figure 53. 3DS-1 Sensor.	88
Figure 54. Transmission signal waveform (a), a signal deformation can be observed due to a capacitance of $C_{TxGND} > 1nF$. Regenerated signal obtained coupling an AO between the Tx pin and the Tx electrode (b). Receiving Rx signal with direct connection (c) between the Tx pin and the Tx electrode. Receiving Rx signal with AO (d) between the Tx pin and the Tx electrode.	91
Figure 55. 25× Magnified view of the printing of the conductive ink on the Type D textile (a) and on the Type E textile (b).	92
Figure 56. 25× Magnified view of the printing of the dielectric and conductive inks on: (a) Type D textile with dielectric Creative 127-48D and a layer of silver ink, (b) Type D textile with dielectric EMS DI-7542 and a layer of silver ink, (c) Type D textile with dielectric INKRON IPD-670 and a layer of silver ink, (d) Type E textile with dielectric Creative 127-48D and a layer of silver ink, (e) Type E textile with dielectric EMS DI-7542 and a layer of silver ink and (f) Type D textile with dielectric IPD-670 and a layer of silver ink.	93
Figure 57. 3DS-2 Design with two construction structures: (a) the textile substrate acting as a dielectric between the Tx electrode and Rx electrode (sensor named 3SD_2a) and (b) the textile substrate covered with polyurethane (sensor named 3SD_2b).	94
Figure 58. Sensor 3DS-2a.	94
Figure 59. Waveform of the transmission signal (a) with buffer due to the capacitance $C_{TxGND} > 1nF$, (b) receiving RX signal with direct connection between the Tx pin and the Tx electrode and (c) receiving RX signal with op-amp between the Tx pin and the Tx electrode.	96
Figure 60. “Artificial hand” provided by Microchip. It is made of styrofoam covered by copper and connected to ground. Some blocks of styrofoam with no covering allow to move the “artificial hand” away from the sensor.	97

Figure 61. Signal Deviation of the different sensors in function of the distance of the hand from the surface of the sensor. The C_{TxRxN} value, in brackets in the legend, has been included as a reference to assess the relationship between capacitance and sensitivity. This relationship is the same in any of the associated capacities.	97
Figure 62. Approach detection.....	99
Figure 63. Flick north to south.....	99
Figure 64. Flick west to east.	100
Figure 65. Airwheel.	100
Figure 66. Complete portable system.....	101
Figure 67. 3D Sensor used as a Wireless mouse with a mobile phone.	101
Figure 68. Standard (left) and Boosted (right) sensors used by Microchip. The standard version consists of 5 RX electrodes on top layer plus a TX electrode on an inner layer. The boosted version has 4 RX and 1 TX electrodes on the top layer. The sensing space is the same in terms of area but is lower in volume in the case of the standard version. Source: Microchip Technology Inc.....	111
Figure 69. Basic design parameters recommended by Microchip for a) Standard sensor and b) Boosted sensor. Source: Microchip Technology Inc.	112
Figure 70. Boosted sensor design: Ground plane layer (a) and Tx-Rx electrodes (b).....	115
Figure 71. 3D gesture sensor developments with the three E-textile technologies: (a) screen-printing, (b) embroidery and, (c) direct application of conductive textile, and with the PCB material (d).	117
Figure 72. Frequency response of fabric relative permittivity.	118
Figure 73. Values of the equivalent capacitor circuit: a) parallel capacitance C_p , b) parallel resistance R_p , c) impedance and d) phase value.	119
Figure 74. “Artificial hand” provided by Microchip made of styrofoam covered by copper and connected to ground.	121
Figure 75. Signal Deviation of the different sensors in function of the distance of the hand from the surface of the sensor. The smallest graph is the magnification of the 10 cm limit.	122
Figure 76. Flexible 3D Boosted sensor manufactured.	122
Figure 77. a) Capacitance variation depending on the humidity at a fixed temperature of 20 °C, b) Capacitance variation depending on the temperature at a fixed humidity of 40% RH.....	123
Figure 78. Normalized resistance variation in a conductor pattern used in the three technologies (fabric, thread and ink) versus number of washes.....	123
Figure 79. a) appearance of the silver ink before washing and, b) after 5 washes.....	124

Figure 80. a) Appearance of the silver ink coated with a heat-sealed film before washing and, b) after 5 washes. The bubbles generated between the substrate and the film and the degeneration of the silver ink are observed..... 124

Figure 81. Characterization of the sensors using an artificial hand: a) PCB reference sensor fixing $Z = 0$ position. b) Textile sensor fixing $Z = 0$ position. c) PCB reference sensor fixing $Z = 3$ cm position. d) Textile sensor fixing $Z = 3$ cm position. e) PCB reference sensor fixing $Z = 5$ cm position. f) Textile sensor fixing $Z = 5$ cm position. 125

Figure 82. Two of the gestures used in the validation: a) flick from north to south and b) flick from west to east. 126

Table List

Table 1. Failures rate (%) for TLD when 1–3 layers of dielectric ink are used.	35
Table 2. Failures rate (%) for OLD when 1–3 layers of dielectric ink are used.....	35
Table 3. Final layer thickness depending on mesh value and number of layers.	36
Table 4. Capacitance (pF) for TLD when 1–3 layers of D2081009D6 ink are used.....	37
Table 5. Capacitance (pF) for OLD when 1–3 layers of D2081009D6 ink are used.	37
Table 6. Capacitance (pF) for OLD and TLD when 1–3 layers of D2070209P6 ink are used for mesh of 175 inches.	38
Table 7. Characteristics of the different fabrics used.	52
Table 8. Light characteristics of the different samples used.	59
Table 9. Values of C_{TxRx} [5–30 pF].....	79
Table 10. Real values of C_{TxGND} [<1 nF].	79
Table 11. Values of C_{RxGND} [5–30 pF].	79
Table 12. Fabric characteristics (I): composition and ligament.	84
Table 13. Fabric characteristics (II): size and weight characteristics.	85
Table 14. Silver ink characteristics.	85
Table 15. Dielectric ink characteristics.	86
Table 16. Polyurethane characteristics.....	86
Table 17. Relative permittivity of the dielectric inks ϵ_r @100 kHz.....	89
Table 18. Relative permittivity of fabrics ϵ_r @100 kHz.	89
Table 19. Capacitance values of 3DS-1a-TA (pF).....	89
Table 20. Capacitance values of 3DS-1b-TA (pF).....	90
Table 21 . Capacitance values of 3DS-2-TA (pF).....	92
Table 22. Relative permittivity of the polyurethanes.	93
Table 23. Capacitance values of 3DS-2a and 3DS-2b (pF).....	95

Table 24. Values of C_{TRX} : theoretical nominal capacity (C_n), with Edge effect (C_{edge}) and real values (C_{real}) (pF).....	98
Table 25. Fabric characteristics.....	113
Table 26. Silver ink characteristics.....	114
Table 27. Embroidery thread silver characteristics.....	114
Table 28. Conductive fabric plain characteristics.....	114
Table 29. Capacitance values (pF) at 104 Hz.....	120
Table 30. Gesture conducted tests results for the 3DBS_Screen sensor.....	127
Table 31. Comparison between proposed Sensors.....	127

Acronyms

ACPEL:	AC Powder Electroluminescent
ADC:	Analog-to-Digital Converter
ASIC:	Application-Specific Integrated Circuit
CAD:	Computer-Aided Design
CIE:	International Commission on Illumination
CNT:	Carbon Nanotube
CVD:	Capacitive Voltage Divider
CSM:	Capacitive Sensing Module
CTMU:	Charging Time Measurement Unit
ECG:	Electrocardiogram
EEG:	Electroencephalogram
ELD:	Electroluminescent Display
EMI:	Electromagnetic Interferences
FPGA:	Field-Programmable Gate Array
FR4:	Fiber Glass-Reinforced Epoxy Laminate Material
GND:	Ground
GPS:	Global Positioning System
GPU	Graphics Processing Unit
HMI:	Human Machine Interaction
HMI:	Human Machine Interface
HCI:	Human-Computer Interaction
Hz:	Hertz
ITO:	Indium Tin Oxide

LCR:	Inductance Capacitance Resistance
LED:	Light-Emitting Diode
MD:	Machine Direction
MVTR:	Moisture Vapor Transmission Rate
OLD:	One Layer Design
OLED:	Organic Light Emission Diode
p-cap:	Projected Capacitive
PCB:	Printed Circuit Board
PCT:	Projected Capacitive Technology
PDMS:	Polydimethylsiloxane
PEDOT:PSS:	Poly(3,4-Ethylenedioxythiophene):Poly(Styrene Sulfonate)
PET:	Polyethylene Terephthalate
PP:	Polypropylene
RF:	Radio Frequency
SCT:	Surface Capacitive Technology
SEM:	Scanning Electron Microscopy
TLD:	Two Layers Design
UV:	Ultraviolet
VAC:	Voltage, Alternating Current
VGA:	Video Graphics Array
V _{P-P} :	Peak to Peak Voltage
ε _r :	Relative Permittivity

Chapter 1

Introduction

1.1. State of the Art

1.1.1. Smart Textiles

Smart textiles have attracted the attention of the scientific community in the last years [1,2]. They are fabrics that can sense or react to the external environment, producing a designed and useful response [3,4]. Since smart textiles are partly made of fabrics, features such as flexibility, softness, wearability and conformability are extended to them. These properties allow them to be used in applications as diverse as Healthcare [5,6], Gaming [7,8], Defence [9-11] Sportwear [12,6] or Automotive [13]. Currently, their potential to be applied in new fields remains unexplored.

One of most important uses of smart textiles is sensing. Smart textile sensors make use of the electrical properties of the involved textile substrates [14]. They are usually combined with external controllers or microprocessor units [15]. Among the applications, it is possible to find antennae for external communications [16,17] or body area networks [18,19], electrodes for Electrocardiogram (ECG) or Electroencephalogram (EEG) measurements [20,21], or sensors for respiration or body postures monitoring [22-24]. In this case, they are also named electronic textiles or e-textiles [25]. The data provided by the sensor to the microprocessor unit can be used for different purposes such as generating alerts [26], detecting situations [27] or tracking behaviours [28,29] among others.

There is a specific subset of sensors focused on movement or gesture detection [30] in order to interact with electronic devices or computers. This field is known as human-computer interaction (HCI) [31] or human machine interaction (HMI) [32]. Some gesture detection sensors enable humans to interact with computers and machines without any physical contact in a more natural way [33]. This is an attractive topic, since it has a huge application range, varying from very simple applications to interact with home appliances [34] to complex systems of telemedicine [35]. This work presents different smart textile solutions for the purpose of hand gesture recognition.

1.1.2. Components of Smart Textiles

Three mainly elements can be differentiated in smart textiles: sensors, actuators and passive components [4]. Sensors transform external parameters into electrical signals that can be read and understood. There is a broad range of sensors for different purposes depending on the used technology [36] or on the parameter to sense [37,38]. Regarding actuators, they usually respond to an event detected by a sensor. Several elements can be considered as actuators, for instance, those that can produce light like electroluminescent screens textiles [39-41], heaters based on resistive materials [42,43] or shape memory fabrics [44]. Finally, the passive elements are those which implement the connectivity of the sensor, such as buses, wires or joining elements [45-47]. All these passive elements should be flexible and stretchable. For these purposes some designs such as serpentines [48-50] and fractal [51] are applied.

1.1.3. Sensor Types

Smart textile sensors can be classified depending on whether they measure resistivity or capacitance variations. On the one hand, resistive sensors measure variations of the resistance of a conductive structure. They could be a wire or a conductive stretchable fabric [52-54]. On the other hand, capacitive sensors use more complex structures that allow one to measure a capacitance between two conductive materials that can be also conductive threads or conductive textiles [55,56]. This technology has been successfully developed in order to measure parameters such as strain [23,56-58], pressure [59-61], movement [62,63], respiration [6,55,64], humidity [65,66], gas [67-69] or temperature [70,71] among others. Moreover, sensors based on conductive surfaces such as electrocardiogram (ECG) [72-76], electromyography (EMG) [28,77,78], electroencephalogram (EEG) [21,79,80] have also been implemented. An example of an ECG sensor made with conductive fabric is presented in Figure 1.



Figure 1. Textile electrodes to be used as ECG and EMG sensors. Source: AITEX.

In addition to conductive threads or conductive fabrics, conductive particles or materials, such as inks, can also be printed on the top of surface of the textile [81]. This technique is known as Printed Electronics [82] and has been successfully applied on flexible substrates [83,84]. Its great potential in terms of flexibility makes possible its use in a huge number of applications. Furthermore, Printed Electronics involves lower costs than the current standard techniques, such as Printed Circuit Board (PCB) manufacturing, which represents an added value [85]. This could lead to an implementation with reel to reel industrial machines [86].

1.1.4. Sensing Technologies

As aforementioned, two main sensing technologies can be found in smart textiles, depending on the electrical parameter that can be measured. The first one uses resistive sensors and is based on the measurement of the variation of the electrical resistance of a conductive structure. It has been successfully been relevant to measure pressure [87], respiration [53] or temperature [70]. This technology is out of the scope of this thesis. An example of a resistive sensors is presented in Figure 2.

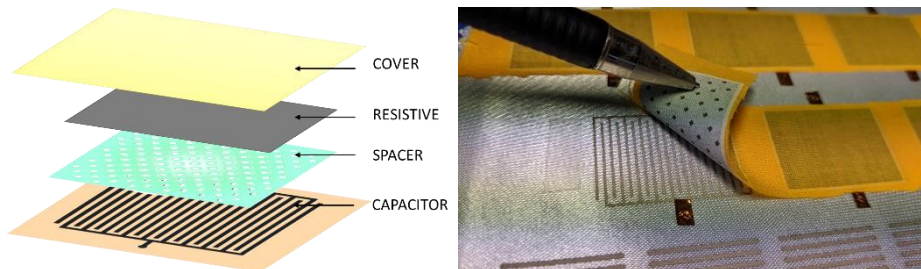


Figure 2. Resistive sensor structure for touch applications.
Source: Screentex Project from AITEX.

The other technology employs capacitive sensors, relying on the measurement of the capacitance at addressable electrodes. Applications such as electromyography [77], humidity [88] or touch sensors [89] make use of capacitive sensors. This thesis is focused in this technology. Capacitive sensors provide some advantages, such as a high linearity, low hysteresis, and fast response time, enabling it to be used in real-life applications [90]. In this type of sensors, the conductivity of the material used is not so critical as in the case of resistive sensors. This is due the measured parameter, the capacitance. This is an important point, since the conductivity can be affected when the used textiles suffer movement, stretching or deterioration. In Figure 3 capacitive sensors printed on textile are shown.



Figure 3. Conductive plates printed on fabric working as electrodes.
Source: Screentex Project from AITEX.

These sensors normally use electrode structures in the same layer or multilayer electrode structures conforming capacitors. The simplest structure of a capacitor consists of two conductors, normally two conductive plates, also named electrodes, separated by a dielectric layer, working as electrical insulator. The capacitance of the resulting capacitor depends basically on three parameters: the area of the surface of the conductive plates, the distance between the plates, given by the resulting thickness of the insulating layer, and the relative permittivity or dielectric constant of the insulating material. The capacitance can be controlled considering that it is directly proportional to the area of the plates and the relative permittivity, and inversely proportional to the distance between the plates.

Capacitive sensors can be used to measure the interaction of the human body with the sensor. There exist two approaches to measure the interaction of a subject with a capacitive sensor. The first one makes use of the variation of the capacitance when a body with capacitive properties approaches to the sensor. For instance, when a finger approaches to a capacitive sensor, the human body becomes part of the electrical circuit and changes the resulting capacitance. This is the base of the functioning of 2D sensors. The second approach make use of the property of capacitors to measure electrical fields. An electrical field is created on the sensors and it is perturbed when a conductive body approaches to the sensor. This perturbation is detected by the sensor. For instance, when a finger approaches to the sensor, the lines of the electrical field are conducted to ground through the human body. 3D sensors use this technique for sensing. In both approaches, the variations in the resulting capacitance or in the electrical field on the sensor, can be used to estimate a position or to detect gestures.

Regarding 2D capacitive touch sensors, they can be grouped in two main categories: Surface Capacitive Technology (SCT) and Projected Capacitive (p-cap) Technology (PCT) [91]. In the SCT, a substrate is uniformly coated with a conductive layer. A voltage signal is applied to all four corners of the sensor, resulting a uniform electrostatic field (Figure 4). When a human finger touches the panel, it forms a capacitance where one plate is the conductive layer and the other the human finger. Depending on the location of the finger touch, different amount of current flows from the four corners. This difference is used to determine the location of the finger.

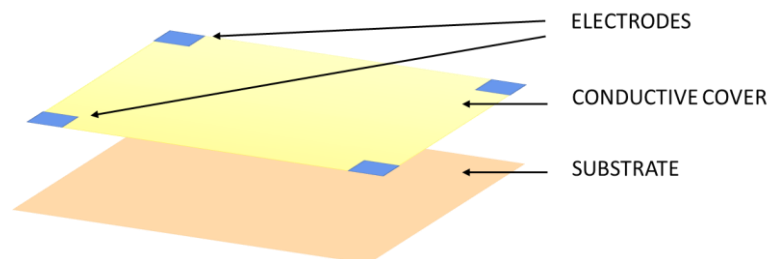


Figure 4. Surface capacitive sensor. Source: Own elaboration.

Projected capacitive technology (PCT) is regarded as the most popular technology for touch sensors. They permit a higher resolution and features that make them ideal for industrial or outdoor applications [92]. PCT is based on some small sensors distributed over a surface. The capacitance of each sensor is measured to detect the position of the finger. They can be implemented using independent feeding lines for each sensor or combining the feeding lines as grids. For the latter, a two layered structure conforms the projected capacitive. Horizontal electrodes are in a layer located in rows and the vertical electrodes are located on another layer as columns (Figure 5). Each sensor has a position that is determined by a row and a column. PCT detect touch by measuring

the capacitance at each addressable sensor. When a finger or a conductive body approaches to a sensor, it disturbs the electromagnetic field and alters the capacitance.

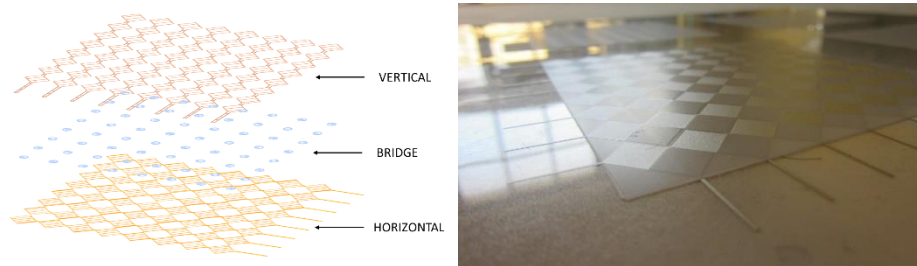


Figure 5. Projected capacitive sensor. Source: Flexitex Project from AITEX.

There exist two types of touch sensing signal acquisition in PCT. The first one is the self-capacitance technology, where each column and row on the screen operates independently. In other words, it is based on measuring the capacitance of a single electrode or line of electrodes with respect to ground (Figure 6). Although this technology offers a faster system response time, it has limitations to register multiple touch points [93].

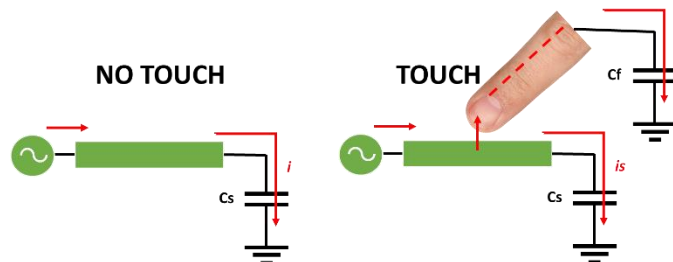


Figure 6. Self-capacitance sensor. Source: Own elaboration based on Walker, G. et al. [91].

The second type of touch sensing in PCT is based on mutual-capacitive sensing technology. This technology measures the capacitance between a pair of electrodes or lines. This technology can detect multi-touch positions, since each electrode intersection is scanned individually [94]. This technology is the most used.

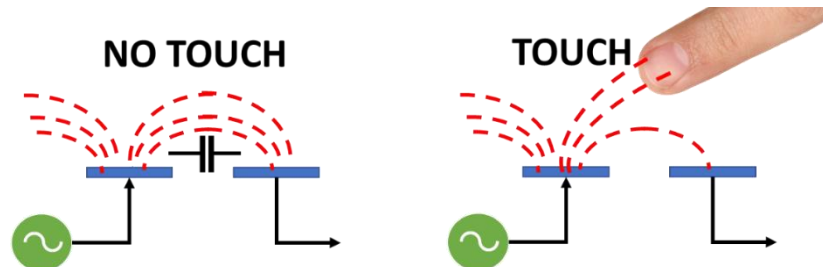


Figure 7. Mutual-capacitance sensor. Source: Own elaboration based on Walker, G. et al. [91].

Regarding 3D sensing technologies, Microchip. Inc, developed the world's first electrical-field based 3D gesture sensor. In this type of sensors an electric field is generated using a transmission electrode. The generated field is received by other reception sensors and converted to electrical signals. When a person places their hands near the emission area, a disturbance of the electric field lines is created. In contrast to PCT, which measures the capacitance, in this technology, the variations of the electric field are measured by the aforementioned reception sensors. Using this technology, the position as well as the distance to the sensor can be estimated. These features allow them to get position tracking, approach detection and recognition of various gestures.

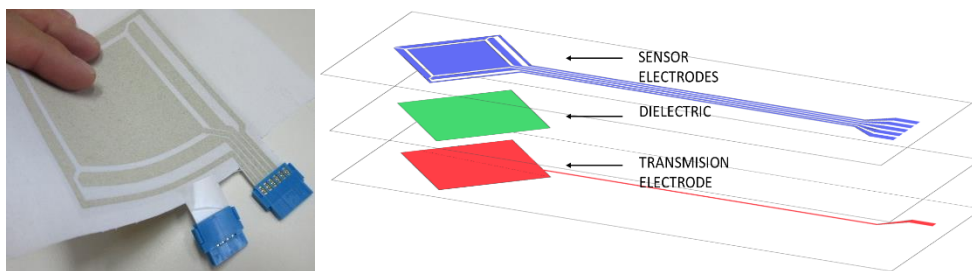


Figure 8. 3D gesture sensor. Source: Own elaboration based on Microchip design recommendations.

1.1.5. Manufacturing Processes

Different techniques can be used to implement the electrodes on a textile surface. Some designs are based on conductive columns and rows that can be simply drawn onto opposite sides of a piece of insulating material using a conductive ink. Another different approach is to use alternating conductive and isolating threads that are glued on the opposite sides of the textile substrate. There also exist implementations where the electronic capabilities are integrated into fiber-based sensors using coating processes on the fiber conforming a dielectric layer sandwiched between two parallel conductive surfaces [95]. Among all the existing technologies, the thick planar printing process with screen printing technology of conductive inks is the most used. This technology can produce entire electronic circuits on a planar fabric board at once and can also re-

produce the identical circuit boards repeatedly. In addition, this system can be easily converted into roll to roll production, resulting in a low cost and high productivity system as flexography or inkjet (Figure 9).

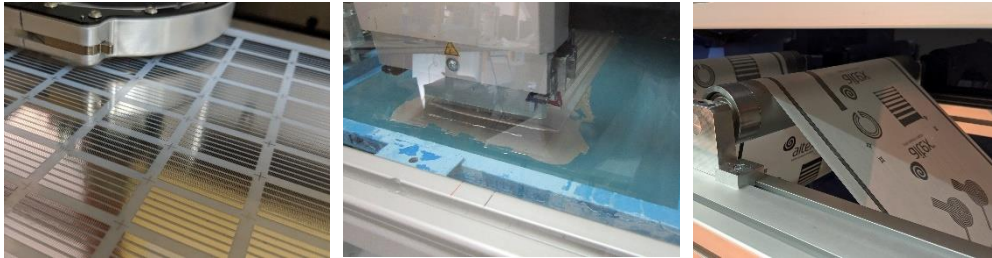


Figure 9. Printing technologies: inkjet, screen and flexography.
Source: Flexitex Project from AITEX.

The most common types of conductive inks are based on conductive nanoparticles or microparticles dispersed into a polymer matrix. These particles are based on carbon metallic particles, such as graphite, silver and gold as well as conductive oxides such as ITO or ZnO. These inks are usually dried or cured by heating, however, laser or UV curing is also possible. When the ink is cured by heat, the binder and solvent are removed, forming a conductive layer on the surface of the substrate. The required curing temperature depends on the type of the ink, but their typically range comes from 100°C to 250°C for 5 to 30 minutes. The curing procedure must be adjusted according to the type of the substrate.

1.1.6. Controller

Sensors usually work together with specific electronic components named controllers. Different electronic companies produce touchpad and touchless gesture detection solutions including sensors, controllers and software. The most important manufacturers are Atmel, Azoteq, Broadcom, Cirque, Cypress, Elan, Infineon, MicroChip, Touch International Silabs or Synaptics among others.

For the case of 2D sensors, different techniques, depending on the manufacturer, are used for the measuring capacitive variations in the SCT or PCT technologies. They are implemented in modules or units:

- Charging Time Measurement Unit (CTMU): uses a constant current that it is applied for a certain time to the circuit. Subsequently, the time of charging and discharging of an internal capacitor, in parallel with the sensor, is measured.
- Capacitive Sensing Module (CSM): uses a fixed current source and a comparator. This creates a circuit that changes its frequency based on the capacitance seen at the sensor.

- **Capacitive Voltage Divider (CVD):** uses an internal capacitor and sensors acting as external capacitors charged to opposite voltages. After a small amount of time, the external and internal capacitors are connected in parallel and the voltage is measured. Then, the process is repeated inverting the voltages. The differential results are measured obtaining the variation.

For this thesis, the 2D touchpad controller selected was the MTCH6102 controller, from Microchip. This capacitive touch controller includes a gesture unit with low-power performance. It utilizes up to 15 channels to support taps, swipes, and scrolling on XY touch pads. This controller includes a CVD module combined with an analog to digital converter. In addition, a digital signal processing unit with an external communication interface is included in the same chip.

For the case of 3D sensors, the only technology found was the corresponding to Microchip. The controller selected was the MGC3XXX controller. This controller transmits a periodic signal from the signal generator to the sensor. This signal generates an electric field on the grid of reception electrodes that form the reception sensors. As aforementioned, when a human finger or hand approaches to the sensor, the electric field is disturbed. The measurement of this variation is carried out by means of a signal registered by the sensor and received in the controller. This is achieved using an analog front end (includes an analog to digital converter). This received signal is processed in the digital signal processing unit obtaining determined results, such as the position or the gesture made. Finally, there can be a data exchange between the controller and some external devices using a communication interface.

1.2. Motivation and Scope

Two main factors contributed to the growth of smart textiles. On the one hand, the miniaturization of the electronics, battery improvements and lower hardware manufacturing costs have made possible to incorporate small electronic devices into our daily lives. On the other hand, the evolution of smart phones and their global use has defined a standard of technological use at the user level. These trends have boosted the use of wearable technology in different products like glasses, watches, bands, but also clothing. Hence, the user and industry demand more integration into the clothing. Although, currently the complete integration in textiles is improvable, the market forecasts are very promising.

To overcome this integration challenge, there are different issues that must be solved. Elements such as the type of textile to be printed or the protection to be used to increase the durability, are critical in the whole design of a smart textile. Each material or element has characteristics that will impact on the final application. Likewise, the typology of inks, their deposition and circuit design, with the added complexity of properties such as flexibility and elasticity, poses a challenge for their fabrication. In addition, another aspect to consider is the interconnection between the flexible smart textile

and the PCB electronics used. The selection of the connectors and attachment systems is also crucial.

During this work, different prototypes have been developed using different technologies that can be used in smart fabrics. All of them will be related to the design and development of fabrics with smart properties, investigating the limitations and scope of the technologies to discover the potential of these applications.

The developed prototypes comply with the minimum requirements of functionality and resistance to use. In addition, the appropriate materials to be used have been selected as well as the optimal conditions of application and manufacturing. It should be noticed that the knowledge acquired during the project, especially that derived from the experimentation in the application of electronic inks on fabrics, will be very useful for future developments, involving the current applications or in other fields.

1.3. Objectives

This thesis is focused on the development of sensors and actuators using printed electronic technology. The general objective of this work is to develop sensors and actuators capable of being integrated into flexible and stretchable substrates such as textiles, using printing conductive polymeric materials, organic polymers and dielectrics.

This general objective is achieved by fulfilling the following specific objectives:

- Design appropriate structures of different materials considering their physical properties that allow them to detect variations of the environment and convert them into signals that can be processed by electronic systems.
- Develop a printed grid of capacitors capable of sensing the closeness of objects, leading to a 2D touchpad touch sensor.
- Develop an electroluminescent grid using transparent conductive inks with the challenge of being applied on flexible substrates. The developed capacitive sensor grid is then complemented with an electroluminescent screen, in order to give feedback that the order or action has been recognized.
- Optimize the fabrication process in order to use as fewer layers as possible considering different designs for each development.
- Demonstrate the potential of these technologies with complete applications, integrating processing electronics or additional components.
- Develop a touchless sensor grid for gesture detection purposes printed on different textiles substrates. Evaluate the textile substrate as the dielectric layer in the sensor structure.

- Enhance the gesture detection sensor considering a boosted design that increase the detection range. Assess alternative manufacturing processes as embroidery or heat fabric lamination.

1.4. Context

All the work developed in this thesis has been done working in AITEX, the Spanish Textile Research Institute sited in Alcoy. AITEX is a private textile research institute which undertakes characterisation proofs and certifications of textile articles and materials with applications in a broad range of sectors. These applications include habitat, clothing, health, cosmetics, workwear, sports, transport, automotive, marine, aeronautics, construction, among others.

The Institute's core mission is to create technical know-how and transfer this knowledge to textile manufacturers and companies. The main objective is to help them to become more competitive, increasing their value and allowing them to access to new business opportunities. Hence, AITEX promotes collaborative research and development (R&D) with companies by means of innovation projects. All the research and experimentation carried out follow scientific processes to end in manufactured products that can be industry transferable.

This R&D work is done through five research groups: Technical Fibers and Nanotechnology; Materials and Sustainability; Smart Textiles and ICT Solutions; Technical, Finishes Health and Biotechnology; Fashion Design and Garment Making. The work developed in this thesis has been done within the Smart Textiles and ICT Solutions Group.

In addition, this thesis is demarcated in the framework of various research projects: The European H2020 SmartLife Project (Smart Clothing Gamification to promote Energy-related Behaviours among Adolescents), the Regional Screentex Project (Electronic printing research on flexible substrate) and the Regional Flexitex Project.

1.4.1. SmartLife

SmartLife was a project co-funded by the Horizon 2020 Programme of the European Commission under Grant Agreement No. 732348.

SmartLife project aimed to create a mobile game that required a lower body movement. It was personalized by physiological feedback measured by smart textiles. To date, no serious games existed able to be personalized according the physical conditions of the player. This was reached by real-time feedback when playing. The objective of the game was to achieve a target physical activity level.

Personalization via smart textiles allows the player to be challenged depending on the current fitness level of the player. Besides, the activity levels change during the game play. This approach can improve current exergames to achieve a higher level of intensi-

ty in physical activity, needed to create a health impact. This can be done considering what is achievable for the person and hence reducing drop-out and injury risks. The smart textile provides immediate physiological feedback (e.g. movement, posture, position), it ensures that exercises are performed at a moderate-to-vigorous intensity level.



Figure 10. Source: Smartlife Project from AITEX.

SmartLife project was the seed to this work. Part of the requirements of the project were to create smart interfaces integrated in the textiles and sensors that could detect gestures and track the gamer movements. These requirements claimed a new technology that was not available at that moment. In parallel, Printed Electronics technologies were emerging and presented new possibilities to integrate sensors on textile substrates.

1.4.2. Screentex

Screentex was a regional project funded by the Conselleria d'Economia Sostenible, Sectors Productius i Treball, through IVACE (Instituto Valenciano de Competitividad Empresarial) and cofounded by ERDF funding from the EU. Application No.: IMAMCI/2017/1.

The main objective of Screentex Project was to transfer printing technology from electronics to textile substrates. This technology is mature in rigid substrates, such as fiberglass or plastics, enabling the creation of commercial products. However, the use of this technology on flexible substrates such as textiles is still incipient. Textiles present additional difficulties due to their mechanical properties such as flexibility and elasticity. Moreover, other aspects such as deformations or the manner they are affected under temperature and humidity variations must be faced.

Currently, defence, healthcare, and entertainment segments have witnessed adoption of smart textiles due to an increasing demand for products with functional properties. Automotive, sports and fitness are other popular segments in the global smart textile market. These segments have a potential to generate high returns due to the expected rise in the adoption of high-end fabrics [96]. The application of this printing technology on fabrics represents a great opportunity due to the boom that smart textiles are

experiencing. All this suggests that Printed Electronics can play a leading role in the coming years in a new phase of evolution of smart textiles and their integration with wearable sensors.

In this project, basic electronic components were implemented such as strip lines and capacitors with several dimensions. In addition, distinct commercial conductive inks for screen printing were used. The inks were printed under different conditions of screen thickness, printing pressures, printing speed, curing temperature and duration. The next step was to apply it on different flexible substrates to compare their performance.

Then, once the behaviour of the inks was determined and multilayer reference capacitors were produced, more challenging electronic designs were undertaken. A grid of capacitors was developed working as a touchpad 2D sensor.

Finally, an advanced touchpad sensor combined with an electroluminescent screen was printed. The main advantage of this design is that it can give feedback to the user when the gesture is recognized.

1.4.3. Flexitex

Flexitex project was a regional project funded by the Conselleria d'Economia Sostenible, Sectors Productius i Treball, through IVACE (Instituto Valenciano de Competitividad Empresarial) and cofounded by ERDF funding from the EU. Application No.: IMAMCI/2018/1, IMAMCI/2019/1.

The stated objective of the project was to undertake the research and development of sensorized fabrics combining electronic printing techniques with flexible and stretchable materials. During the project, several multilayer circuits were printed to obtain a range of sensors using conductive, dielectric and resistive inks. The resulting embedded electronic designs were characterised. Besides, operational aspects including their ability to flex and stretch were analysed. Challenges such as the encapsulation of printed circuits were also addressed to improve their durability and level of protection.

In this project, new inks were used with resistive and stretchability properties. Heater textiles were faced combining conductive and resistive inks. These fabrics can be used as seats, jackets or gloves heaters. Moreover, the stretch property of some conductive inks was tested. For this purpose, different textiles were printed with these inks. Then, some tests were performed measuring the conductivity while they were stretched. In addition, solutions of conductive electrodes to measure heart rate were considered.

Following the research line of developing interfaces based on sensors, a 3D gesture recognition sensor was designed. The objective was to improve the previous touchpad, developing touchless sensors which do not need direct contact. Different combinations of printed materials were considered evaluating their performance as a 3D gesture recognition sensor.

1.5. Thesis overview

This thesis has been written as a compendium of publications, following *the Universitat Politècnica de València* regulation about doctoral studies. The organization and content of each chapter of this thesis is summarized below.

Chapter 1, as Introduction, provides a description of the state of the art of smart textiles which clearly motivates the realization of the presented work. Besides, a basic introduction of the different employed technologies was presented. In addition, the chapter presents the related projects that have offered a framework for the development of this thesis. Then, the specific objectives are presented and how the thesis is structured to fulfil them.

Chapter 2 presents the use of touchpad sensors as tools to interact in wearable solutions. The principles of projected capacitors technologies are analysed. Two designs of a textile touchpad sensor based on a diamond pattern are presented. Then, the procedure of fabrication with screen-printing technology is included considering different textiles substrates. Finally, the results and conclusions were presented.

Chapter 3 describes the work and results obtained when combining a touchpad 2D with an electroluminescent lamp grid using screen-printing technique on a textiles substrate. This solution improves the effectiveness in the use of touch interfaces since the user receives feedback when the action has been recognized. Some challenges are faced, such as the electromagnetic interferences detected distorting the signal in the touchpad produced by the electroluminescent lamp or the printing order to assure good performance.

Chapter 4 introduces touchless gesture sensors and their importance to allow humans to interact with computers and machines without any physical contact. The design and working principles for developing a 3D gesture sensor are presented. Then, two three-conductive layer designs of a gesture sensor are shown. They use five electrodes printed on a textile substrate. Next, the results in terms of sensitivity of the two presented designs in function of different materials are discussed. Moreover, the real capacitance values obtained for each individual electrode are presented and compared with the theoretical ones. Finally, a real-world application is presented, a gesture-controlled mouse for a mobile phone.

Chapter 5 describes the work and results obtained with a boosted 3D gesture sensor. Three manufacturing techniques have been considered as alternatives: screen printing with conductive ink, embroidery with conductive thread and thermostealing with conductive fabric. The main critical parameters are analysed for each prototype, such as the capacitance or the sensitivity of the sensor. Moreover, a user validation is performed, testing several gestures with different subjects. Finally, in order to evaluate the stability and strength of the solutions, some tests have been performed to assess their washing tolerance.

The thesis concludes with Chapter 6, where the general conclusions are summarized. Moreover, the main limitations found during the work are analysed. At the end of the chapter, future research lines derived from this work are also presented.

To finalize this chapter, a graphic diagram is presented showing the different parts of the thesis and the connections between them.

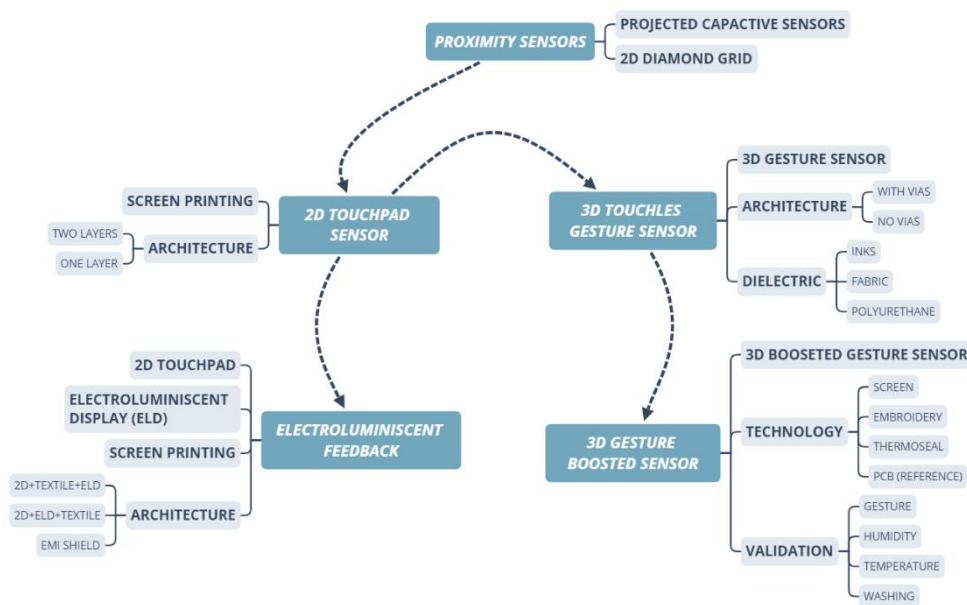


Figure 11. Thesis diagram

1.6. Scientific Publications

The following publications have been included in the compendium of this work:

- Ferri, J.; Lidón-Roger, J.V.; Moreno, J.; Martinez, G.; Garcia-Breijo, E. A wearable textile 2D touchpad sensor based on screen-printing technology. *Materials (Basel)*. **2017**, *10*(12), 1450. <https://doi.org/10.3390/ma10121450> (Impact factor: 2.467, Q2-Material Science, Multidisciplinary)
- Ferri, J.; Fuster, C.P.; Llinares Llopis, R.; Moreno, J.; Garcia-Breijo, E. Integration of a 2D touch sensor with an electroluminescent display by using a screen-printing technology on textile substrate. *Sensors* **2018**, *18*(10), 3313. <https://doi.org/10.3390/s18103313> (Impact factor: 3.031, Q1-Instruments & Instrumentation)

- Ferri, J.; Llinares Llopis, R.; Moreno, J.; Ibañez Civera, J.; Garcia-Breijo, E. A Wearable Textile 3D Gesture Recognition Sensor Based on Screen-Printing Technology. *Sensors* **2019**, *19*, 5068. <https://doi.org/10.3390/s19235068> (Impact factor: 3.275, Q1-Instruments & Instrumentation)
- Ferri, J.; Llinares Llopis, R.; Martinez, G.; Lidon, J.V.; Garcia-Breijo, E. Comparison of E-Textile Techniques and Materials for 3D Gesture Sensor with Boosted Electrode Design. *Sensors* **2020**, *20*(8), 2369. <https://doi.org/10.3390/s20082369> (Impact factor (2018): 3.031, Q1-Instruments & Instrumentation)

1.7. Academic Contributions

In this section the journal papers and conference strongly related but not included in the compendium are presented.

International Journals:

- Schwarz, A.; DeSmet, A.; Cardon, G.; Chastin, S.; Costa, R.; Grilo, A.; Ferri, J.; Domenech, J.; Stragier, J. Mobile exergaming in adolescents' everyday life—contextual design of where, when, with whom, and how: The Smartlife case. *Int. J. Environ. Res. Public Health* 2018, *15*, 1-15. <https://doi.org/10.3390/ijerph15050835> (Impact factor: 2.468, Q2-Public, Environmental & Occupational Health)
- Ferri, J.; Llinares Llopis, R.; Moreno, J.; Vicente Lidón-Roger, J.; Garcia-Breijo, E. An investigation into the fabrication parameters of screen-printed capacitive sensors on e-textiles. *Textile Research Journal*. J. 2020. <https://doi.org/10.1177/0040517519901016> (Impact factor (2018): 1.613, Q1-Material Science, Textiles)
- Ferri, J.; Moreno, J.; Rodes, A.; Garcia-Breijo, E. Learning how to print sensors onto stretchable substrates. *Technical Textiles International*. A. 2019, *28*, 31-33.

International Conferences:

- Ferri, J., Moreno, J., Martinez, G., Lidón-Roger, J. V., & Garcia-Breijo, E. (2017, September). Printed Textile Touchpad. In Proceedings of the Eighth International Conference on Sensor Device Technologies and Applications (SensorDevices2017), Rome, Italy (pp. 10-14).

- Costa, R., Oliveira, P., Grilo, A., Schwarz, A., Cardon, G., Desmet, A., Ferri, J., Domenech, J., Pomazanskyi, A. SmartLife smart clothing gamification to promote energy-related behaviours among adolescents. 2017 Int. Conf. Eng. Technol. Innov. Eng. Technol. Innov. Manag. Beyond 2020 New Challenges, New Approaches, ICE/ITMC 2017 - Proc. 2018, 2018-Janua, 1489–1495.
- Doménech, J., Ferri, J., Costa, R., Oliveira, P., Grilo, A., Cardon, G., DeSmet, A., Schwarz, A., Stragier, J., Pomazansky, A., Danilins, J. (2018, November). SmartLife–Exergames and Smart Textiles to Promote Energy-Related Behaviours among Adolescents. In Joint International Conference on Serious Games (pp. 288-293). Springer, Cham.
- Ferri, J., Moreno, J., Rodes, A., Mira, E., Garcia-Breijo, E., Llinares, R. (2018, October). Embedded Sensors on Stretchable Substrates Research Project. In 9th Workshop on Flexible & Printed Electronics Industry, Athens, Greece.
- Ferri, J., Domenech, J., Costa, R., Oliveira, P., Grilo, A., Pomazansky, A., Danilins, J., Schwarz, A., Chastin, S., Cardon, G., DeSmet, Ann. (2018, September). A Mobile Game with Smart Textiles Promoting Healthy Lifestyles among Adolescents. In NanoInnovation 2018, Rome, Italy.
- Ferri, J., Domenech, J., Costa, R., Oliveira, P., Grilo, A., Pomazansky, A., Danilins, J., Schwarz, A., Chastin, S., Cardon, G., DeSmet, Ann. (2018, November). Smart Textiles Promoting Healthy Lifestyles Among Adolescents. In Aachen-Dresden-Denkendorf International Textile Conference, Aachen, German.
- Ferri, J., Costa, R. (2018, December). Personal Digital Twin: AI meets physical exercise. In ICT 2018: Imagine Digital - Connect Europe, Vienna, Austria.

1.8. Rights

The figures and infographics included in this chapter were taken or made during the development of the described projects and are owned by AITEX.

References

- 1 Sarif Ullah Patwary, M.S. Smart Textiles and Nanotechnology: A General Overview. *J. Text. Sci. Eng.* **2015**, 05, 1–7.
- 2 Baurley, S. Interactive and experiential design in smart textile products and applications. *Pers. Ubiquitous Comput.* **2004**, 8, 274–281.
- 3 Wicaksono, I.; Paradiso, J.A. FabricKeyboard : Multimodal Textile Sensate Media as an Expressive and Deformable Musical Interface. *Nime* **2017**, 348–353.
- 4 Kongahage, D.; Foroughi, J. Actuator materials: Review on recent advances and future outlook for smart textiles. *Fibers* **2019**, 7.
- 5 Mostafalu, P.; Tamayol, A.; Rahimi, R.; Ochoa, M.; Khalilpour, A.; Kiaee, G.; Yazdi, I.K.; Bagherifard, S.; Dokmeci, M.R.; Ziaie, B.; et al. Smart Bandage for Monitoring and Treatment of Chronic Wounds. *Small* **2018**, 1703509.
- 6 Molinaro, N.; Massaroni, C.; Lo Presti, D.; Saccomandi, P.; Di Tomaso, G.; Zollo, L.; Perego, P.; Andreoni, G.; Schena, E. Wearable textile based on silver plated knitted sensor for respiratory rate monitoring. *Proc. Annu. Int. Conf. IEEE Eng. Med. Biol. Soc. EMBS 2018, 2018-July*, 2865–2868.
- 7 Mann, G.; Oatley, G. Positive design of smart interactive fabric artifacts for people with dementia. *2017 IEEE 5th Int. Conf. Serious Games Appl. Heal. SeGAH 2017, 2017*.
- 8 Costa, R.; Oliveira, P.; Grilo, A.; Schwarz, A.; Cardon, G.; Desmet, A.; Ferri, J.; Domenech, J.; Pomazanskyi, A. SmartLife smart clothing gamification to promote energy-related behaviours among adolescents. *2017 Int. Conf. Eng. Technol. Innov. Eng. Technol. Innov. Manag. Beyond 2020 New Challenges, New Approaches, ICE/ITMC 2017 - Proc. 2018, 2018-Janua*, 1489–1495.
- 9 Shi, H.; Zhao, H.; Liu, Y.; Gao, W.; Dou, S.C. Systematic Analysis of a Military Wearable Device Based on a Multi-Level Fusion Framework: Research Directions. *Sensors (Basel)*. **2019**, 19.
- 10 Nayak, R.; Wang, L.; Padhye, R. *Chapter 11 - Electronic textiles for military personnel*; Elsevier Ltd., 2015; ISBN 9780081002018.
- 11 Bulgun, E.Y. Smart Textiles for Soldier of the Future. *Defence Science Journal*, **2005**, 55(2), 195.

- 12 Ferraro, V. Smart Textiles and Wearable Technologies for Sportswear: A Design approach. 2015, S3005.
- 13 Drean, E.; Schacher, L.; Adolphe, D.; Bauer, F. Smart textiles for automotive: Application to airbag development. *Exp. Tech.* **2008**, *32*, 44–48.
- 14 Gehrke, I.; Tenner, V.; Lutz, V.; Schmelzeisen, D.; Gries, T. Sensor and Production Technologies for Industrial Smart Textiles Smart Textiles Production; ISBN 9783038974970.
- 15 Bosowski, P.; Hoerr, M.; Mecnika, V.; Gries, T.; Jockenhövel, S. *Design and manufacture of textile-based sensors*; 2015; ISBN 9780081002230.
- 16 Vornholt, K.; Alshrafi, W.; Reiffenrath, M. Design and Evaluation of a Textile-Integrated GPS Receiver. **2015**, 1–7.
- 17 Klemm, M.; Troester, G. Textile UWB Antennas for Wireless Body Area Networks. *IEEE Trans. Antennas Propag.* **2006**, *54*, 3192–3197.
- 18 Dar, S.H.; Ahmed, J. Wearable textile antenna design in body centric wireless communications: a systematic literature review. **2017**, *28*, 3716–3720.
- 19 Virkki, J.; Wei, Z.; Liu, A.; Ukkonen, L.; Björninen, T. Wearable passive E-textile UHF RFID tag based on a slotted patch antenna with sewn ground and microchip interconnections. *Int. J. Antennas Propag.* **2017**, *2017*, 27–29.
- 20 Soroudi, A.; Hernández, N.; Wipenmyr, J.; Nierstrasz, V. Surface modification of textile electrodes to improve electrocardiography signals in wearable smart garment. *J. Mater. Sci. Mater. Electron.* **2019**, *30*, 16666–16675.
- 21 Shu, L.; Xu, T.; Xu, X. Multilayer Sweat-Absorbable Textile Electrode for EEG Measurement in Forehead Site. *IEEE Sens. J.* **2019**, *19*, 5995–6005.
- 22 Merritt, C.R.; Nagle, H.T.; Grant, E. Textile-based capacitive sensors for respiration monitoring. *IEEE Sens. J.* **2009**, *9*, 71–78.
- 23 Mattmann, C.; Amft, O.; Harms, H.; Tröster, G.; Clemens, F. Recognizing upper body postures using textile strain sensors. In Proceedings of the Proceedings - International Symposium on Wearable Computers, ISWC; 2007; pp. 29–36.
- 24 Mecnika, V.; Hoerr, M.; Krievins, I.; Jockenhoevel, S.; Gries, T. Technical Embroidery for Smart Textiles: Review. *Mater. Sci. Text. Cloth. Technol.* **2015**, *9*, 56.

- 25 Stoppa, M.; Chiolerio, A. Wearable electronics and smart textiles: A critical review. *Sensors (Switzerland)* **2014**, *14*, 11957–11992.
- 26 Fischer, M.; Renzler, M.; Ussmueller, T. Development of a Smart Bed Insert for Detection of Incontinence and Occupation in Elder Care. *IEEE Access* **2019**, *7*, 118498–118508.
- 27 Chuang, M.C.; Windmiller, J.R.; Santhosh, P.; Ramírez, G.V.; Galik, M.; Chou, T.Y.; Wang, J. Textile-based Electrochemical Sensing: Effect of Fabric Substrate and Detection of Nitroaromatic Explosives. *Electroanalysis* **2010**, *22*, 2511–2518.
- 28 Colyer, S.L.; McGuigan, P.M. Textile electrodes embedded in clothing: A practical alternative to traditional surface electromyography when assessing muscle excitation during functional movements. *J. Sport. Sci. Med.* **2018**, *17*, 101–109.
- 29 Yang, G.; Deng, J.; Pang, G.; Zhang, H.; Li, J.; Deng, B.; Pang, Z.; Xu, J.; Jiang, M.; Liljeberg, P.; et al. An IoT-Enabled Stroke Rehabilitation System Based on Smart Wearable Armband and Machine Learning. *IEEE J. Transl. Eng. Heal. Med.* **2018**, *6*, 1–10.
- 30 Plan, W.; Cardoso, D.P. Automotive Gestures Recognition Based on Capacitive Sensing for Safer HMI. **2016**.
- 31 Conway, F. Finding Common Ground: A Survey of Capacitive Sensing in Human-Computer Interaction. *J. Women Aging* **2018**, *30*, 365.
- 32 Herbert, R.; Kim, J.H.; Kim, Y.S.; Lee, H.M.; Yeo, W.H. Soft material-enabled, flexible hybrid electronics for medicine, healthcare, and human-machine interfaces. *Materials (Basel)*. **2018**, *11*.
- 33 Santos, L.; Carbonaro, N.; Tognetti, A.; González, J.; de la Fuente, E.; Fraile, J.; Pérez-Turiel, J. Dynamic Gesture Recognition Using a Smart Glove in Hand-Assisted Laparoscopic Surgery. *Technologies* **2018**, *6*, 8.
- 34 Lai, H.Y.; Ke, H.Y.; Hsu, Y.C. Real-time hand gesture recognition system and application. *Sensors Mater.* **2018**, *30*, 869–884.
- 35 Karim, R.A.; Zakaria, N.F.; Zulkifley, M.A.; Mustafa, M.M.; Sagap, I.; Md Latar, N.H. Telepointer technology in telemedicine: A review. *Biomed. Eng. Online* **2013**, *12*, 1.

- 36 Ponnamma, D.; Kumar, K.; Chaoying, S.; Sabu, W.; Mariam, T.; Alma 'adeed Editors, A.-A. Springer Series on Polymer and Composite Materials Flexible and Stretchable Electronic Composites.
- 37 Manjakkal, L.; Dang, W.; Yogeswaran, N.; Dahiya, R. Textile-Based Potentiometric Electrochemical pH Sensor for Wearable Applications. **2019**, 1–12.
- 38 Stempien, Z.; Kozicki, M.; Korzeniewska, E.; Owczarek, G.; Poscik, A. Ammonia gas sensors ink-jet printed on textile substrates. *2016 IEEE SENSORS* 1–3.
- 39 Hu, B.; Li, D.; Ala, O.; Manandhar, P.; Fan, Q.; Kasilingam, D.; Calvert, P.D. Textile-based flexible electroluminescent devices. *Adv. Funct. Mater.* **2011**, *21*, 305–311.
- 40 De Vos, M.; Torah, R.; Glanc-Gostkiewicz, M.; Tudor, J. A Complex Multilayer Screen-Printed Electroluminescent Watch Display on Fabric. *J. Disp. Technol.* **2016**, *12*, 1757–1763.
- 41 Janczak, D.; Zych, M.; Raczyński, T.; Dybowska-Sarapuk, Ł.; Peplowski, A.; Krzemiński, J.; Sosna-Głębska, A.; Znajdek, K.; Sibiński, M.; Jakubowska, M. Stretchable and Washable Electroluminescent Display Screen-Printed on Textile. *Nanomaterials* **2019**, *9*, 1276.
- 42 Mbise, E.; Dias, T.; Hurley, W. Design and manufacture of heated textiles. *Electron. Text. Smart Fabr. Wearable Technol.* **2015**, 117–132.
- 43 Sadi, M.S.; Yang, M.; Luo, L.; Cheng, D.; Cai, G.; Wang, X. Direct screen printing of single-faced conductive cotton fabrics for strain sensing, electrical heating and color changing. *Cellulose* **2019**, *26*, 6179–6188.
- 44 Jahid, M.A.; Hu, J.; Wong, K.H.; Wu, Y.; Zhu, Y.; Luo, H.H.S.; Zhongmin, D. Fabric Coated with shape memory polyurethane and its properties. *Polymers (Basel)*. **2018**, *10*, 1–13.
- 45 Yokus, M.A.; Foote, R.; Jur, J.S. Printed Stretchable Interconnects for Smart Garments: Design, Fabrication, and Characterization. *IEEE Sens. J.* **2016**, *16*, 7967–7976.
- 46 Agcayazi, T.; Chatterjee, K.; Bozkurt, A.; Ghosh, T.K. Flexible Interconnects for Electronic Textiles. *Adv. Mater. Technol.* **2018**, *3*, 1–32.

- 47 Mecnika, V.; Scheulen, K.; Anderson, C.F.; Hörr, M.; Breckenfelder, C. Joining technologies for electronic textiles. *Electron. Text. Smart Fabr. Wearable Technol.* **2015**, 133–153.
- 48 Jahanshahi, A.; Gonzalez, M.; Brand, J. Van Den; Bossuyt, F.; Vervust, T.; Verplancke, R.; Vanfleteren, J.; Baets, J. De. Stretchable Circuits with Horseshoe Shaped Conductors Embedded in Elastic Polymers. *Japanese Journal of Applied Physics.* **2013**. 52(5S1), 05DA18.
- 49 Nagels, S.; Deferme, W. Fabrication Approaches to Interconnect Based Devices for Stretchable Electronics: A Review. *Materials (Basel).* **2018**, *11*.
- 50 Axisa, F.; Bossuyt, F.; Missine, J.; Verplancke, R.; Vervust, T.; Vanfleteren, J. Stretchable engineering technologies for the development of advanced stretchable polymeric systems. *PORTABLE-POLYTRONIC 2008 - 2nd IEEE Int. Interdiscip. Conf. Portable Inf. Devices 2008 7th IEEE Conf. Polym. Adhes. Microelectron. Photonics* **2008**, 1–8.
- 51 Fan, J.A.; Yeo, W.-H.; Su, Y.; Hattori, Y.; Lee, W.; Jung, S.-Y.; Zhang, Y.; Liu, Z.; Cheng, H.; Falgout, L.; et al. Fractal design concepts for stretchable electronics. *Nat. Commun.* **2014**, *5*, 1–8.
- 52 Jin, H.; Matsuhisa, N.; Lee, S.; Abbas, M.; Yokota, T.; Someya, T. Enhancing the Performance of Stretchable Conductors for E-Textiles by Controlled Ink Permeation. *Adv. Mater.* 2017, 29.
- 53 Ejupi, A.; Menon, C. Detection of talking in respiratory signals: A feasibility study using machine learning and wearable textile-based sensors. *Sensors (Switzerland)* **2018**, *18*.
- 54 Capineri, L. Resistive sensors with smart textiles for wearable technology: from fabrication processes to integration with electronics. *Procedia Eng.* **2014**, *87*, 724–727.
- 55 Merritt, C.R.; Nagle, H.T.; Grant, E.; Member, S. Textile-Based Capacitive Sensors for Respiration Monitoring. **2009**, *9*, 71–78.
- 56 Zhang, Q.; Wang, Y.L.; Xia, Y.; Zhang, P.F.; Kirk, T. V.; Chen, X.D. Textile-Only Capacitive Sensors for Facile Fabric Integration without Compromise of Wearability. *Adv. Mater. Technol.* **2019**, 1900485, 1900485.

-
- 57 Shyr, T.-W.; Shie, J.-W.; Jiang, C.-H.; Li, J.-J. A Textile-Based Wearable Sensing Device Designed for Monitoring the Flexion Angle of Elbow and Knee Movements. *Sensors* **2014**, *14*, 4050–4059.
- 58 Mattmann, C.; Clemens, F.; Tröster, G. Sensor for measuring strain in textile. *Sensors* **2008**, *8*, 3719–3732.
- 59 Enokibori, Y.; Suzuki, A.; Mizuno, H.; Shimakami, Y.; Mase, K. E-textile pressure sensor based on conductive fiber and its structure. *Proc. 2013 ACM Conf. Pervasive ubiquitous Comput. Adjunct. Publ. - UbiComp '13 Adjunct.* **2013**, 207–210.
- 60 Sergio, M.; Manaresi, N.; Tartagni, M.; Guerrieri, R.; Canegallo, R. 5.4: A Textile Based Capacitive Pressure Sensor. *Sensors*, **2002**. *Proc. IEEE 2002*, 1625–1630 vol. 2.
- 61 Cheng, J.; Sundholm, M.; Zhou, B.; Hirsch, M.; Lukowicz, P. Smart-surface: Large scale textile pressure sensors arrays for activity recognition. *Pervasive Mob. Comput.* **2016**, *30*, 97–112.
- 62 Paradiso, R.; De Rossi, D. Advances in textile technologies for unobtrusive monitoring of vital parameters and movements. *Annu. Int. Conf. IEEE Eng. Med. Biol. - Proc.* **2006**, 392–395.
- 63 Farrington, J.; Moore, A.J.; Tilbury, N.; Church, J.; Biemond, P.D. Wearable sensor badge & sensor jacket for context awareness. *Int. Symp. Wearable Comput. Dig. Pap.* **1999**, 107–113.
- 64 Guo, L.; Ratnarathorn, S.; Berglin, L.; Wiklund, U.; Sandsjö, L. ‘Disappearing Sensor’ -Textile Based Sensor for Monitoring Breathing. *Int. Conf. Control Autom. Syst. Eng.* **2011**, 1.
- 65 Gonçalves, C.; Ferreira da Silva, A.; Gomes, J.; Simoes, R. Wearable E-Textile Technologies: A Review on Sensors, Actuators and Control Elements. *Inventions* **2018**, *3*, 14.
- 66 Li, B.; Xiao, G.; Liu, F.; Qiao, Y.; Li, C.M.; Lu, Z. A flexible humidity sensor based on silk fabrics for human respiration monitoring. *Journal of Materials Chemistry C*. **2018**, *6*(16), 4549–4554.
- 67 Ju Yun, Y.; Hong, W.G.; Choi, N.-J.; Hoon Kim, B.; Jun, Y.; Lee, H.-K. Ultrasensitive and Highly Selective Graphene-Based Single Yarn for Use in Wearable Gas Sensor. *Sci. Rep.* **2015**, *5*, 10904.

- 68 Kincal, D.; Kumar, A.; Child, A.D.; Reynolds, J.R. Conductivity switching in polypyrrole-coated textile fabrics as gas sensors. *Synth. Met.* **1998**, *92*, 53–56.
- 69 Yun, Y.J.; Hong, W.G.; Kim, D.Y.; Kim, H.J.; Jun, Y.; Lee, H.K. E-textile gas sensors composed of molybdenum disulfide and reduced graphene oxide for high response and reliability. *Sensors Actuators, B Chem.* **2017**, *248*, 829–835.
- 70 Polanský, R.; Soukup, R.; Řeboun, J.; Kalčík, J.; Moravcová, D.; Kupka, L.; Švantner, M.; Honnerová, P.; Hamáček, A. A novel large-area embroidered temperature sensor based on an innovative hybrid resistive thread. *Sensors Actuators, A Phys.* **2017**, *265*, 111–119.
- 71 Husain, M.D.; Kennon, R. Preliminary investigations into the development of textile-based temperature sensor for healthcare applications. *Fibers 2013*, **2013**, *1*, 2–10.
- 72 Pola, T.; Vanhala, J. Textile electrodes in ECG measurement. *Proc. 2007 Int. Conf. Intell. Sensors, Sens. Networks Inf. Process. ISSNIP 2007*, 635–639.
- 73 Tao, X.; Koncar, V.; Huang, T.H.; Shen, C.L.; Ko, Y.C.; Jou, G.T. How to make reliable, washable, and wearable textronic devices. *Sensors (Switzerland)* **2017**, *17*.
- 74 Paul, G.; Torah, R.; Beeby, S.; Tudor, J. Novel active electrodes for ECG monitoring on woven textiles fabricated by screen and stencil printing. *Sensors Actuators, A Phys.* **2015**, *221*, 60–66.
- 75 Kim, S.; Leonhardt, S.; Zimmermann, N.; Kranen, P.; Kensche, D.; Müller, E.; Quix, C. Influence of contact pressure and moisture on the signal quality of a newly developed textile ECG sensor shirt. **2008**, 256–259.
- 76 Kaya, M.; Alkhidir, T.; Abdul, Y.; Liao, K. Sensors and Actuators B : Chemical Graphene-clad textile electrodes for electrocardiogram monitoring. *Sensors Actuators B. Chem.* **2015**, *221*, 1469–1474.
- 77 Ng, C.L.; Reaz, M.B.I. Evolution of a capacitive electromyography contactless biosensor: Design and modelling techniques. *Meas. J. Int. Meas. Confed.* **2019**, *145*, 460–471.
- 78 Paul, G.M.; Cao, F.; Torah, R.; Yang, K.; Beeby, S.; Tudor, J. A smart textile based facial emg and eog computer interface. *IEEE Sens. J.* **2014**, *14*, 393–400.
- 79 Seoane, F.; Thordstein, M.; Academy, S. Textile Electrodes for EEG Recording — A Pilot Study. *Sensors*, *12*(12), **2012**, 16907–16919.

-
- 80 Muthu Kumar, N.; Thilagavathi, G. Design and development of textile electrodes for EEG measurement using copper plated polyester fabrics. *J. Text. Apparel, Technol. Manag.* **2014**, *8*.
- 81 Gräbner, D.; Tintelott, M.; Dumstorff, G.; Lang, W. Low-Cost Thin and Flexible Screen-Printed Pressure Sensor. *Proceedings* **2017**, *1*, 616.
- 82 Khan, S.; Lorenzelli, L.; Dahiya, R.S. Technologies for printing sensors and electronics over large flexible substrates: A review. *IEEE Sens. J.* **2015**, *15*, 3164–3185.
- 83 Chang, J.; Zhang, X.; Ge, T.; Zhou, J. Fully printed electronics on flexible substrates: High gain amplifiers and DAC. *Organic Electronics*, *15*(3), **2014**, 701-710.
- 84 Li, Z.; Zhang, R.; Moon, K. S.; Liu, Y.; Hansen, K.; Le, T. Highly Conductive, Flexible, Polyurethane - Based Adhesives for Flexible and Printed Electronics. *Adv. Funct. Mater.* **2013**, *23*(11), 1459-1465.
- 85 Subramanian, V.; Chang, J.B.; De La Fuente Vornbrock, A.; Huang, D.C.; Jagannathan, L.; Liao, F.; Mattis, B.; Molesa, S.; Redinger, D.R.; Soltman, D.; et al. Printed electronics for low-cost electronic systems: Technology status and application development. *ESSCIRC 2008 - Proc. 34th Eur. Solid-State Circuits Conf.* **2008**, 17–24.
- 86 Salam, B.; Shan, X.C.; Zhanhong, C.; Lok, B.K. Multilayer Roll-to-Roll Screen-Printing for Printed Electronics Applications. *2018 IEEE 20th Electron. Packag. Technol. Conf.* **2019**, 359–362.
- 87 Lin, X.; Seet, B.C. Battery-Free Smart Sock for Abnormal Relative Plantar Pressure Monitoring. *IEEE Trans. Biomed. Circuits Syst.* **2017**, *11*, 464–473.
- 88 Komazaki, Y.; Uemura, S. Stretchable, printable, and tunable PDMS-CaCl₂ micro-composite for capacitive humidity sensors on textiles. *Sensors Actuators, B Chem.* **2019**, *297*, 126711.
- 89 Nelson, A.; Singh, G.; Robucci, R.; Patel, C.; Banerjee, N. Adaptive and Personalized Gesture Recognition Using Textile Capacitive Sensor Arrays. *IEEE Trans. Multi-Scale Comput. Syst.* **2015**, *1*, 62–75.
- 90 Atalay, O. Textile-based, interdigital, capacitive, soft-strain sensor for wearable applications. *Materials (Basel)*. **2018**, *11*.
- 91 Walker, G. A review of technologies for sensing contact location on the surface of a display. *J. Soc. Inf. Disp.* **2012**, *20*, 413–440.

- 92 Bhalla, M.R.; Bhalla, A.V. Comparative Study of Various Touchscreen Technologies. *Int. J. Comput. Appl.* **2010**, *6*, 2–8.
- 93 Gray, T.; Gray, T. *Projected Capacitive Touch Basics*; **2019**; ISBN 9783319983912.
- 94 Du, L.; Ieee, M. An Overview of Mobile Capacitive Touch Technologies Trends.
- 95 Gu, J.F.; Gorgutsa, S.; Skorobogatiy, M. Soft capacitor fibers using conductive polymers for electronic textiles. **2014**.
- 96 Sharma K (2019) Smart textile market by function (energy harvesting, sensing, thermoelectricity, luminescent, and others) and end user (healthcare, military and defense, entertainment, automotive, sport and fitness) global opportunity analysis and industry forecast, 2014 2022. Allied market research, series: emerging and next generation technology.

Chapter 2

2D Touchpad Sensor Printed on Textile Substrate



Impact factor: 2.467

Q2-Material Science, Multidisciplinary

2.1. Introduction

The flexibility and portability that wearables devices can bring have increased their development and their use. The interface devices, among all wearable devices, can be considered as indispensable tools for the user to interact with other devices both external and wearable [1]. Different strategies have been devised to integrate electronics as wearables such as smartwatches [2], rings [3], bracelets [4] as well as garments [5] identified as smart textiles or smart garments [6]. Each one of them has its advantages and limitations, being perhaps a complex garment, but, on the contrary, it is supposed to be more comfortable due to its comfort, flexibility, fashion, ergonomics and possibilities of integration in a transparent way [7,8].

An important factor to take into account in the use of wearable devices is the communication between the person and the electronic control system. This is carried out through the interfaces, such as keyboards, buttons and touchpads. The typical characteristics of these interfaces are the necessity of a stretchable or flexible setup to follow the action of human body [9] and a significant sensor area to detect the fingers [10].

Regarding touchpads, different technologies have been developed during the last years as solutions for “touch panel” and “touchscreen” [11]. From all of them, analog resistive and capacitive touch technologies dominate the touch landscape today [12]. Others have used optical sensing [13], force sensing [14], or even inductive sensing [15]. In combination uses, flexible and stretch sensing approaches have also been popular using contact resistances between threads [16,17], with piezoelectric [18] and capacitive designs [19,20].

Several designs and techniques have been used for touchpad application in textiles; in general, they can be classified into two main techniques: weaving the pattern by using fibers [21] or drawing the pattern on the fabric by using a printing techniques [22].

With regard to fibers, and depending on the sensor technology, different approaches of structures multilayer are developed. In the last years, Gu [20] reported a capacitor fiber highly flexible with a dielectric multilayer structure and conductive polymer composite films, manufactured by drawing techniques. Gorgutsa [23] built a fully woven 2D touchpad sensor and a 1D slide sensor manufactured with soft conductive-polymer-based capacitor. A flexible textile keyboard, using carbon nanotube (CNT) filled polypropylene (PP) composite fibers, is introduced [24] using conductive buttons made with threads combined with a metallic thread layer using a spacer material between both layers. The use of a textile polymer based conducting yarn and its characteristics are discussed in [21], giving details of the development of a touch control woven fabric keypad. A 7-bit dynamic range of pressure sensing at each taxel of piezoresistive multi-touch arrays is achieved in [25] for musical applications using multitouch arrays sensing sandwiched structures with non-conductive pieces of fabric combined with parallel lines of conductive thread sewn into them. Hamdan [26] presented Grabrics, a two-

dimensional textile sensor that is manipulated by grabbing a fold and moving it between fingers by using sewing techniques.

Regarding transferring a pattern on the textile, Takamatsu [1] presented a PEDOT:PSS based stretchable keyboard which is based on capacitance sensors; the electrodes are patterned on a knitted textile by using spin-coat technique. Dong-Ki Kim [27] reported a touchpad based on a contact-resistance-type force sensor manufactured by using screen-printing techniques.

In this article we will demonstrate a novel touchpad design fabricated over textile layer using the screen printing technique [28]. The well-known screen-printing technique is widely used in the graphic arts industry, ceramics, etcetera, and, in recent years, it has been introduced into the Printed Electronics industry. Its direct application in manufacturing allows reducing costs, while increasing profitability and reproducibility. Directly printing the touchpad on textile with this industrial technique would allow its easy production in series and its application in various areas.

2.2. Design and Working Principle

The working principle used is based on projected capacitive (pro-cap) technologies [29], which are commonly used for display systems but can also be used in other applications, as presented in this work. Pro-cap technologies detect touch by measuring the capacitance at each addressable electrode; in other words, when a finger approaches an electrode, the electromagnetic field is disturbed and alters the capacitance. The X, Y location, where the touch has occurred, can be located by measuring the variation of the capacitance with an electronic equipment.

There are two main types of pro-cap sensing methods, namely self-capacitance and mutual capacitance, each having its own advantages and disadvantages.

There are several pro-cap controllers which offer both self-capacitance and mutual-capacitance types. MTCH6102 from Microchip has been used in this work. This device is a turnkey projected capacitive touch controller that simplifies adding gestures to touch interface designs with industry-leading low-power performance. It utilizes up to 15 channels to support taps, swipes, and scrolling on XY touch pads and touch screens [30].

MTCH6102 has an embedded Capacitive Voltage Divider (CVD) acquisition engine which requires only an Analog-to-Digital Converter (ADC) to perform capacitive touch sensing. Capacitive Voltage Divider is a charge/voltage-based technique to measure relative capacitance on a pin using only the ADC module. The advantages of this technique are low power supply dependence, low-frequency noise rejection, low temperature dependence and minimal hardware requirements.

2.2.1. Sensor Pattern

Sensor pattern is a very important aspect of capacitive sensor design because the capacitance of touch is dependent on the sensor pattern design. Features, such as X-Y layer-to-layer spacing, electrode geometry and pitch, on front panel thickness and shielding must be considered when looking for the best design pattern. Attributes such as accuracy, resolution and linearity of touch position are greatly dependent on the sensor pattern as well.

The sensor pattern of touchpad commonly consists of a set of electrodes in a row and columns to form a matrix. Based on this structure, several touchpad sensor pattern designs can be found, which are usually referred to by names that are indicative of the shape or construction of the pattern, such as telephone poles, snowflakes, triangles, diamonds, and streets and alleys.

Among the well-known pattern designs, the diamond pattern [31-33] is one of the most commonly used. It consists of diamonds interconnected with a narrow neck sections (Figure 12a).

The structure consists of two layers, each having a host of conductive electrodes organized parallel to each other. An individual sensors node is formed by the region between the edges of the X and Y electrodes (Figure 12a).

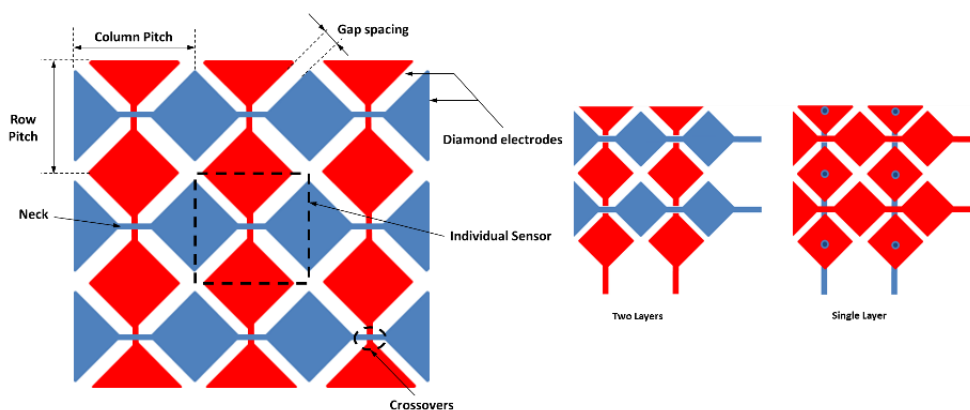


Figure 12. (a) Diamond pattern; and (b) 2D array sensors in the case of single layer or two layers.

The diamond shape elements are used to maximize the exposure of sensor electrodes to a touch. There are two main parameters related to diamond pattern, namely pitch and gap. The pitch is the distance between the electrodes (Figure 12a) and its dimension determines the range of finger sizes that can reliably be detected. Typical dimensions [32] of the pitch are a minimum of 4 mm and a maximum of 10 mm. The gap between the X and Y electrodes (Figure 12a) defines how far a signal is projected and the level of noise in the measured signal as well. A sensor with a larger gap can detect a user

further away, but it will have more noise than a sensor with a smaller gap. A minimum of 0.1 mm and maximum of 0.5 mm have been reported [32].

The Y electrodes are arranged among rows on the top layer and the X electrodes are arranged along columns on the top layer or bottom layer (Figure 12b), forming a two-dimensional array of sensors. The layers isolated from each other.

A ground ring around the touchpad can be placed to reduce the electromagnetic interference (EMI) to the active sensor area.

The low power projected capacitive touch pad development kit (Microchip DM160219) based on MTCH6102 Microchip device is an example of diamond pattern capacitive sensor but manufactured with Printed Circuit Board (PCB) technology. In this case, a matrix of nine X-electrodes and six Y-electrodes is used. Pitch (Row and Column) of 6.2 mm and Gap of 0.3 mm are the dimensions of this design. The capacitance measure between electrodes is 20 pF (1 kHz) (Agilent U1731A LCR Meter).

2.2.2. Textile Touchpad Design

2.2.2.1 Screen-Printed Technology

Manufacturing technology used to implement this type of sensor was based on serigraphic technology of thick film. The screen-printing process consists of forcing pastes of different characteristics over a substrate through some screens using squeegees. Openings in the screen define the pattern that will be printed on the substrate by serigraphy. The final thickness of the pastes can be adjusted by varying the thickness of the screens.

2.2.2.2 Two Layers Design [TLD]

A sensor matrix formed by 9×6 electrodes has been designed. The sensor has been developed with two conductive layers for horizontal and vertical tracks and another layer of dielectric. The three patterns are shown in the Figure 13: Vertical or X layer (a); dielectric layer (b); Horizontal or Y layer (c); and the complete design (d).

The Pitch (Row and Column) of 8 mm and Gap of 0.4 mm are the main dimensions of pattern.

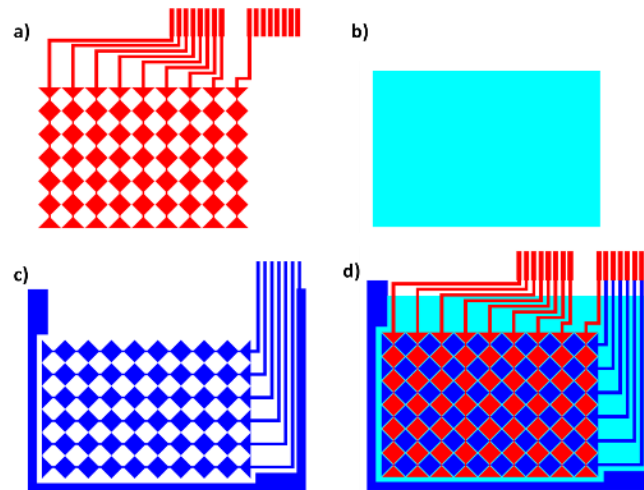


Figure 13. Two Layers Design (TLD): (a) Vertical or X layer; (b) dielectric layer; (c) Horizontal or Y layer; and (d) the complete design.

2.2.2.3 One Layers Design [OLD]

A sensor matrix also formed by 9×6 electrodes has been designed with only one layer of horizontal-vertical (X-Y) conductive tracks. Despite being a one-layer design, two extra layers are needed because the horizontal or vertical tracks have to be connected to avoid short circuits between them. Therefore, an extra conductive layer is added to make the connection and another extra dielectric layer is added to provide via-holes. The three patterns are shown in Figure 14: conductive layer for connection tracks (a); dielectric layer with via-holes (b); X-Y layer (c); and the complete design (d).

The Pitch (Row and Column) of 8.3 mm, Gap of 0.5 mm and through-hole diameter of 1.6 mm are the main dimensions of pattern.

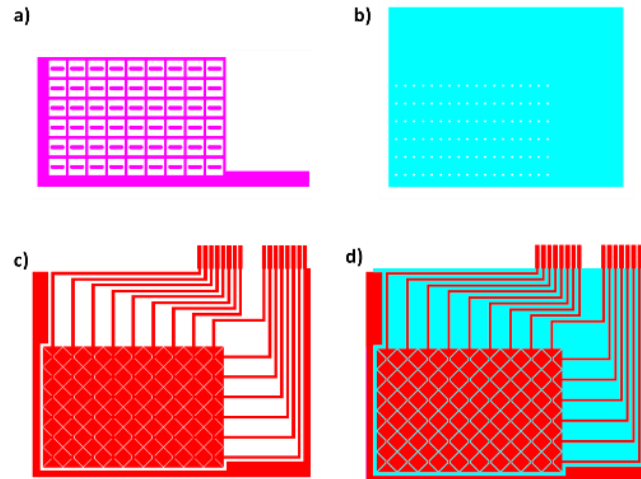


Figure 14. One Layer Design (OLD): (a) conductive layer for connection tracks; (b) dielectric layer with via-holes; (c) X-Y layer; and (d) the complete design.

2.2.3. Design of Electronic System

The MTCH6102 low-power projected capacitive touch controller from Microchip was used to design the electronic system. As master controller, a PIC16LF1454 was used. Finally, to make the system portable, a Bluetooth module was used.

2.3. Materials and Methods

2.3.1. Sensor Development

When screen-printing technology is used, it is necessary to manufacture frames with screen mesh for each layer of the design. Therefore, to build the sensor matrices, three screens were made in both designs.

The screen for the conductors was a 230 mesh polyester material (PET 1500 90/230-48 from Sefar) and the screen for dielectric layer was a 175 mesh polyester material (PET 1500 68/175-64 PW from Sefar). Afterwards, to transfer the stencil to screen mesh, a UV film Dirasol 132 (Fujifilm) was used. The final screen thickness was 10 μm for the screen for conductors and 15 μm for the screen for the dielectric. The patterns were transferred to the screen by using a UV light source unit.

The materials used were, the textile Mediatex TT ACQ 120 μm (Technohard) for the substrate, C2131014D3 Silver paste-58, 85% (Gwent Group) as conductive paste and D2081009D6 Polymer dielectric (Gwent Group) as dielectric paste. Flexibility is one of the most important characteristics of these inks to use them with textiles.

Printing was carried out by using Ekra E2 XL screen- printer with a 75° shore squeegee hardness, 3.5 bar force, and 8 mm/s. After inks depositing, these were cured in an air oven at 130 °C for 10 min.

A high failure rate was found due to short-circuits between conductive layers. These short-circuits are due to pinholes in dielectric layer (Figure 15), which occur during the curing process.

To avoid this trouble, two solutions were found. The first solution was to increase the number of dielectric layers; however, this solution implies an increase in cost and processing time. Therefore, the ideal solution would be to minimize the number of dielectric layers by using a different mesh screen size. For this reason, a study about the influence of dielectric layer mesh screen size was made. The mesh screen sizes selected were 123 inches (PET 1500 48/123-70 PW from Sefar), 137 inches (PET 1500 54/137-70 PW from Sefar), 175 inches (PET 1500 68/175-64 PW from Sefar), 230 inches (PET 1500 90/230-48 PW from Sefar) and 330 inches (PET 1500 130/330-34 PW from Sefar).

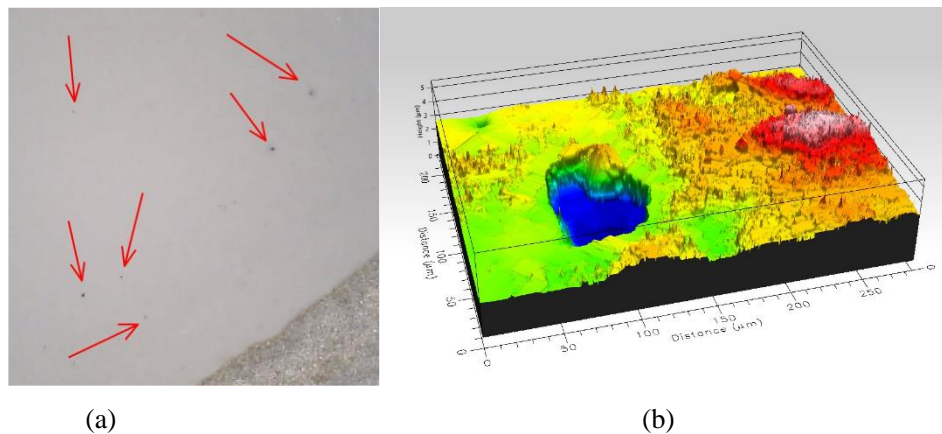


Figure 15. Pinholes in the dielectric layer; and (b) detail of pinhole.

A single design pattern was designed (Figure 16) to study the influence of the mesh screen size for both cases, TLD and OLD. In both cases, three different single electrode sizes, which are designed called A, B and C; the conductive plates are square, and their areas are 18, 24.5 and 32 mm², respectively. Type C corresponds to the size of the electrodes used in the general design. The number of dielectric layers varied between one and three layers; to obtain the different layers, first one layer was printed and it was cured thermally; then the second one was printed and thermally cured; and, finally, the third one with the same process.

Tables 1 and 2 show the percentage of failures found. Table 3 shows the dielectric layer total thickness obtained for each mesh value and number of layers. For total layer

thicknesses less than 10 μm , insulation faults are detected, as shown in Tables 1 and 2. As a result, with a minimum of two layers, and using a mesh between 123 and 230, no errors are obtained in the manufacture of the devices. It is important to note that, as can be seen in Table 3, a similar layer thickness with two or three layers of dielectric can be obtained. For example, the thickness obtained with two layers and mesh 137 is similar to the thickness obtained with three layers and 175 mesh. However, in the case of three layers, the surface obtained is more uniform than in the case of two layers, so a design with three layers would be more reliable than one with two layers. This may be because the ink is distributed through the different hollows left in the lower layers.

Table 1. Failures rate (%) for TLD when 1–3 layers of dielectric ink are used.

Mesh (Inch)	1 Layer			2 Layers			3 Layers		
	Type			Type			Type		
	A	B	C	A	B	C	A	B	C
330	100	100	50	0	100	0	0	100	0
230	50	0	50	0	0	0	0	0	0
175	0	0	0	0	0	0	0	0	0
137	0	0	0	0	0	0	0	0	0
123	0	0	0	0	0	0	0	0	0

Table 2. Failures rate (%) for OLD when 1–3 layers of dielectric ink are used.

Mesh (Inch)	1 Layer			2 Layers			3 Layers		
	Type			Type			Type		
	A	B	C	A	B	C	A	B	C
330	100	100	100	100	100	50	0	50	100
230	50	100	100	0	0	0	0	0	0
175	50	100	100	0	0	0	0	0	0
137	100	100	50	0	0	0	0	0	0
123	50	50	50	0	0	0	0	0	0

Table 3. Final layer thickness depending on mesh value and number of layers.

Mesh (Inch)	1 Layer	2 Layers	3 Layers
330	$2.8 \pm 0.6 \mu\text{m}$	$7.8 \pm 0.3 \mu\text{m}$	$12.7 \pm 1.1 \mu\text{m}$
230	$4.8 \pm 2.1 \mu\text{m}$	$11.8 \pm 0.8 \mu\text{m}$	$18.1 \pm 1.2 \mu\text{m}$
175	$7.5 \pm 2.4 \mu\text{m}$	$15.4 \pm 1.2 \mu\text{m}$	$22.9 \pm 1.5 \mu\text{m}$
137	$9.1 \pm 1.1 \mu\text{m}$	$20.3 \pm 1.4 \mu\text{m}$	$30.3 \pm 0.9 \mu\text{m}$
123	$10.3 \pm 0.2 \mu\text{m}$	$21.6 \pm 2.1 \mu\text{m}$	$34.7 \pm 2.3 \mu\text{m}$

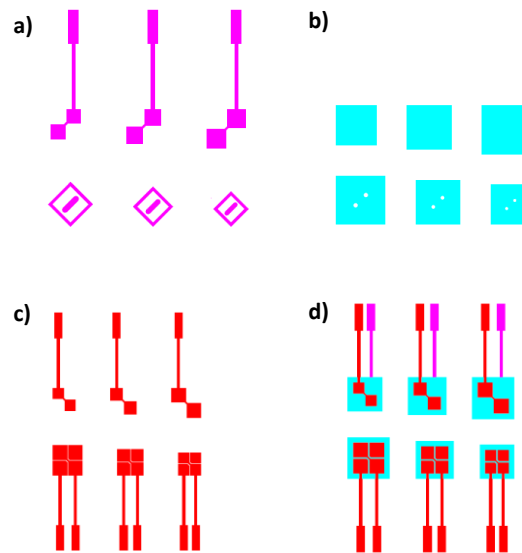


Figure 16. (a) First conductive layer, above for TLD and below for OLD; (b) dielectric layer; (c) second conductive layer; and (d) complete Design.

To look for dielectrics with different viscosities, a second solution was used. However, this change of viscosity adds a problem: the dielectric constant of the ink can change the value of the capacitance; therefore, it was necessary to study the influence of the dielectric on the value of the electrode capacitance. The ink D2081009D6 (Gwent) has a viscosity of 13.0–17.0 Pas (Haake VT550, PK1.1° at 230 s⁻¹ at 25 °C) so a new dielectric ink was used, D2070209P6 (Gwent), which has a viscosity of 1.4–2.3 Pas (Haake VT550, PK1.1° at 230 s⁻¹ at 25 °C).

The capacitances of the sensors were measured by using an inductance-capacitance-resistance (LCR) meter at 1 kHz (Agilent U1731A). Tables 4 and 5 show capacitances for the dielectric D2081009D6. It is observed that there is very little variation (between

9 and 13) in capacitance in the case of the TLD design. However, in the OLD design, there is greater variation (between 13 and 60 pF) because, in this design, the influence of the variation of the surface of the electrodes and of their layer thickness is more noticeable. At higher mesh value, the layer thickness decreases; therefore, the capacitance increases, and the greater the surface of the electrode, the greater the capacitance.

Table 4. Capacitance (pF) for TLD when 1–3 layers of D2081009D6 ink are used.

Mesh (Inch)	1 Layer			2 Layers			3 Layers		
	Type			Type			Type		
	A	B	C	A	B	C	A	B	C
330	-	-	6.79	6.1	-	6.47	5.89	-	7.02
230	7.54	6.74	7.33	6.81	6.56	6.87	6.43	6.01	7.05
175	6.72	6.28	6.24	11.8	12.5	13	5.82	5.67	5.97
137	6.91	6.75	6.99	5.6	5.26	5.58	5.4	5.2	5.8
123	5.21	5.61	6.37	5.85	6.73	6.09	5.35	4.46	5.35

Table 5. Capacitance (pF) for OLD when 1–3 layers of D2081009D6 ink are used.

Mesh (Inch)	1 Layer			2 Layers			3 Layers		
	Type			Type			Type		
	A	B	C	A	B	C	A	B	C
330	-	-	-	-	-	78	27.15	106	-
230	53.42	-	-	17.72	19.81	25.76	14.79	15.05	18.32
175	53.7	-	-	21.3	25.43	32.45	12.29	13.65	16.34
137	36	-	99	12.1	13.3	17.2	9.5	10.34	12.64
123	19.6	30.8	38.3	11.69	12.2	23	9.2	9.5	11

The measurements for dielectric D2070209P6 show an increase in the capacitance of the electrodes (Table 6; to simplify, in this case, only the results are shown for a mesh of 175). The resulting capacitances are higher than those obtained with dielectric D2081009D6. Dielectric D2081009D6 was chosen for the final development of the touchpad since an increase of the capacitance supposes an incorrect operation of the controller.

Table 6. Capacitance (pF) for OLD and TLD when 1–3 layers of D2070209P6 ink are used for mesh of 175 inches.

Type of Design	1 Layer			2 Layers			3 Layers		
	Type			Type			Type		
	A	B	C	A	B	C	A	B	C
TLD	-	10.9	15.1	9.13	7.71	9.44	9.1	7.64	9.1
OLD	-	-	-	80.6	94.1	121	57.5	66.8	85.8

The dielectric layer for the final designs was made with a screen of 175 mesh, using ink D2081009D6 and with two layers of dielectric in each prototype.

2.4. Results

2.4.1. Physical Parameters

The magnification view of the two designs with their dimensions are shown in Figure 17 (Figure 17a for TLD; and Figure 17b for OLD). The dimensions considered in the design have been obtained after manufacturing with an almost negligible error.

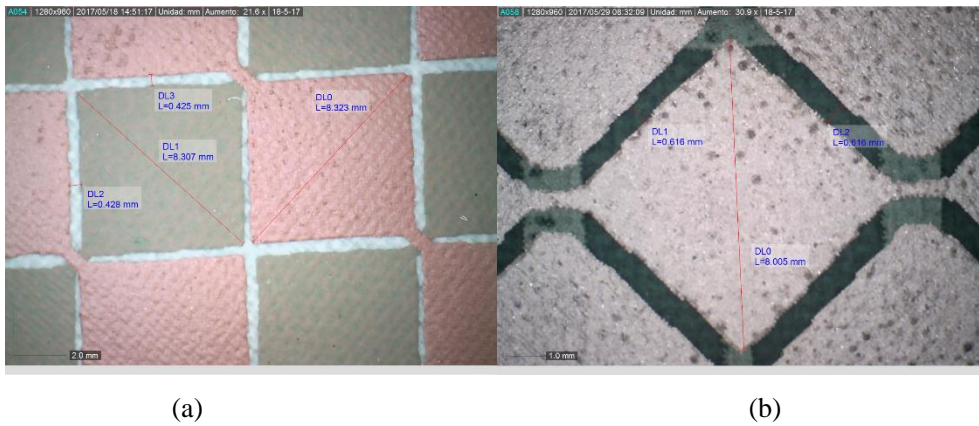


Figure 17. (a) Two-layer design; and (b) one-layer design magnification views.

2.4.2. Electrical Parameters

The capacitance of the sensors has been measured using a RCL meter to 1 kHz (Agilent U1731A). Figure 18a,b shows the capacitance distribution in each sensor. The TDL has an average of 13 pF and OLD of 50 pF. In the case of the OLD design, a difference is observed over the value obtained in the simple electrodes previously performed, which may be due to the influence of the rest of the sensor array; this effect is

not so noticeable in the case of TDL. In any case, they do not influence the correct operation of the touchpad.

Scattering observed in both cases is due to the fabrication process because the thickness of different layers is not exactly the same along substrate, and, in the case of OLD, it could also be due to an incorrect alignment between the layers which entails different geometries along the substrate (Figure 18).

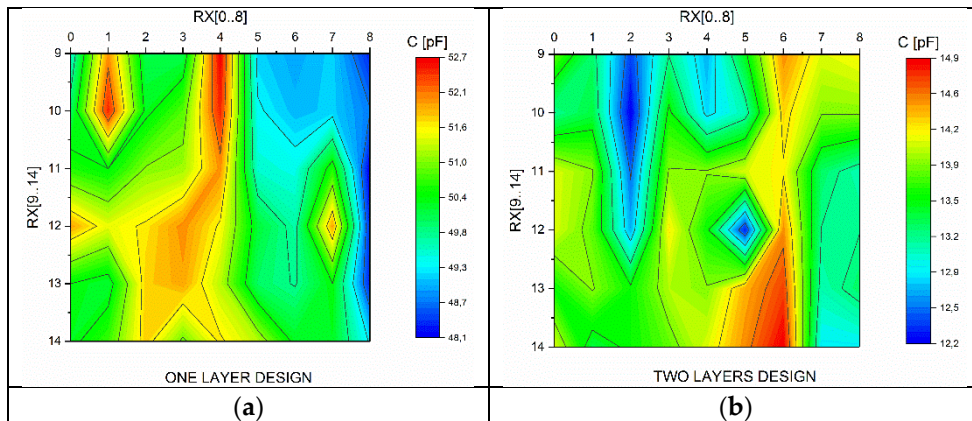


Figure 18. (a) Capacitance distribution on OLD; and (b) capacitance distribution on TLD.

With regard to TLD, the signal recorded on the RX0 line in “released case” (Figure 19a) shows a difference of 54 mV, while, in the “pressed case” (Figure 19b), it is 88 mV.

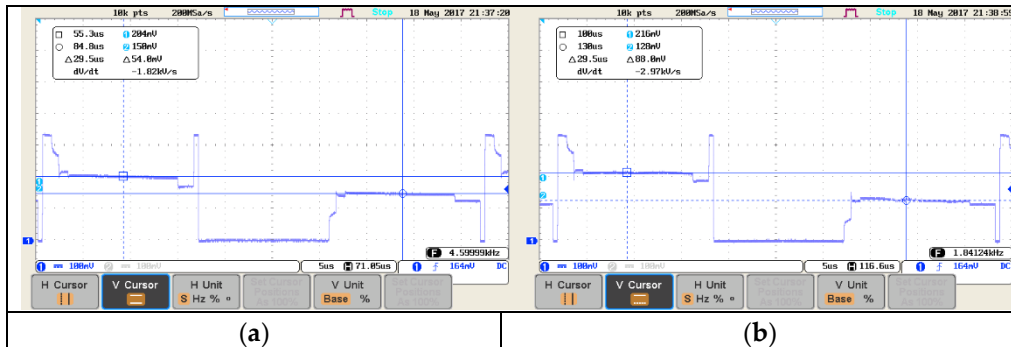


Figure 19. Two-layer design: (a) “released” signal; and (b) “pressed” signal.

With respect to OLD, the signal recorded on the RX0 line in “released case” shows a difference of 160 mV (Figure 20a), while, in the “pressed case”, it is 168 mV (Figure 20b).

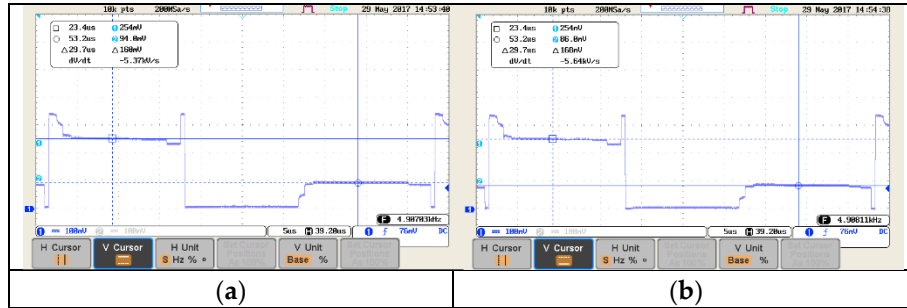


Figure 20. One-layer design: (a) “released” signal; and (b) “pressed” signal.

2.4.3.4.3. Design Using Different Types of Fabrics

Finally, after verifying the correct operation of the sensor, both TLD and OLD have been manufactured using the different types of fabrics shown in the Table A1.

Figure 21 shows the results for each type of fabric. In the case of OLD, all but Mediatex presented problems. The capacitance in this case is similar to that obtained previously. In TLD, there were no failures, but the capacitance was not equal in all cases, with some dispersion of values in some cases such as that of 100% raw cotton. In the best cases, the capacitance was similar to that obtained previously.

	Mediatex 100% Polyester	100% Polyester	65% Polyester 35% Cotton	100% Cotton	100% Cotton Raw	100% Cotton Waterproof
OLD	50.4±1.2 pF	Failure	Failure	Failure	Failure	Failure
TLD	13.6±0.6 pF	19.3±1.3 pF	20.2±0.6 pF	17.4±0.9 pF	31.5±12.9 pF	16.7±0.8 pF

Figure 21. Capacitances and failures for each type of fabric and design.

The reason for failures and value dispersion may be due to loose threads, because they do not allow the dielectric to be an insulating layer. This is more notable in OLD as they have more conductive area faced.

2.4.4. Design Reducing the Size

A new version of OLD was designed; the size of electrodes was reduced in this new version. The main dimensions of this new design pattern are: Pitch (Row and Column) of 6 mm, Gap of 0.5 mm and through-hole diameter of 1.2 mm (Figure 22). The prototype works properly and similarly to its larger version.

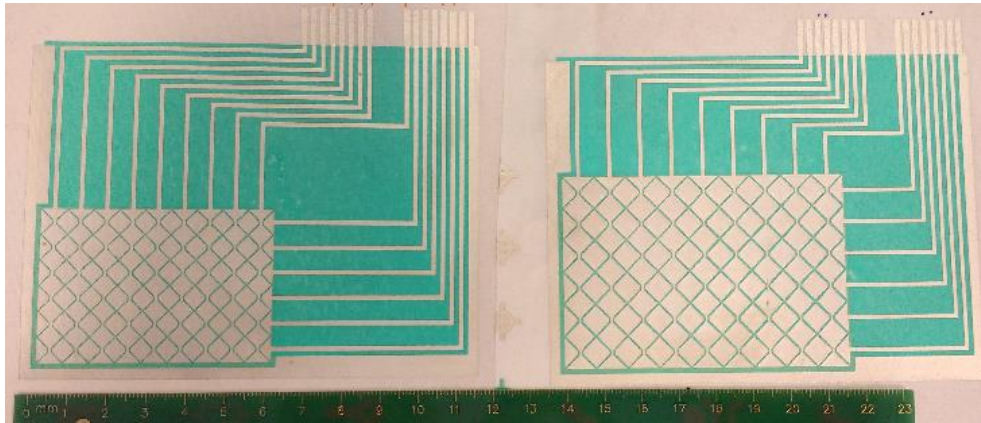


Figure 22. Touchpads with the same design but different size.

2.4.5. Operation

The MTCH6102 GUI utility allows checking all gesture detection of this device: Single Click, Click and Hold, Double Click, Right Swipe, Right Swipe and Hold, Left Swipe, Left Swipe and hold, Up Swipe, Up swipe and Hold, Down Swipe, and Down Swipe and Hold. Both designs were connected to the electronic system and tested with this GUI utility.

In both designs, the operations worked correctly and all possible gestures could be checked; Figure 23a touching on a curved surface in two different points, and Figure 23b touching in the same point but on a flat surface (left) and on a curved surface (right), in both cases the resulting point is the same.

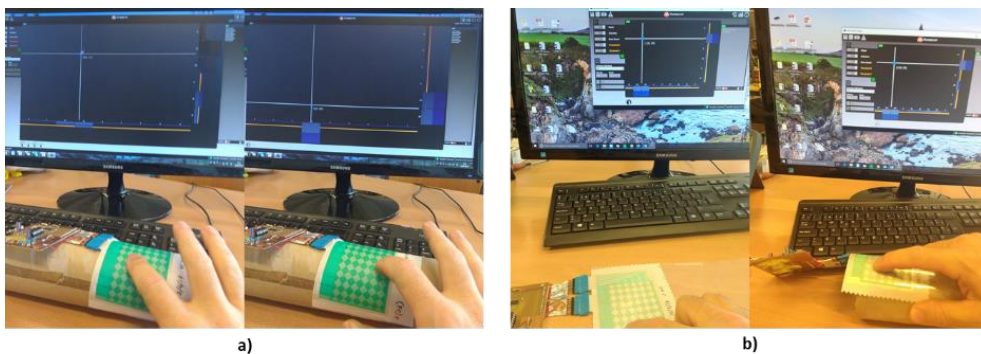


Figure 23. (a) Performance test on a curved surface touching two different points; and (b) performance test touching on the same point but on a flat and a curved surface, obtaining the same result.

2.5. Conclusions

The capacitance obtained in both cases was similar to Microchip's PCB design, but lower in the case of TLD. Capacitors in both cases have the same size; the difference lies in the dielectric: in TLD, there is a dielectric layer between the two conductive layers, whereas, in OLD, there is no dielectric layer. Despite the technology used, the distribution of capacitance along the sensors is quite uniform. Due to its low capacitance, the differential voltage obtained with TLD is higher than that obtained with OLD, as well as higher than Microchip's PCB design. The initial failures found due to the manufacturing process have been solved.

A touchpad based on projected capacitive (pro-cap) technologies has been developed to be used with textile substrates using a low cost and habitual in the textile industry printing technique: screen-printing. The system works on both flat and curved surfaces, which allows it to be used in parts of clothes, such as sleeves, trouser legs or textiles for furniture such as sofas, armchairs, etc.

Touchpad design is based on a diamond type pattern. Two types of architecture with different sizes of electrodes and different types of textiles have been developed, and their correct operation has been verified. Being capacitive electrodes, the control of the capacitance is vital, which is why studies have been made on all those aspects that can modify the capacitance. The most important factor that conditions the capacitance is the thickness, thus it has been emphasized in the study of the factors that affect the thickness.

The application of this device to textiles depends on the type of textile surface, since it can modify the internal structure of the electrode; therefore, it is advisable to modify the surface of the fabric with a layer of dielectric.

References

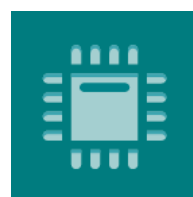
- 1 Takamatsu, S.; Lonjaret, T.; Ismailova, E.; Masuda, A.; Itoh, T.; Malliaras, G.G. Wearable keyboard using conducting polymer electrodes on textiles. *Adv. Mater.* **2016**, *28*(12), 4485–4488.
- 2 Mcmillan, D.; Brown, B.; Lampinen, A. Situating Wearables: Smartwatch Use in Context. In *Proceedings of the 2017 CHI Conference on Human Factors in Computing Systems (CHI '17)*, **2017**, 3582–3594.
- 3 Nirjon, S.; Gummesson, J.; Gelb, D.; Kim, K.-H. TypingRing: A Wearable Ring Platform for Text Input. *Proc. 13th Annu. Int. Conf. Mob. Syst. Appl. Serv. - MobiSys '15* **2015**, 227–239.
- 4 Rekimoto, J. GestureWrist and GesturePad: unobtrusive wearable interaction devices. *Proc. Fifth Int. Symp. Wearable Comput.* **2001**, 21–27.
- 5 Kim, K.; Joo, D.; Lee, K.-P. Wearable-object-based interaction for a mobile audio device. *Proc. 28th Int. Conf. Ext. Abstr. Hum. factors Comput. Syst. - CHI EA '10* **2010**, 3865–3870.
- 6 Suh, M.; Carroll, K.; Cassill, N. Critical Review on Smart Clothing Product Development. *J. Text. Appar.* **2010**, *6*, 1–18.
- 7 Yoon, S.H.; Huo, K.; Ramani, K. Wearable textile input device with multimodal sensing for eyes-free mobile interaction during daily activities. *Pervasive Mob. Comput.* **2016**, *33*, 17–31.
- 8 Van Heek, J.; Schaar, A.K.; Trevisan, B.; Bosowski, P.; Ziefle, M. User requirements for wearable smart textiles. Does the usage context matter (medical vs. sports)? In *Proceedings of the 8th International Conference on Pervasive Computing Technologies for Healthcare (PervasiveHealth '14)*, **2014**, 205–209.
- 9 Rogers, J.A.; Someya, T.; Huang, Y. Materials and Mechanics for Stretchable Electronics. *Science* **2010**, *327*, 1603–1607.
- 10 Fan, J.A.; Yeo, W.-H.; Su, Y.; Hattori, Y.; Lee, W.; Jung, S.-Y.; Zhang, Y.; Liu, Z.; Cheng, H.; Falgout, L.; et al. Fractal design concepts for stretchable electronics. *Nat. Commun.* **2014**, *5*, 1–8.
- 11 Bhalla, M.R.; Bhalla, A.V. Comparative Study of Various Touchscreen Technologies. *Int. J. Comput. Appl.* **2010**, *6*, 2–8.

- 12 Walker, G. A review of technologies for sensing contact location on the surface of a display. *J. Soc. Inf. Disp.* **2012**, *20*, 413–440.
- 13 Pedersen, H.C.; Jakobsen, M.L.; Hanson, S.G.; Mosgaard, M.; Iversen, T.; Korsgaard, J. Optical touch screen based on waveguide sensing. *Appl. Phys. Lett.* **2011**, *99*, 2–5.
- 14 Emamian, S.; Avuthu, S.G.R.; Narakathu, B.B.; Eshkeiti, A.; Chlahawi, A.A.; Bazuin, B.J.; Joyce, M.K.; Atashbar, M.Z. Fully printed and flexible piezoelectric based touch sensitive skin. In Proceedings of the 2015 IEEE *SENSORS*, **2015**, 1–4.
- 15 George, B.; Zangl, H.; Bretterkieber, T.; Brasseur, G. A Combined Inductive–Capacitive Proximity Sensor for Seat Occupancy Detection. *IEEE Trans. Instrum. Meas.* **2010**, *59*, 1463–1470.
- 16 Gunnarsson, E.; Karlsteen, M.; Berglin, L.; Stray, J. A novel technique for direct measurements of contact resistance between interlaced conductive yarns in a plain weave. *Text. Res. J.* **2015**, *85*, 499–511.
- 17 Parzer, P.; Sharma, A.; Vogl, A.; Olwal, A.; Haller, M. SmartSleeve: Real-time Sensing of Surface and Deformation Gestures on Flexible, Interactive Textiles, using a Hybrid Gesture Detection Pipeline. In *Proceedings of the 30th Annual ACM Symposium on User Interface Software and Technology (UIST '17)*, **2017**, 565–577.
- 18 Donneaud, M.; Honnet, C.; Strohmeier, P. Designing a Multi-Touch eTextile for Music Performances. In *Proceedings of the 17th International Conference on New Interfaces for Musical Expression (NIME '17)*, **2017**, 7–12.
- 19 Enokibori, Y.; Suzuki, A.; Mizuno, H.; Shimakami, Y.; Mase, K. E-textile pressure sensor based on conductive fiber and its structure. *Proc. 2013 ACM Conf. Pervasive ubiquitous Comput. Adjunct. Publ. - UbiComp '13 Adjunct.* **2013**, 207–210.
- 20 Gu, J.F.J.F.; Gorgutsa, S.; Skorobogatiy, M. A fully woven touchpad sensor based on soft capacitor fibers. *arXiv Prepr. arXiv1106.3881* **2011**, 1–19.
- 21 Govindaraj, M.; Brookstein, D. Multi-component Multiple-layer Woven Textiles for Electronic Applications. In Proceedings of the *Ambience'08*, **2008**, 72–78.
- 22 Wei, Y.; Torah, R.; Li, Y.; Tudor, J. Dispenser printed capacitive proximity sensor on fabric for applications in the creative industries. *Sens. Actuators A Phys.* **2016**, *247*, 239–246.

- 23 Gorgutsa, S.; Gu, J.F.; Skorobogatiy, M. A woven 2D touchpad sensor and a 1D slide sensor using soft capacitor fibers. *Smart Mater. Struct.* **2012**, *21*, 15010.
- 24 Guo, L.; Soroudi, A.; Berglin, L.; Mattila, H.; Skrifvars, M.; Torstensson, H. Fibre-based single-wire keyboard—The integration of a flexible tactile sensor into e-textiles. *Autex Res. J.* **2011**, *11*, 106–109.
- 25 Roh, J.; Mann, Y.; Freed, A.; Wessel, D.; Berkeley, U.C.; Freed, A.; Street, A.; Wessel, D. Robust and Reliable Fabric and Piezoresistive Multitouch Sensing Surfaces for Musical Controllers. *Proc. Int. Conf. New Interfaces Music. Expr.* **2011**, 393–398.
- 26 Al-huda Hamdan, N.; Heller, F.; Wacharamanotham, C.; Thar, J.; Borchers, J. Grabrics : A Foldable Two-Dimensional Textile Input Controller. *CHI Ext. Abstr. Hum. Factors Comput. Syst.* **2016**, 2497–2503.
- 27 Kim, D.K.; Kim, J.H.; Kwon, H.J.; Kwon, Y.H. A touchpad for force and location sensing. *ETRI J.* **2010**, *32*, 722–728.
- 28 Ferri, J.; Moreno, J.; Martinez, G.; Lidón-Roger, J.V.; Garcia-Breijo, E. Printed Textile Touchpad. In Proceedings of the Eighth International Conference on Sensor Device Technologies and Applications (SensorDevices2017), **2017**, 118–123.
- 29 Barrett, G.; Omote, R. Projected-capacitive touch technology. *Information Display*, **2010**, *26*, 16–21.
- 30 Davison, B. AN1478: mTouch™ Sensing Solution Acquisition Methods Capacitive Voltage Divider. *Microchip Technology Incorporated*, 28.
- 31 Qtouch Surface Design Guide; Application Note, AT11849; Atmel: San Jose, CA, USA, **2015**.
- 32 A Short Guide on Trackpad Layout; Application Note, AZD068; Azoteq: Paarl, South Africa, **2016**.
- 33 FAQs-Sensor Design Guidelines; Application Note, AD120007-001; Microchip Technology Inc.: Chandler, AZ, USA, **2012**.

Chapter 3

A 2D Touch Textile Sensor with an Electroluminescent Display



sensors

Impact factor: 3.031

Q1-Instruments & Instrumentation

3.1. Introduction

To improve the effectiveness of interfaces such as touchpads, buttons, or keyboards, a feedback mechanism is necessary to confirm to the user that the order or action has been recognized by the system. Many types of solutions have been studied and developed in order to provide this user feedback. In this sense, there exist solutions based on haptic feedback by vibrating the touchpad surface [1]. This type of solution has been applied in the automotive industry to assess its effectiveness in real driving situations [2]. On the other hand, the use of tiny sounds used as feedback has also been studied to inform the user that the action has been recognized in combination with or without vibration systems [3,4]. For blind people, different approaches have been studied, such as small braille mechanisms integrated under the touchpad, which emerge as the user interacts with the system [5]. Regarding touchpads, different technologies have been developed as solutions for keyboards, touch panels [6], and touchscreens [7]. From all of them, capacitive and resistive touch technologies master the touch landscape now [8]. Other solutions have been investigated, such as optical sensors [9], force sensors [10], or even inductive sensors [11]. In addition, flexible and stretch sensing approaches have also been popular using contact resistances between threads [12,13], with piezoelectric [14] and capacitive designs [15-17].

Recently, there has been a considerable growing interest in the development of new interfaces that could be printed onto, embedded or attached into textile, giving them a wearable new feature. These interfaces should be flexible, comfortable, and cheap to be suitable for integration into textiles that become smart textiles, fabrics, or garments. The application of these interfaces is very promising with possibilities of interaction with computers, smartphones, or Internet of Things (IoT) devices. In a recent work, our team has designed and developed different touchpad prototypes based on capacitive (pro-cap) technologies using textile substrates [6]. The technique used in these touchpads, screen-printing, is low cost and quite habitual in the textile printing industry.

On the other hand, in spite of the fact that the electroluminescent lamps are not a new technology, electroluminescent display (ELDs) have seen an increase in interest lately due to smart fabrics. Flexible displays have experienced a significant development in recent years, with interest being driven by the expanding wearable technology market. Several experiments using different materials for the different layers, especially for the phosphor and transparent conductive layers, have been performed characterizing the material properties [18]. Other approaches consider including flexible substrates as fabrics evaluating flexibility and breathability [19]. Also, complex seven-segment digital displays have been developed using screen-printing electroluminescent printed on fabric substrates [20].

There are different alternatives to electroluminescent ones like displays based on electrochromic materials [21,22]. Thus, fiber-based visualizers [21] and those based on electrochromic tissues [23] have been reported. The new OLED (Organic Light Emission Diode) technologies still have little implementation in textiles but some develop-

ments have already been reported [22,24-26]. Finally, polymeric optical fiber fabrics have also been used for illumination and sensorial applications in textiles [27,28].

Yet, to date, there have been only limited papers on solutions combining simple interfaces with light emission as feedback. Some solutions are based on flexible and stretchable substrates, such as PDMS, combined with an ELD [29]. This innovative solution can be used as a button or keyboard that is illuminated, as soon as the user pulsation is detected. Other authors address its application on paper and textiles as substrates with the use of capacitive buttons [30].

In this work, we introduce a novel solution that combines complex interface, a touchpad 2D with an electroluminescent ELD. This approach physically has two circuits over a flexible textile substrate using the screen-printing technique for wearable electronics applications. In addition, different layer structures are presented, considering different fabric materials and inks, to obtain the best results.

3.2. Materials and Methods

3.2.1. Device Architecture Development

The architecture of the device consists of, on the one hand, a 2D touchpad whose design is similar to one developed by Ferri, J. et al. [6], and on the other hand, an ELD whose classic design has two conductive external electrodes [31]. In order to manufacture the 2D touchpad sensor in combination with the display, one of the conductive electrodes of ELD must be isolated, specifically the emitting electrode. Two designs can be used for the device:

- Using the fabric as a base, silk-screen printing is done, first corresponding to the ELD and next, corresponding to the 2D sensor. An insulator must be inserted between the two layers (Figure 24a).
- Using the own fabric as part of the emitting electrode, the different layers of the electroluminescent are printed in the lower part of the fabric and the 2D sensor in the upper part. This upper part is conveniently insulated in those cases in which the conductive material of the emitting electrode is completely embedded in the fabric (Figure 24b).

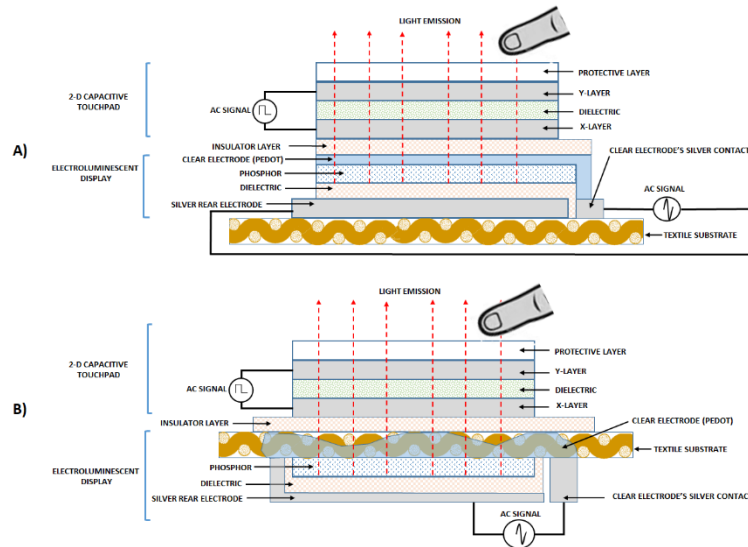


Figure 24. ELD + 2D touchpad architecture: All the design on one side of the textile (a); Using the textile itself as a separating element, on one side the ELD and on the other one the 2D touchpad sensor (b). ELD: electroluminescent display.

The second structure has been chosen for this work, since the fabric can be used as a support for the transparent conductor and at the same time as an insulating layer, saving layers in the process. The development of each of the elements, the ELD on the one hand and the 2D on the other one, are detailed below.

3.2.1.1 Electroluminescent Display Development

There are two standard configurations for a printed ELD, also named ACEPEL (AC Powder Electroluminescent) [32]. In the first one, the light is emitted through a transparent substrate, whereas in the second one, the light is emitted through a printed transparent conductor [33]. To avoid the use of a transparent conductive film (indium tin oxide (ITO) type) required by the first configuration, the second option has been used in this work. Four layers are needed to build the ELD; they are shown in Figure 25: rear conductor layer (a); dielectric layer (b); phosphor layer (c); and clear conductive layer (d).

Thus, to build the ELD, four screens were made. The screen for the conductors (Figure 25 a,d), Silver and PEDOT:PSS, was a 230 mesh polyester material (PET 1500 90/230-48 from Sefar) and the screen for the Dielectric and Phosphor layers (Figure 25b,c), was a 175 mesh polyester material (PET 1500 68/175-64 PW from Sefar). Afterwards, to transfer the stencil to a screen mesh, a Dirasol 132 (Fujifilm) UV film was used. The final screen thicknesses were 10 μm for the screen for the conductors and 15 μm for the

screen for the dielectric and phosphor. The patterns were transferred to the screen by using a UV light source unit.

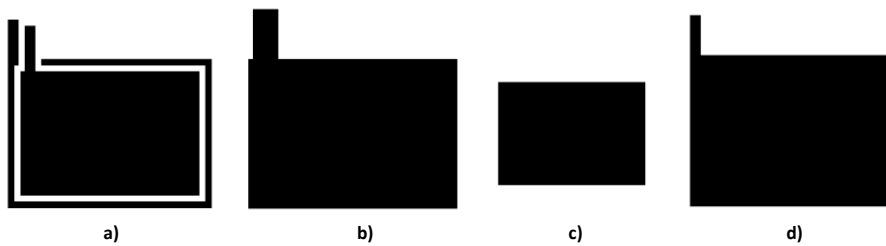


Figure 25. ELD Design: Conductive silver electrode (a); dielectric layer (b); Phosphor layer (c); and clear conductor (d).

The inks used were C2131014D3 Silver paste (Gwent Group) as rear electrode layer, D2070209P6 White Dielectric Ink (Gwent Group) as dielectric layer, C2070126P5 White Phosphor Ink (Gwent Group) as phosphor layer and C2100629D1 Clear conductor ink (Gwent Group) as emitting electrode. Flexibility is one of the most important characteristics of these inks to use them with textiles.

Printing was carried out by using an Ekra E2 XL screen-printer with a 75° shore squeegee hardness, 3.5 bar force, and 8 mm/s. After inks depositing, these were cured in an air oven (MEMMERT UNB-100) at 130 °C for 10 min.

Several materials were used for the substrate: Mediatex TT ACQ 120 μm (Technohard) 100% polyester (Fabric_A), a mix of 65% polyester–35% cotton (Fabric_B), a 100% cotton (Fabric_C), a 100% cotton waterproof (Fabric_D). In order to compare the color, luminosity, and transmission of the textiles, two totally transparent substrates were tested as well: an ITO film and a transparent polyurethane (Inspire® 2370, Coveris™ Advanced Coatings). In the case of the 75 μm ITO/PET film F2071018D1 (Gwent Group), the clear conductor layer was the own ITO. Figure 26 shows the substrates used and their characteristics are shown in Table 7.

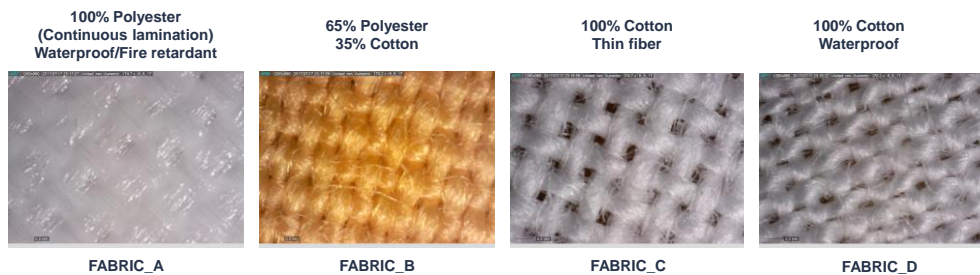


Figure 26. Different types of fabrics used as substrates.

Table 7. Characteristics of the different fabrics used.

Fabric	Weft Densi-ty (Thread/cm)	Warp Densi-ty (Thread/cm)	Ligament	Grammage (g/m ²)	Weft Ma-terial	Warp Material	Thick-ness (μ m)
(A) Mediatex	25	40	Taffeta	115	Polyester	Polyester	110
(B) 65% Pol/35% Cot	30	46	Taffeta	110	Cotton	Polyester	200
(C) 100% Cotton	30	30	Taffeta	120	Cotton	Cotton	190
(D) 100% Cotton Waterproof	34	45	Taffeta	120	Cotton	Cotton	130

In order to improve the response of the clear conductor ink, two compounds were used: Triton™ X-100 (Sigma-Aldrich) as nonionic surfactant to improve the wettability and Glycerol (Sigma-Aldrich) to improve the mobility [34,35]. The behavior of the PEDOT:PSS has been studied in the natural fibers, which allow an absorption of this material (Fabric_B and Fabric_C), not so the Fabric A and D samples since the Fabric_A is 100% waterproof polyester and the Fabric_D is cotton but with a water-resistant treatment. The PEDOT:PSS was tested alone and adding the two aforementioned compounds: Triton™ X-100 (Sigma-Aldrich) for wettability and Glycerol (Sigma-Aldrich) for mobility. Therefore, three more samples have been studied: Fabric_C + Triton (2.0 wt %), Fabric_C + Glycerol (10 wt %) and Fabric_C + Triton + Glycerol.

3.2.1.2 2D Touchpad Development

A sensor matrix formed by 9×6 electrodes has been designed. The sensor has been developed with two conductive layers for horizontal and vertical tracks and another layer of dielectric. The three patterns are shown in the Figure 27: Vertical or X layer (a); dielectric layer (b); and Horizontal or Y layer (c). The Pitch (Row and Column) of 8 mm and Gap of 0.4 mm are the main dimensions of pattern.

To build the sensor matrices, three screens were made. The screen for the conductors (Figure 27a,c) was a 230 mesh polyester material (PET 1500 90/230-48 from Sefar) and the screen for the dielectric layer (Figure 27b) was a 175 mesh polyester material (PET 1500 68/175-64 PW from Sefar). Afterwards, to transfer the stencil to a screen mesh, a Dirasol 132 (Fujifilm) UV film was used. The final screen thicknesses were 10 μ m for the screen for the conductors and 15 μ m for the screen for the dielectric. The patterns were transferred to the screen by using a UV light source unit.

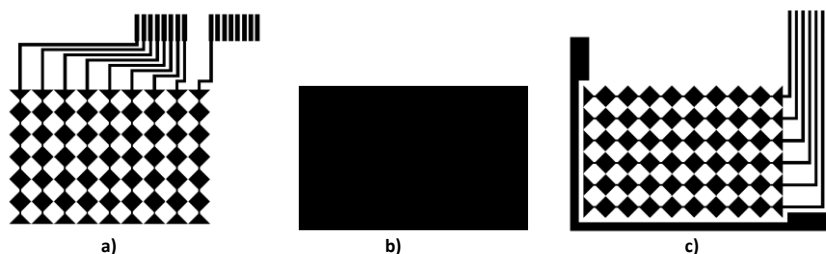


Figure 27. 2D Touchpad Design: Vertical or X layer (a); dielectric layer (b); and Horizontal or Y layer (c).

The inks used were C2131014D3 Silver paste (Gwent Group) as conductive layers, D2081009D6 Transparent Green Colored ink (Gwent Group) as dielectric layer. Two layers of dielectric are needed to improve the design as it is explained in Ferri, J. et al. [6].

Printing was carried out by using an Ekra E2 XL screen-printer with a 75° shore squeegee hardness, 3.5 bar force, and 8 mm/s. After the deposition of the inks, these were cured in an air oven (MEMMERT UNB-100) at 130 °C for 10 min.

Substrates are the same detailed in the previous point.

3.2.2. Electronic Systems Development

The electronic systems consist of four blocks. A master controller implemented with a PIC16LF1454 that controls other two blocks: one for the ELD and the other one for the 2D touchpad (Figure 28). The last block corresponds to a Bluetooth module to make the system portable. Figure 28a shows the complete system with the two control blocks, one for the ELD and one for the touchpad, and the master block, with the different integrated circuits in each block. Figure 28b shows an application of the system implementing a mouse for a mobile phone through a Bluetooth communication.

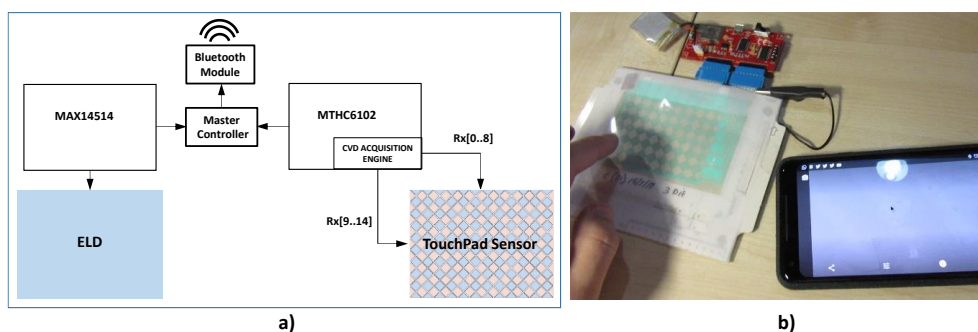


Figure 28. Electronic System Block Diagram (a); real electronic system applied to a mouse control in a mobile phone (b).

3.2.2.1 ELD Electronic Block

The ELDs are a parallel plate “lossy capacitors”, an active electroluminescent phosphor is embedded in dielectric. The application of an AC voltage to both plates generates a changing field within the active layer that causes the phosphor to emit light.

Electroluminescent displays require special frequency, voltage and waves types characteristics. Thus, for its excitation it is necessary to apply a sinusoidal or square alternating signal of amplitude between 100 to 400 V and of frequency of the order of 50 to 900 Hz.

In order to use stand-alone power sources (batteries), an electronic circuit is needed which, from a direct voltage, provides us with the alternating signal required by the electroluminescent lamp. The integrated circuit MAX14514 (Maxim Integrated) has been selected. The MAX14514 features a +2.7 V to +5.5 V input range that allows the device to accept a wide variety of voltage sources, including single-cell lithium-ion (Li+) batteries. The lamp outputs of the device generate up to 300 V_{P-P} for maximum lamp brightness.

3.2.2.2 2D Touchpad Electronic Block

MTCH6102 (Microchip) has been used in this work. This device is a turnkey projected capacitive touch controller that simplifies adding gestures to touch interface designs with industry-leading low-power performance. It utilizes up to 15 channels to support taps, swipes, and scrolling on XY touch pads and touch screens. The operation and the scheme are explained and showed in Ferri, J. et al. [6].

3.3. Results and Discussion

3.3.1. Physical Parameters

The profilometer Profilm3D (Filmetrics) has been used to measure the thickness of the set of layers on each side of the fabric. Figure 29 shows the profilometry of the two faces of the fabric. In Figure 4a, the ELD layers with a final average thickness of 70 μm are shown for the Fabric_A substrate, distributed in approximately 3 μm of PEDOT:PSS, 26 μm of phosphorus, 35 μm of dielectric and 6 μm of silver. In this type of substrate, the thickness of the PEDOT:PSS layer can be measured since it does not penetrate the fabric, in the rest of the substrates with cotton part of the PEDOT:PSS remains embedded in the fabric. Figure 4b shows the layers of the 2D touchpad, in this case for a Fabric_B type substrate to assess the influence of the insulating layer. The resulting average thickness is 80 μm , distributed in approximately 30 μm of insulation, 9 μm of silver X-layer, 31 μm of dielectric and 10 μm of silver Y-layer.

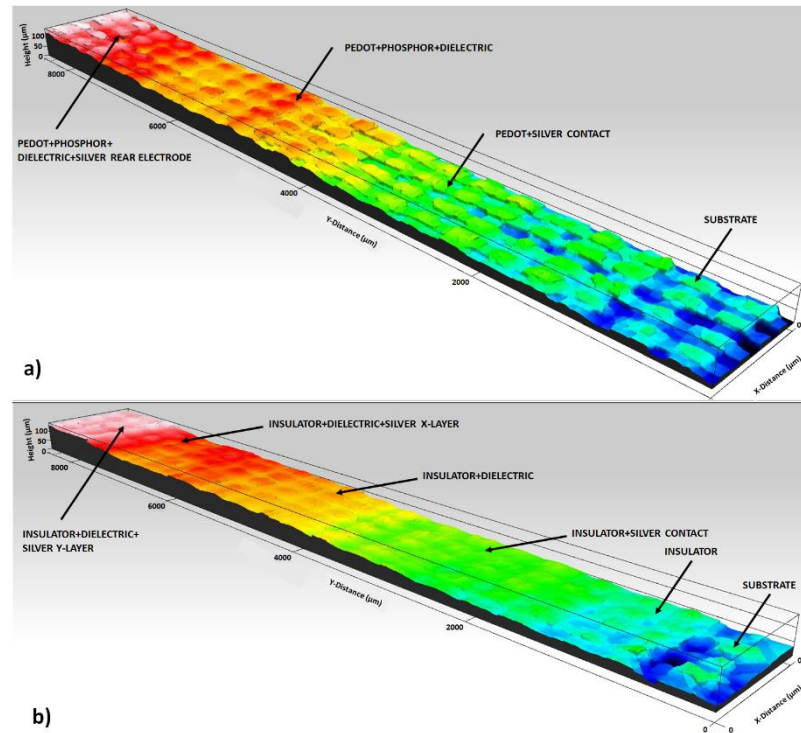


Figure 29. Electroluminescent Display layers profilometry (a). 2D Touchpad layers profilometry, in this case fabrics A and B are studied in order to value the insulator layer (b).

In the Fabric_B and Fabric_C samples, the PEDOT:PSS is partially embedded inside the threads but it covers its surface. Scanning electron microscopy (SEM) images (JEOL JSM6300) have been carried out to verify how the PEDOT interacts with the fibers (Figure 30). In Figure 30a, the cotton fabric without PEDOT:PSS is shown and in Figure 30b the cotton fabric with PEDOT:PSS is shown. A comparison between two images reveals that a PEDOT:PSS coating of the fibers takes place and, in addition, PEDOT:PSS intertwines with the fibers like a ligament [36].

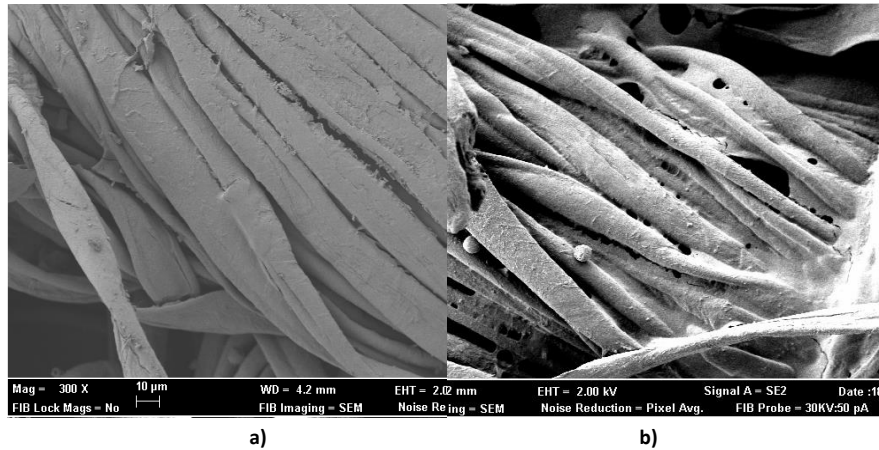


Figure 30. Cotton fibers without PEDOT: PSS (a) and after the screen printing of PEDOT: PSS (b).

Finally, a SEM micrograph cross-section of the whole system is shown in Figure 31 to highlight the multilayer structure of the device. Figure 31a shows the Fabric_A sample, the touchpad is on the upper part of the fabric and the ELD on the bottom. In a box, in the bottom right corner, the virgin fabric 100% polyester is shown. Figure 31b shows the Fabric_C sample, on the upper part of the fabric is the touchpad and on the lower part the ELD. In a box, in the bottom right corner, the 100% cotton fabric is shown virgin. In this case, the insulator layer can be observed. This layer avoids the contact between the cotton with PEDOT: PSS and the Silver X-Layer. Moreover, this layer allows to soften the uneven surface of the woven fabric to provide a more heterogeneous surface for the subsequent layers to be printed.

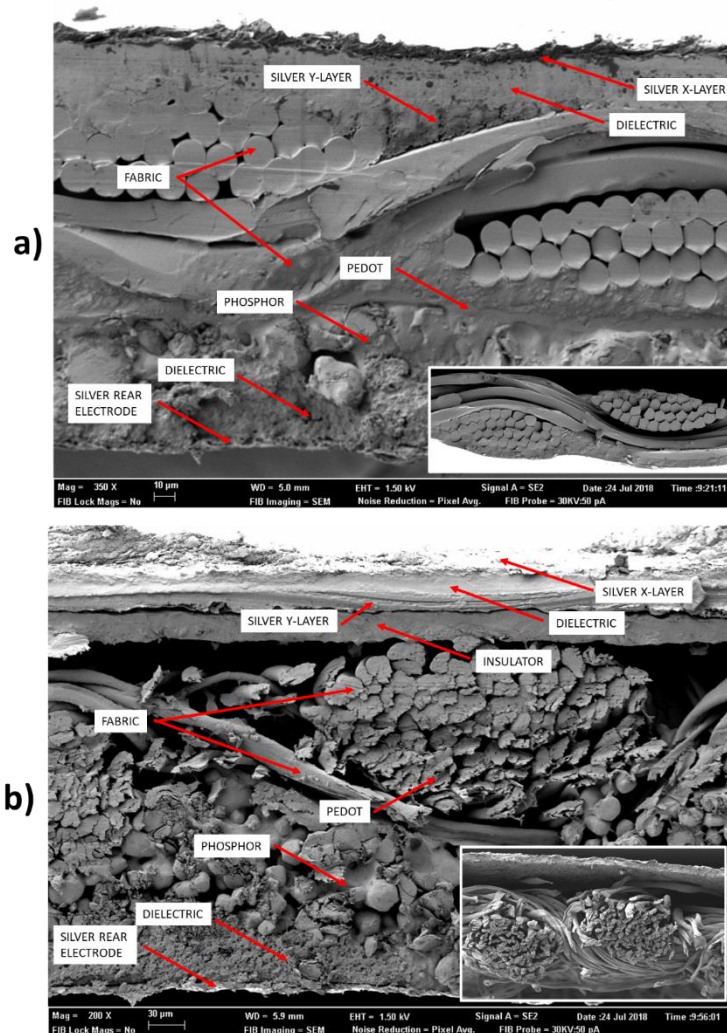


Figure 31. SEM micrograph showing device cross-section. Fabric_A (a) and Fabric_C (b). In a box, in the bottom right corner of each figure, the virgin fabric is shown.

3.3.2. Electroluminescent Display Results

The ELD has been tested using four devices, a programmable AC power source (Chroma Programmable AC Source Model 61601) that allows supplying output voltage from 0 to 300 VAC, and frequencies from 15 to 1000 Hz, a fiber-based spectrometer (Thorlabs Compact Spectrometer CC5200/M) with a wave range between 350 and 70 nm, and a digital luxometer, a device for precise light measurements of up to 200,000 lux (Koban Digital Lux Meter KL1330). The light transmission has been

measured with an Instrument System Model Digilux 9500 system photometer in base on the standard NF P38-511:1969.

To measure the ELD, the ink colours will be defined based on the CIE colour system. The CIE colour system provides a quantitative link between distributions of wavelengths in the electromagnetic visible spectrum, and physiologically perceived colours in human vision. The different displays have been tested at the same conditions applying typical values of 100 V AC and frequency of 400 Hz. Notice that brightness of the display can be increased by a higher voltage and frequency, however both these will shorten the life of the display. The results of the chromaticity, luminance, and light transmission are presented in Figure 32 and Table 8. Although the phosphor ink is the same and has been applied with the same procedure, there are variations in the colour, mainly due to the fabric. A totally transparent test sample (A) is used as a basis of comparison. Fabric_A (B), Fabric_B (C), Fabric_C (D), and Fabric_D (E) are close to the test sample, and with very similar parameters in colour but significantly smaller in order of luminance (three times smaller in the best case (B)) due to the fabric tissue absorbance. No significant improvements have been achieved in the substrates in which an attempt to improve the PEDOT:PSS response has been made (G, H, and I), chromaticity and luminance have not been affected.

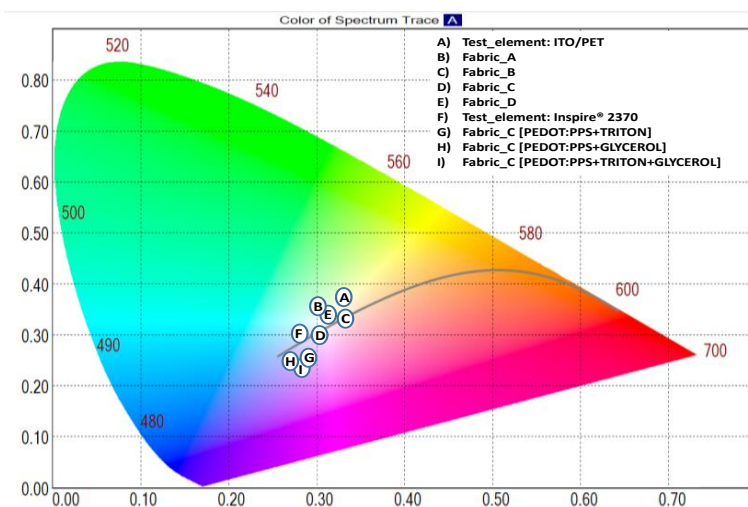


Figure 32. Chromaticity diagram according to the CIE 1931 standard.

Table 8. Light characteristics of the different samples used.

pe	Substrate	Clear Conductor	lux	CIE 1931 Standard				Light Trans
				x	y	z	Dominant	
A	PET	ITO	217	0.3294	0.3745	0.2961	549.59	79%
B	Fabric_A	PEDOT:PSS	74.1	0.3195	0.3553	0.3253	514.31	27%
C	Fabric_B	PEDOT:PSS	11.3	0.3479	0.3428	0.3093	583.37	14%
D	Fabric_C	PEDOT:PSS	11.2	0.3059	0.3112	0.3829	480.36	32%
E	Fabric_D	PEDOT:PSS	29.2	0.3084	0.3374	0.3542	493.81	30%
F	Inspire 2370	PEDOT:PSS	170	0.2821	0.3328	0.3851	491.58	49%
G	Fabric_C	PEDOT:PSS + TRITON	15	0.2764	0.2503	0.4733	465.84	33%
H	Fabric_C	PEDOT:PSS + GLYCEROL	14	0.2701	0.2529	0.4770	471.12	32%
I	Fabric_C	PEDOT:PSS + GLYCEROL + TRITON	10	0.2813	0.2470	0.4717	457.22	33%

3.3.3. 2D Touchpad Results

The operation of the system is explained in Ferri, J. et al. [6]. The touch controller used, MTCH6102, transmits a train of square pulses of 50 μ s (20 kHz) of duration with a frequency of 50 Hz. Figure 33a shows the typical signal emitted by the MTCH6102.

The touchpad works correctly when the ELD is switched off, but a problem is detected when turning on the ELD. The ELD produces electromagnetic interferences (EMI) that distort the signal in the touchpad. The signal affected by the emissions is shown in Figure 33b; in the spectrum the 50 Hz frequency suffers a degradation of 10 dB and the 20 kHz frequency decreases 6 dB. Different waveforms, voltage levels, and working frequencies have been studied but an efficient reduction of the emission is not achieved. Therefore, an EMI isolation is needed.

An EMI shielding limits the penetration of electromagnetic fields into a space, by blocking them with a barrier made of a conductive material [37]. Different materials can be used as EMI shielding as Al/Cu foil tape, silver paint, copper paint, nickel paint, metal cables, or conductive elastomers depending on the applications [38-40]. To isolate the 2D touchpad, an EMI shield must be inserted between the ELD and the 2D Touchpad. The premise is that the EMI shield must be transparent. For this reason, an ITO film, which is transparent to visible light but still electrically conducting at the frequencies of interest for EMI shielding (GHz to DC), has been used. Although indium tin oxide (ITO) films have been extensively used in electronic and photoelectronic applications because of their low electrical resistivity, there are few publications discussing the electromagnetic shielding effectiveness of this material. Nevertheless, according to different studies, they can be used as electromagnetic shields [41,42]. The

ITO attenuation in different frequencies have been tested, the fewer frequency applied, the more attenuation obtained. If the surface resistance is around $80 \Omega/\text{sq}$, the attenuation at 200 Hz can be around 150 dB [42].

The film used is a $50 \mu\text{m}$ printed ITO (Multek) and has been fixed to the fabric with a screen-printed adhesive SILPURAN® 2114 A/B (Wacker).

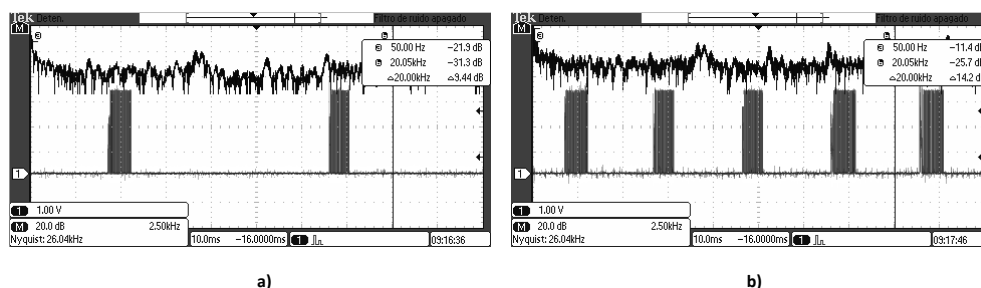


Figure 33. Train of pulses sent by the Touch Controller. Normal signal (a) and disturbed signal (b).

3.3.4. Final Design

A final design with an EMI shield was made as can be seen in Figure 34. This device allows to turn ELD on or off from the control electronics (Appendix A, Figure A4a). A later version, in which the ELD has been redesigned so that only the zone that has been touched is turned on, has been made (Figure 35).

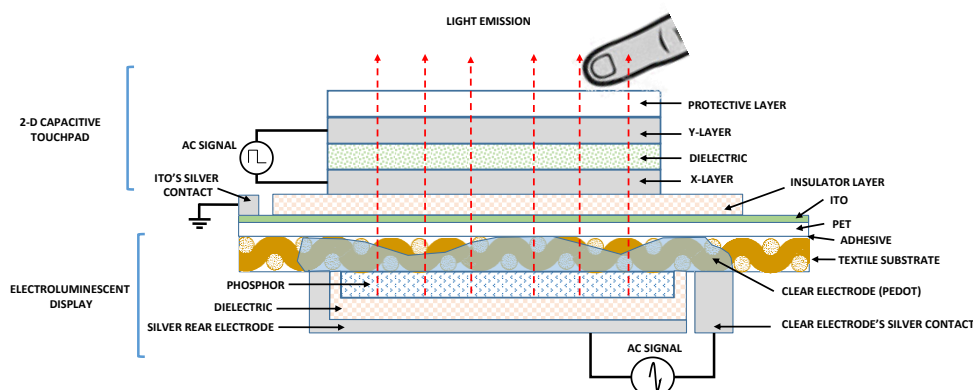


Figure 34. ELD + 2D touchpad architecture with ITO EMI shield. ELD: electroluminescent display; ITO: indium tin oxide; EMI: electromagnetic interferences.

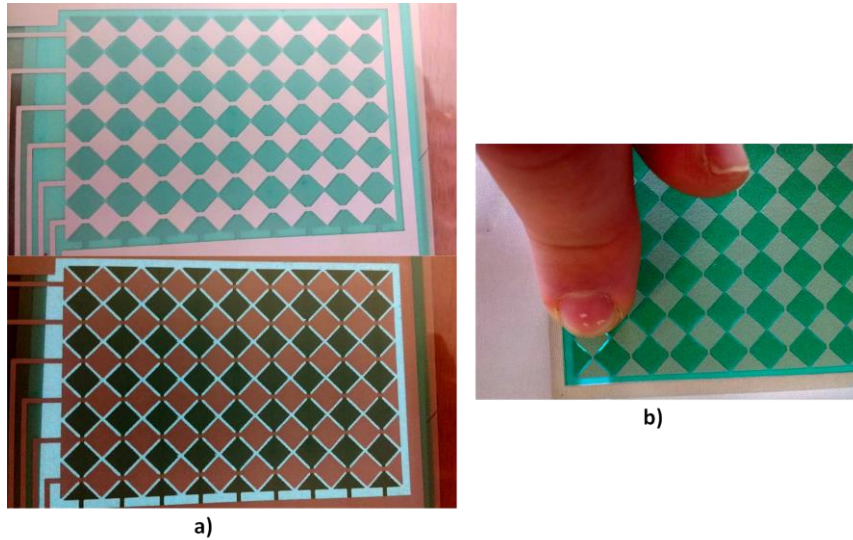


Figure 35. 2D touchpad with ELD on and off (a). Redesign in order to turn on only the zone that has been touched (b). The design has been manufactured with Fabric_A.

3.4. Conclusions

A novel solution that combines a touchpad 2D with an electroluminescent (EL) matrix has been presented, using screen-printing technique on a textile substrate. The integration of a 2D touch sensor with an electroluminescent display is not directly due to the electromagnetic fields emitted by the ELD, so an EMI shield must be incorporated into the assembly, which makes it difficult, but not impossible, to translate it into the industrial field. The application of the ELD on textile reduces considerably the luminosity compared to using transparent substrate based on ITO, used as reference. Two solutions have been presented as alternatives to improve the luminosity, the ELD on a transparent substrate based on ITO and of polyurethane with PEDOT:PSS like emitting electrode and later to anchor it to the textile. However, in those cases in which the integration of an ITO film is not possible, and there are no excessive luminosity requirements, the full printed presented solution can be considered, taking into account the limitations previously explained. The entire screen-printing process adds a maximum of 200 μm to the textile, so it remains flexible, and the inks used are flexible, so there is no breakage when working with the material. Regarding the fabrics studied, all of them have a similar behaviour with the 2D sensor, but the highest luminous efficiency is obtained with Fabric_A. The developed equipment allows feedback with the user in the different applications of this type of system

References

- 1 Blattner, A.; Bengler, K.; Hamberger, W.; Schnieder, S. Comparison of in-car touchpads with adaptive haptic feedback. *Proc. - 2012 IEEE Symp. Haptic Audio-v. Environ. Games, HAVE 2012*, **2012**, 62–65.
- 2 Ishizuka, H.; Hatada, R.; Cortes, C.; Miki, N. Development of a fully flexible sheet-type tactile display based on electrovibration stimulus. *Micromachines* **2018**, *9*, 230.
- 3 Hoggan, E.; Crossan, A.; Brewster, S.; Kaaresoja, T. Audio or Tactile Feedback: Which Modality When? *In Proceedings of the SIGCHI Conference on Human Factors in Computing Systems*, **2009**, 2253–2256.
- 4 Chang, A.; O’Sullivan, C. Audio-haptic Feedback in Mobile Phones. *CHI '05 Ext. Abstr. Hum. Factors Comput. Syst.* **2005**, 1264–1267.
- 5 Jung, J.; Youn, E.; Lee, G. PinPad: Touchpad Interaction with Fast and High-Resolution Tactile Output. *CHI '17 Proc. 2017 CHI Conf. Hum. Factors Comput. Syst.* **2017**, 2440–2448.
- 6 Ferri, J.; Moreno, J.; Martinez, G.; Lidón-Roger, J.V.; Garcia-Breijo, E. Wearable Textile 2D Touchpad Sensor Based on Screen-Printing Technology. *Materials* **2017**, *10*, 1450.
- 7 Bhalla, M.R.; Bhalla, A.V. Comparative Study of Various Touchscreen Technologies. *Int. J. Comput. Appl.* **2010**, *6*, 12–18.
- 8 Walker, G. A review of technologies for sensing contact location on the surface of a display. *J. Soc. Inf. Disp.* **2012**, *20*, 413–440.
- 9 Pedersen, H.C.; Jakobsen, M.L.; Hanson, S.G.; Mosgaard, M.; Iversen, T.; Korsgaard, J. Optical touch screen based on waveguide sensing. *Appl. Phys. Lett.* **2011**, *99*, 2–5.
- 10 Emamian, S.; Avuthu, S.G.R.; Narakathu, B.B.; Eshkeiti, A.; Chlaihawi, A.A.; Bazuin, B.J.; Joyce, M.K.; Atashbar, M.Z. Fully printed and flexible piezoelectric based touch sensitive skin. *In Proceedings of the 2015 IEEE SENSORS*, **2015**, 1–4.
- 11 George, B.; Zangl, H.; Bretterkieber, T.; Brasseur, G.A. Combined Inductive–Capacitive Proximity Sensor for Seat Occupancy Detection. *IEEE Trans. Instrum. Meas.* **2010**, *59*, 1463–1470.

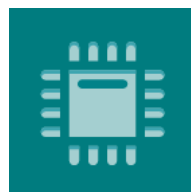
- 12 Gunnarsson, E.; Karlsteen, M.; Berglin, L.; Stray, J. A novel technique for direct measurements of contact resistance between interlaced conductive yarns in a plain weave. *Text. Res. J.* **2015**, *85*, 499–511.
- 13 Parzer, P.; Sharma, A.; Vogl, A.; Steimle, J.; Olwal, A.; Haller, M. SmartSleeve: Realtime sensing of surface and deformation gestures on flexible, interactive textiles, using a hybrid gesture detection pipeline. *UIST 2017 - Proc. 30th Annu. ACM Symp. User Interface Softw. Technol.* **2017**, 565–577.
- 14 Donneaud, M.; Honnet, C.; Strohmeier, P. Designing a Multi-Touch eTextile for Music Performances. *Nime* **2017**, 7–12.
- 15 Enokibori, Y.; Suzuki, A.; Mizuno, H.; Shimakami, Y.; Mase, K. E-textile pressure sensor based on conductive fiber and its structure. *Proc. 2013 ACM Conf. Pervasive ubiquitous Comput. Adjunct. Publ. - UbiComp '13 Adjunct.* **2013**, 207–210.
- 16 Gu, J.F.J.F.; Gorgutsa, S.; Skorobogatiy, M. A fully woven touchpad sensor based on soft capacitor fibers. *arXiv Prepr. arXiv1106.3881* **2011**, 1–19.
- 17 Nunes, J.S.; Castro, N.; Gonçalves, S.; Pereira, N.; Correia, V.; Lanceros-Mendez, S. Marked Object Recognition Multitouch Screen Printed Touchpad for Interactive Applications. *Sensors*, **2017**, *17*, 1–9.
- 18 Shon, P.K.; Shin, J.H.; Kim, G.C.; Lee, S.N. Enhanced luminescence related to transparent conductive oxide in ZnS-based EL device fabricated by screen printing method. *J. Lumin.* **2012**, *132*, 1764–1767.
- 19 De Vos, M.; Torah, R.; Beeby, S.; Tudor, J. Functional electronic screen-printing-Electroluminescent lamps on Fabric. *Procedia Eng.* **2014**, *87*, 1513–1516.
- 20 De Vos, M.; Torah, R.; Glanc-Gostkiewicz, M.; Tudor, J. A Complex Multilayer Screen-Printed Electroluminescent Watch Display on Fabric. *J. Disp. Technol.* **2016**, *12*, 1757–1763.
- 21 Weng, W.; Chen, P.; He, S.; Sun, X.; Peng, H. Smart electronic textiles. *Angew. Chem. Int. Ed.* **2016**, *55*, 6140–6169.
- 22 Cochrane, C.; Meunier, L.; Kelly, F.M.; Koncar, V. Flexible displays for smart clothing: Part I—Overview. *Indian J. Fibre Text. Res.* **2011**, *36*, 422–428.
- 23 Cochrane, C.; Meunier, L.; Kelly, F.M.; Koncar, V. Flexible displays for smart clothing: Part II—Electrochromic displays. *Indian J. Fibre Text. Res.* **2011**, *36*, 429–435.

- 24 Matsuhisa, N.; Kaltenbrunner, M.; Yokota, T.; Jinno, H.; Kuribara, K.; Sekitani, T.; Someya, T. Printable elastic conductors with a high conductivity for electronic textile applications. *Nat. Commun.* **2015**, *6*, 7461.
- 25 Kim, W.; Kwon, S.; Lee, S.M.; Kim, J.Y.; Han, Y.; Kim, E.; Choi, K.C.; Park, S.; Park, B.C. Soft fabric-based flexible organic light-emitting diodes. *Org. Electron.* **2013**, *14*, 3007–3013.
- 26 Kim, W.; Kwon, S.; Han, Y. C.; Kim, E.; Kim, H. C.; Choi, K.C.; Kang, S. H.; Park, B.-C. OLEDs on Textile Substrates with Planarization and Encapsulation using Multilayers for Wearable Displays. *SID Symp. Digest Tech. Pap.* **2014**, *45*, 364–366.
- 27 Harlin, A.; Makinen, M.; Vuorivirta, A. Development of polymeric optical fibre fabrics as illumination elements and textile displays. *Autex Res. J.* **2003**, *3*, 8.
- 28 Selm, B.; Gürel, E.A.; Rothmaier, M.; Rossi, R.M.; Scherer, L.J. Polymeric optical fiber fabrics for illumination and sensorial applications in textiles. *J. Intell. Mater. Syst. Struct.* **2010**, *21*, 1061–1071
- 29 Wessely, M.; Orsay, F.-; Mackay, W.E. Stretchis: Fabricating Highly Stretchable User Interfaces. *Proc. 29th Annu. Symp. User Interface Softw. Technol. - UIST '16* **2016**, 697–704.
- 30 Van de Zande, T.; Lockton, D. Printerface: Screen Printed Electroluminescent Touch Interface. In Proceedings of the 2017 ACM International Conference on Interactive Surfaces and Spaces, Brighton, UK, 17–20 October **2017**.
- 31 Hart, J.A.; Lenway, S.A.; Murtha, T. A History of Electroluminescent Displays. Available online: <http://www.indiana.edu/~hightech/fpd/papers/ELDs.html> (accessed on 28 September **2018**).
- 32 Chen, F.; Kitai, A.H. Handbook of Visual Display Technology. *Springer International Publishing*: New York, NY, USA, **2016**.
- 33 Kronfli, R. A Novel Design for Fully Printed Flexible AC-Driven Powder Electroluminescent Devices on Paper. Ph.D. Thesis, University of Toronto, Toronto, ON, Canada, **2014**.
- 34 Tevi, T.; Saint Birch, S.W.; Thomas, S.W.; Takshi, A. Effect of Triton X-100 on the double layer capacitance and conductivity of poly(3,4-ethylenedioxythiophene):poly(styrenesulfonate) (PEDOT:PSS) films. *Synth. Met.* **2014**, *191*, 59–65.

- 35 Shi, H.; Liu, C.; Jiang, Q.; Xu, J. Effective approaches to improve the electrical conductivity of PEDOT:PSS: A review. *Adv. Electron. Mater.* **2015**, *1*, 1500017–1500032.
- 36 Hu, B.; Li, D.; Ala, O.; Manandhar, P.; Fan, Q.; Kasilingam, D.; Calvert, P.D. Textile-Based Flexible Electroluminescent Devices. *Adv. Funct. Mater.* **2011**, *21*, 305–311.
- 37 Li, H.; Li, Z.; Zhang, B.; Tang, W.K.; Halang, W.A. Suppressing electromagnetic interference in direct current converters. *IEEE Circuits Syst. Mag.* **2009**, *9*, 4.
- 38 Håkansson, E.; Amiet, A.; Kaynak, A. Electromagnetic shielding properties of polypyrrole/polyester composites in the 1–18 GHz frequency range. *Synth. Met.* **2006**, *156*, 917–925.
- 39 Devender; Ramasamy, S.R. Review of EMI shielding and suppression materials. In Proceedings of the Proceedings of the International Conference on Electromagnetic Interference and Compatibility, **1997**, 459–466.
- 40 Huang, J.L.; Yau, B.S.; Chen, C.Y.; Lo, W.T.; Lii, D.F. The electromagnetic shielding effectiveness of indium tin oxide films. *Ceram. Int.* **2001**, *27*, 363–365.
- 41 Sarto, F.; Sarto, M.S.; Larciprete, M.C.; Sibilina, C. Transparent films for electromagnetic shielding of plastics. *Rev. Adv. Mater. Sci.* **2003**, *5*, 329–336.
- 42 Eite, J.; Spencer, A.G. Indium Tin Oxide for transparent EMC shielding and Anti-static applications. In Proceedings of the EMC-UK, **2004**.

Chapter 4

A Textile 3D Gesture Recognition Textile Sensor



sensors

Impact factor: 3.275

Q1-Instruments & Instrumentation

4.1. Introduction

The ability of computers to recognize hand gestures is essential for progress in human-computer interaction (HCI) and human machine interaction (HMI) [1]. Gesture recognition enables humans to interact with computers and machines without any physical contact in a more natural way. It is an alternative method for interacting with computers without using traditional peripheral devices, such as the keyboard or the mouse. One of the most relevant devices is the Microsoft Kinect sensor, now updated as Azure Kinect DK sensor, both consisting of advanced sensing hardware combining a VGA (Video Graphics Array) video camera, an infrared depth sensor and a multi-array microphone allowing people to interact with the games using their body [2]. In addition, this device includes a complex microprocessor that is able to run advanced machine-learning algorithms on a graphics processing unit (GPU) in parallel, tracking simultaneously up to six people. Although face and other body parts, considered as full body interaction [3], can be used to interact with computers, hand gesture recognition is the most popular solution for different reasons. Factors such as end-user application, reliability, cost, and context influence the choice of one technology in detriment of another.

Hand gesture recognition based human machine interface (HMI) is an attractive topic because it is especially important in both industrial and domestic applications, to evolve the way we interact with our environment. Hand gesture recognition allows us to control elements in a 3D space, rather than traditional interfaces, such as the mouse or the keyboard, that are limited to a 2D environment. These features have an important impact on CAD (Computer-Aided Design) applications, 3D gaming, or Virtual Reality. Hence, gesture recognition has a huge application ranging from very simple applications to interact with home appliances such as the TV [4] to complex systems of telemedicine [5]. In addition, hand gesture recognition has a promising future in some circumstances where hands are not able to touch equipment, such as in medical environments [6], helping impaired people to communicate [7], game-based rehabilitation applications [8,9], cooking scenarios [10], controlled robots at industrial environments [11], vehicle interfaces [12,13], or military needs [14].

The design of a successful hand gesture recognition system must address two main characteristics: functionality and usability [15]. Functionality refers to the set of functions, gestures, or services that the system offers to the users, whereas usability refers to the performance and user experience to perform specific purposes efficiently. Generally, the video technology is used for general motion recognition and has also been used for hand gesture recognition. Most of the systems based on video technology, although able to detect many gestures, are faced with other challenges, such as lighting variation, hand location, orientation, or the changes in the background. Nevertheless, this technology has promising results as soon as the complex algorithms needed for real time applications are able to be embedded on hardware such as FPGA (Field-Programmable Gate Array) or ASIC (Application-Specific Integrated Circuit) devices. As a drawback, the powerful microprocessors required raise the price of the final prod-

uct. Another factor to consider is the invasion of privacy inherent in video-based recognition.

As an alternative, there exist wearable devices for user interaction with bending sensors [16,17], LEDs (Light-Emitting Diode) [18], electrical impedance sensors on the skin [19], and accelerometers to be worn on gloves. These alternatives have shown good results with high classification accuracy but also some disadvantages such as the calibration of the orientation or the need to use gloves that may be uncomfortable for the user.

Another group of solutions are based on proximity sensors that have limited gesture recognition but good accuracy and low price. These sensors use different technologies depending on the way they process the signals involved. Sensors based on radar signals [20-22] make use of transmission and reflection of RF (Radio Frequency) waves, determining the time delay between transmitted and received waveforms. Other sensors, sound sensors, apply similar techniques but working in different frequencies [23,24]. These solutions use sonar systems that transmit inaudible sound signals and track the echoes of the hand with its microphones.

Analysing commercial products and the evolution of the gesture recognition market, there is a natural evolution from the touchpads [25-27], where contact with sensors is needed [28], to touchless sensors [29]. Regarding touchpad technologies, two main types of sensors can be found: capacitive and resistive [30]. Of the two, only capacitive sensors can be used as touchless detecting hand gestures. In this field, there exist different approaches, but all of them have presented good results in low power consumption, seamless integration, and low cost [31].

Focusing on hand gesture recognition with capacitive touchless sensors [32,33], the literature presents many approaches. Some authors have classified the technologies as active or passive. Other authors have found up to four different modes of operation [34]. Each one has benefits and limitations but, despite the limitations, capacitive sensors have been shown to be able to sense human activities. Moreover, one of the advantages of this technology is that it is possible to use capacitive sensors on non-rigid substrates, supporting flexible and stretchable substrates [35,36]. All these features offer an opportunity to overcome challenges that smart textiles demand [37] as user interfaces embedded into textiles and fabrics [38]. Applications such as a sofa pillow that integrates a smart TV remote control, an intuitive embedded interface to activate a recliner armchair, or smart cloths that are able to interact with external computers are examples that could take advantage of this innovation [39].

This paper shows the behaviour and influence of different smart textile materials used as capacitive sensors for the purpose of hand gesture recognition. The electrodes that conform the sensor structure are printed on textiles substrates using screen printing technology. All the study uses is the 3D GestIC® sensor from Microchip Technology Inc. (Chandler, Arizona, USA) with their MGC3130 processor. The different smart

textiles prototypes presented are compared with the reference sensor that fits with the design recommendations of Microchip. The research is divided in two different parts, one corresponding to the design and working principles and the other one focusing on the development of the system and the obtained results. Two three-conductive layers designs are presented. Both of them present five reception electrodes and one transmission electrode. The studied parameters are the conductivity and relative permittivity for the different used inks as well as the thickness and relative permittivity of the fabrics. Moreover, the real capacitance values obtained for each individual electrode are presented and compared with the theoretical ones. The research also presents the sensitivity of each individual development and the results detecting gestures. Finally, a real-world application is presented, a mouse for a mobile phone.

4.2. Design and Working Principle

This section presents the design of the proposed system based on a 3D GestIC® sensor from Microchip Technology Inc. The 3D GestIC® sensor is a combination of a gesture Microchip controller and a set of sensor electrodes. Microchip's GestIC® is a 3D sensor technology which utilizes an electric field for advanced proximity sensing. Usually this sensor is made by using a PCB (Printed Circuit Board) technology on a rigid or flexible substrate normally of polymer materials [40].

4.2.1. Working Principle

The functioning of the sensor is based on the modification, in this case due to the proximity of hands, of the lines of an electric field. The variation of the distribution of the lines of the electric field is detected by a controller and interpreted by means of an algorithm, into different types of gestures that can be visualized conveniently. To generate a spatial electric field, i.e., in three dimensions, an electrode acting as an antenna is utilized. This electrode conducts an alternating signal and is usually named transmission electrode or Tx electrode. The behaviour of the non-radiative near field (reactive) of the electromagnetic fields dominates close to the transmitter. Using an electrode with a geometry much smaller than the wavelength and working close to the electrode, the magnetic component of the generated field is insignificant and there is no wave propagation. The electric component is quasi-static, enabling to detect possible conducting elements modifying the mentioned field with hands, fingers, etc. That is, if a person places their hands inside of the emitting area, a perturbation of the lines of the electric fields is created, due to the deviation of the lines to ground using the intrinsic conductivity of the human body. Using a series of reception electrodes, Rx electrodes, it is possible to determine the value and position in the electric field (Figure 36).

Microchip Technology's MGC3130 is a three-dimensional (3D) gesture recognition, motion tracking and approach detection controller based on Microchip's patented GestIC® technology for embedded usage. It enables user command input with natural hand and finger movements [41,42]. MGC3130 is able to generate a Tx signal of about 100

kHz, that corresponds to a wavelength of 3 km and has the capacity to acquire signals from 4 or 5 Rx electrodes. Using a sensor with electrodes in the 4 cardinal points and an electrode in the centre, this integrated circuit is able to recognize the variations and position of the perturbations of field that a hand produces in the delimited area over the sensor. The maximum range of detection is 15 cm in the perpendicular axis to the sensor. The central electrode is usually used as a touchpad and can be removed in case the sensor is only used to detect gestures. As aforementioned, the MGC3130 controller utilizes an algorithm to detect the following gestures: approach detection, position tracking in 3D, sensor touch (touch, multitouch, tap and double tap), flick gestures, circle gestures, and airwheel (Figure 37).

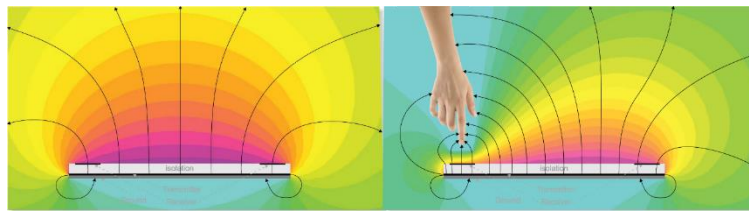


Figure 36. Field lines generated by the transmission Tx electrode. The reception Rx electrodes are located inside of the generated field. On the left side of the Figure, the field lines are shown when they are not modified by any conductor object. On the right side of the Figure, a hand is causing a modification of the field lines, leading to a variation in the signal received by the Rx electrodes. Source: Microchip Technology Inc.

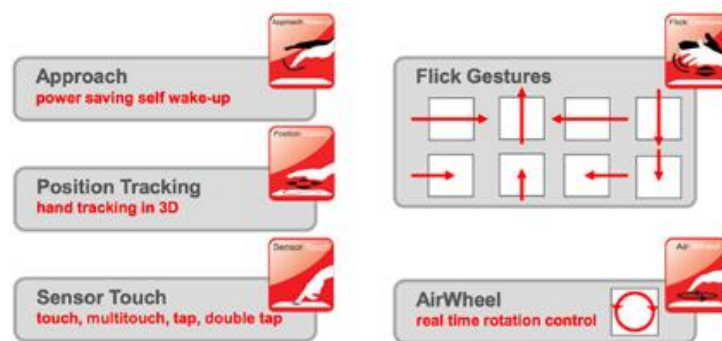


Figure 37. Gestures recognized by the internal algorithm of MGC3130: approach detection, position tracking in 3D, sensor touch (touch, multitouch, tap, and double tap), flick gestures, circle gestures, and airwheel. Source: Microchip Technology Inc.

The design suggested by Microchip [40] consists of a sensor made in rigid or double-sided flexible PCB (Printed Circuit Board), where the Rx electrodes are distributed on the four cardinal points of the upper face and on the centre. The Tx electrode is located on the underside. This design is used when the operation does not need a battery, and the electrical noise is low. When the external noise is high or the functioning uses a

battery, three layers are needed due to the addition of a ground plane. In the PCB designs, four conductive layers are implemented, leaving one of them with no use. In the case of utilizing a four layer design, the upper layer is used for Rx electrodes, the second internal layer for the Tx signal and the underside layer for the ground plane (Figure 38).

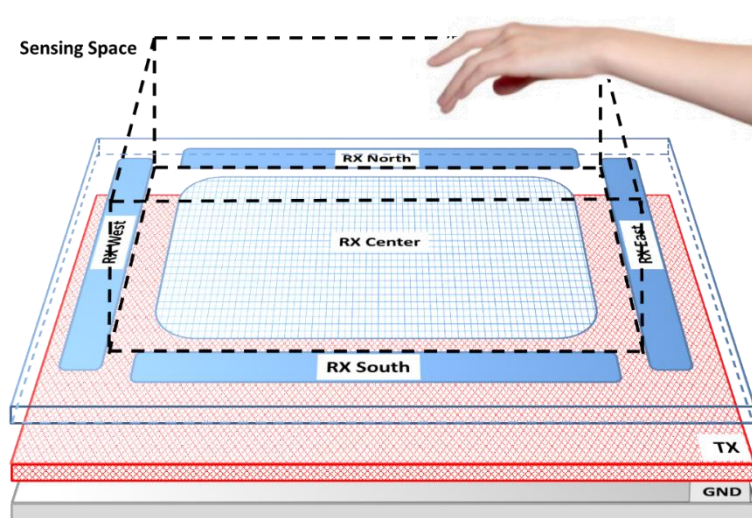


Figure 38. Standard sensor used by Microchip. It consists of a first layer where four Rx electrodes are located on each of the cardinal points as well as a central Rx electrode. This layer is separated from the bottom layer that contains the Tx electrode by a dielectric. The ground plane layer is optional and would be located below the Tx electrode layer. The sensitive area is just delimited by the four perimeter Rx sensors. Source: Microchip Technology Inc.

The Rx and Tx layers must be of conductive material such as copper but can be of indium-tin oxide (ITO) or similar. The electrode isolation can be made of any non-conductive material (FR4, glass, PET, etc.). Microchip proposes two designs [40] for MGC3130, of different and compatible sensors:

- Standard sensor (Tx signal amplitude of 2.85 V). Useful for small or medium-sized devices and mandatory for devices with a weak connection to ground, that is, with battery.
- Booster sensor (Tx signal amplitude between 5 and 18 V) allowing bigger sensors and recognition ranges.

Figure 39 shows the block diagram of the MGC3130 controller. It consists of the analogue front-end unit connected to the Tx and Rx electrodes, the signal processing unit that receives data from the front-end and is assisted by a GestIC library and, finally, a communication interface for the data interconnection between MGC3130 and another microcontroller.

The MGC3130 controller is parameterizable, that is, it can be reconfigured for each type of sensor and application. Thus, the most important part of the design of this system is the sensor characterization. It can be used to detect hand movements or only finger movements, influencing in the size of the sensor. This research uses the hand, which can be used in parallel, perpendicularly or with a certain angle to the sensitive area. The sensitive area is always defined inside of the four cardinal Rx electrodes. The geometrical form of the sensitive area is a key factor. This depends on the electrode geometry but also on the electrode location. For the design of the sensor, it is necessary to have some knowledge of its electrical parameters (shown in Figure 40). This electrical model allows us to evaluate the characteristics of the system and points out the dependencies between the electrodes, the MGC3130 controller and the hand. In particular, the capacitances of the electrodes which are coupled to the input/output sections of the MGC3130 integrated circuit.

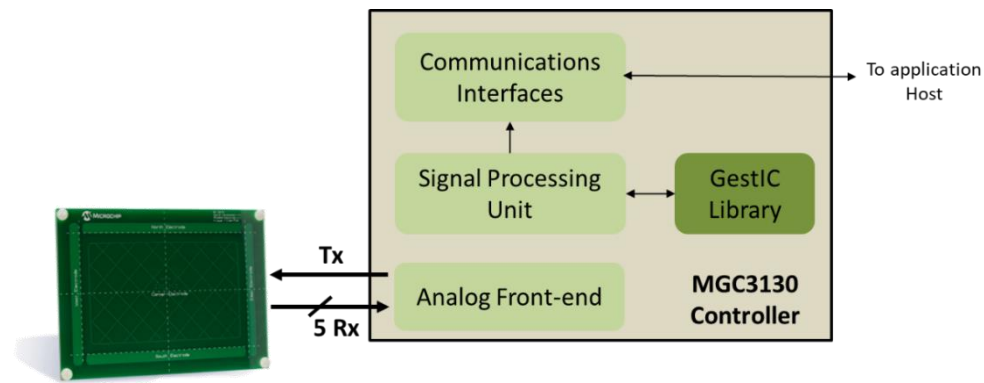


Figure 39. MGC3130 Block Diagram, composed of an analog front-end module that allows to generate the transmission Tx signal and receive the signals from the 5 Rx electrodes. The signals, properly processed, are transferred to the Signal Processing Unit that, together with the GestIC library, processes and converts them into the different programmed gestures. Lastly, there is a communication block with a host. Source: Microchip Technology Inc.

The output signal, V_{Tx} , is found on the Tx pin of the MGC3130 integrated circuit, whose capacitance to ground is C_{TxG} . e_{Tx} and e_{Rx} represent the transmission and reception electrodes. The parameterization of the corresponding circuit is based on the C_{RxTx} , C_{RxG} , and C_L capacitances. C_{RxTx} is the capacitance between the Tx and Rx electrodes, C_{RxG} is the capacitance between the Rx electrode and ground and C_L is the coupled capacitance between the transmission Tx pin and the Rx reception line. Finally, C_H is the capacitance between the hand and the Rx electrode. C_H is represented as a variable capacitor, since the corresponding capacitance depends on the hand and its position regarding the Rx electrodes. The e_{Rx} reception electrode measures the electric field potential. When a conductive object, like a hand, interacts with the electric field, the C_H capacitance of the reception electrode changes in the range of femtofarads and the cor-

responding variation is detected by the MGC3130 integrated circuit. The embedded table in Figure 40 shows the typical range of these capacitances.

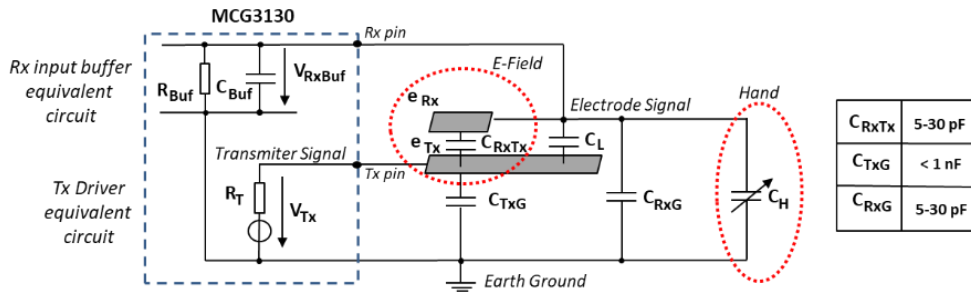


Figure 40. Equivalent simplified circuit of the combination sensor-MGC3130. Source: Microchip Technology Inc.

4.2.2. Microchip Sensor Design

The sensor can have different sizes and shapes, such as square, circular, oval, or rectangular, as long as the 1:3 length to width ratio is not exceeded. Microchip recommends a maximum of 140×140 mm (or a 140 mm diameter) and a minimum of 20×20 mm (diameter of 20 mm). The sensor must have a minimum of two layers but can be made with three layers: Rx on the upper layer, Tx on the bottom layer and, if necessary, GND as a third layer [40].

Figure 41 shows a typical design. On the upper layer, the four perimeter electrodes can be observed, as well as the optional central electrode, whereas the Tx electrode is located on the bottom layer. The size of the Rx electrodes determines the sensitive area. These Rx electrodes must always remain delimiting the aforementioned sensitive area to obtain the maximum resolution for the x, y, and z coordinates.

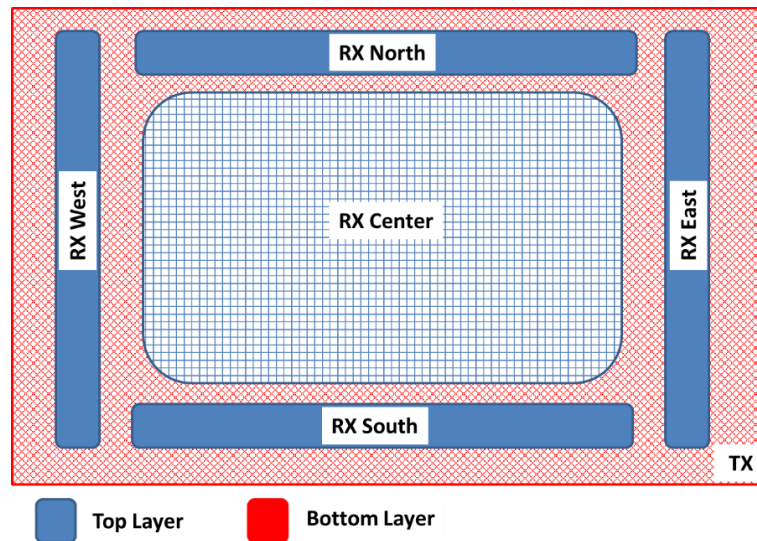


Figure 41. Basic scheme of the gesture sensor recommended by Microchip. Source: Microchip Technology Inc.

With the aim of obtaining a high sensitivity in the sensitive area, the area of the reception electrodes and the hand should be of the same order of magnitude. Hence, the four Rx electrodes of the cardinal points should have a lengthened shape to increment the coupling between the Rx electrodes and the hand. If the recognition range must be symmetric in both directions, the electrode design must be symmetric. In any case, the length of both vertical and horizontal electrodes must be balanced. The recommended distance between the Rx electrodes is of 1 to 5 mm. The most influential factor of the sensitivity to the hand is the width of the perimeter Rx electrodes. The bigger the width of the electrode is, the higher the sensitivity is. The receiver signal sensitivity measures the influence of the hand capacitance when a hand approaches the system. As a consequence, the Rx signal changes in presence of a hand, deviating from a reference value. The value of the deviation is measured and named Signal Deviation. It is the basis for the recognition of gestures [41]. Microchip references the signal deviation obtained in MGC3130 with respect to the distance of the hand compared with the width of the Rx electrodes (Figure 42). Logically, the larger the distance of the hand on the sensitive area is, the less the signal deviation is. The width of the electrode also influences the signal deviation. The wider the Rx electrode is, the greater the signal deviation is. However, an increase in the area of the Rx electrode implies a limitation in the range of gesture recognition. A best practice is to choose an Rx electrode width between 4% and 7% of the length. Moreover, an overly large Rx electrode causes higher capacitance between Rx and Tx and also between Rx and the ground. As a result of that, a loss of signal sensitivity is produced.

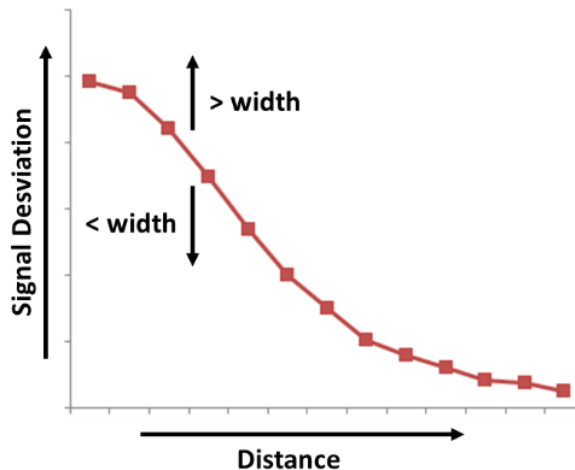


Figure 42. Variation of signal deviation received by Rx in function of the distance of the hand to the sensor and of the Rx electrode width.

In the case of the central Rx electrode, a meshed design is recommended. The mesh design increases the sensitivity due to the reduction of the effective area of the Rx electrode and to the coupling to the Tx electrode. An acceptable value for the mesh would be around 5% and 20%.

The C_{RxGND} capacitance must be as low as possible. That is, the distance between the Rx electrodes and ground must be as high as possible.

Regarding the Tx electrode, it must be located under the Rx electrodes and must have a shape and size to cover all the reception area. On the other hand, the Tx electrode must have a low coupling with the Rx electrodes (C_{RxTx}) and with ground (C_{TxG}). To reduce the C_{RxTx} capacitance, the distance between the Tx and the Rx electrodes must be as long as possible. The optimum distance between these two layers (t) will depend on the relative permittivity (ϵ_r) of the isolation material between both layers. Microchip recommends a $t > \epsilon_r/5$, hence, for a FR4 material (glass-reinforced epoxy laminate material $\epsilon_r = 5$), the thickness can be of 1 mm, for plastic ($\epsilon_r = 3$), it can be of 0.6 mm and, for glass ($\epsilon_r = 6$), it can be of 1.2 mm. Microchip recommends a minimum value between 1 to 2.5 mm, a value of 50% to 100% of the Rx electrode width being considered optimal. In any case, the calculated thickness will be the minimum one, achieving a better response as this distance increases.

Regarding the C_{TxGND} capacitance, it cannot be greater than the conductive capacitance of MGC3130 that is 1 nF. To reduce it, the Tx electrode must have a large surface and a meshed design of between 20% and 50% of the surface. When the C_{TxGND} capacitance is not low enough, an operational amplifier (op-amp) must be inserted between the Tx pin and the Tx electrode (Figure 43). Lastly, Microchip recommends an overlap

between the Tx electrode and the external edges of the Rx electrodes greater than 3 mm (Figure 44).

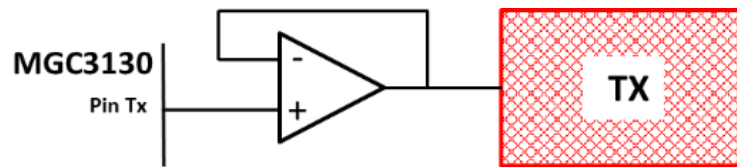


Figure 43. An op-amp buffer must be inserted between the Tx pin and the Tx electrode in case C_{TxGND} is greater than 1 nF. Source: Microchip Technology Inc.

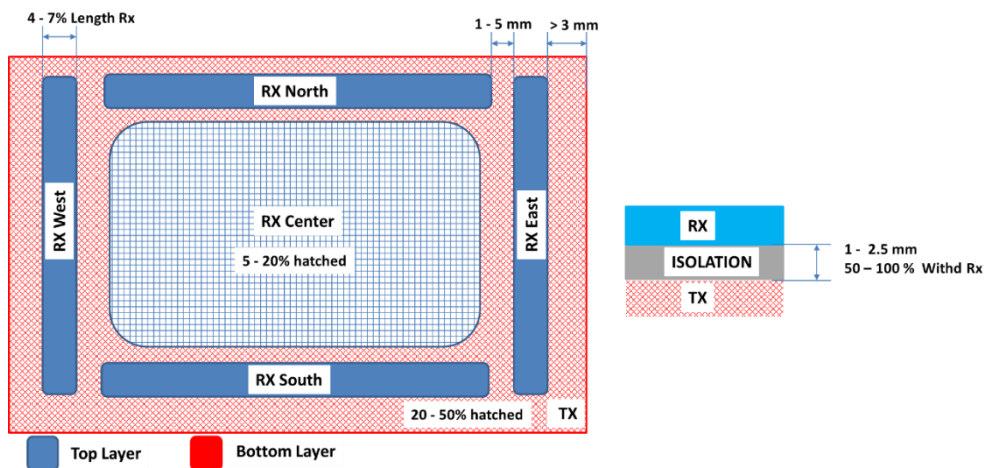


Figure 44. Basic design parameters recommended by Microchip. Source: Microchip Technology Inc.

Apart from the Rx and Tx layers, a third layer, GND, must be added in case of systems with no battery in high noise environments or in case of battery operation. When the system operates with batteries, this GND layer is mandatory but, in systems with ground connection, this layer is optional. In any case, the GND layer confers stability and noise immunity but at the expense of losing sensitivity, between 10% and 20%. As aforementioned, the C_{TxGND} capacitance must be lower than 1 nF. To achieve this, the thickness between the Tx and GND layers must be increased using materials with a greater relative permittivity and mesh design.

The Rx and Tx electrodes are not only limited to the sensitive area of the sensor but are also formed by the conductive lines that join these electrodes with the MGC3130 controller. Hence, these conductive lines influence the gesture detection as well. For this reason, these lines must be designed with as shorter length as possible, inside of the sensitive area and, if possible, with a distance from the Tx electrode larger than 0.15 mm.

Before proceeding with the design of the sensor with a textile, a study of the sensor of Microchip was performed. The reference sensor had a sensitive area of 95 x 60 mm with a size of 120 x 85 mm. This study helped with the validation of the results obtained with the textile version. The sensor characteristics are shown in Figure 45.

The PCB (Printed Circuit Board) follows a four layers design. The Rx electrodes are located on the upper layer, the second layer (internal) is not used, the third layer (internal) contains the Tx electrode, and the bottom layer includes the GND plane. The dielectric between the conductive layers is of FR4 material. The cross distribution of the PCB is shown in Figure 46. The relative permittivity (ϵ_r) of FR4 is considered to be 4.8.

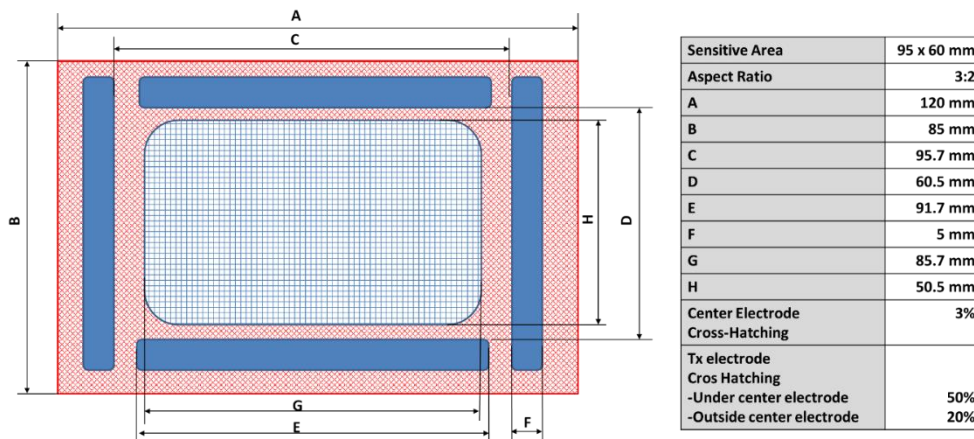


Figure 45. General characteristics of the 95 × 60 sensor from Microchip.
Source: Microchip Technology Inc.

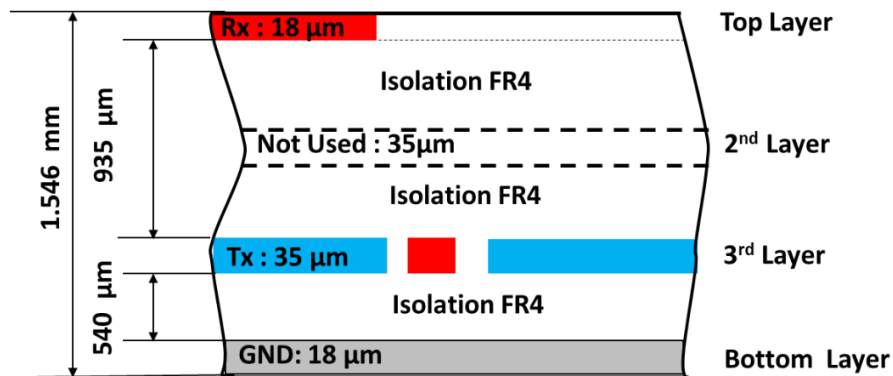


Figure 46. Crosscut of the PCB of the 95 x 60 sensor; dimensions and number of layers.
Source: Microchip Technology Inc.

Table 9 shows the different values obtained for C_{TxRx} . The range acceptable by Microchip for this capacitance oscillates between 5 and 30 pF. The value for this PCB provided by Microchip is shown as well. Note the higher value corresponding to the central electrode due to its larger area.

Table 9. Values of C_{TxRx} [5–30 pF].

	l (mm)	w (mm)	t (mm)	Microchip (pF)	Value (pF)
R _{xN}	91.7	5.0	0.935	20.00	33.92 ± 10.67
R _{xS}	91.7	5.0	0.935	20.00	34.66 ± 10.69
R _{xE}	70.5	5.0	0.935	18.00	30.09 ± 10.60
R _{xW}	70.5	5.0	0.935	18.00	30.62 ± 10.61
R _{xC}	85.7	50.5	0.935	65.00	68.22 ± 11.36

Table 10 shows the different values obtained for C_{TxGND} . The value for this capacitance acceptable by Microchip is lower than 1 nF.

Table 10. Real values of C_{TxGND} [<1 nF].

	l (mm)	w (mm)	t (mm)	Microchip (pF)	Value (pF)
Tx	120	85	0.540	590.00	635.00 ± 22.70

Table 3 shows the different values obtained for C_{RxGND} . The range for this capacitance acceptable by Microchip oscillates between 5 and 30 pF.

Table 11. Values of C_{RxGND} [5–30 pF].

	l (mm)	w (mm)	t (mm)	Value (pF)
R _{xN}	91.7	5	0.1512	34.31 ± 10.68
R _{xS}	91.7	5	0.1512	33.19 ± 10.66
R _{xE}	70.5	5	0.1512	30.30 ± 10.60
R _{xW}	70.5	5	0.1512	30.17 ± 10.60
R _{xC}	120.0	85	0.1512	62.85 ± 11.25

Figure 47.a shows the Tx signal generated by MGC3130, in this case of frequency 115 kHz and amplitude 2.84 V. Figure 47.b shows the signal received from one of the Rx electrodes when there is no object on the sensitive area modifying the electrical field. As expected, the frequency is 115 kHz, but the amplitude of the received signal is 1.82 V. Figure 47.c shows the same Rx signal but introducing an object in the sensitive area. The amplitude of the signal varies up to 2.18 V.

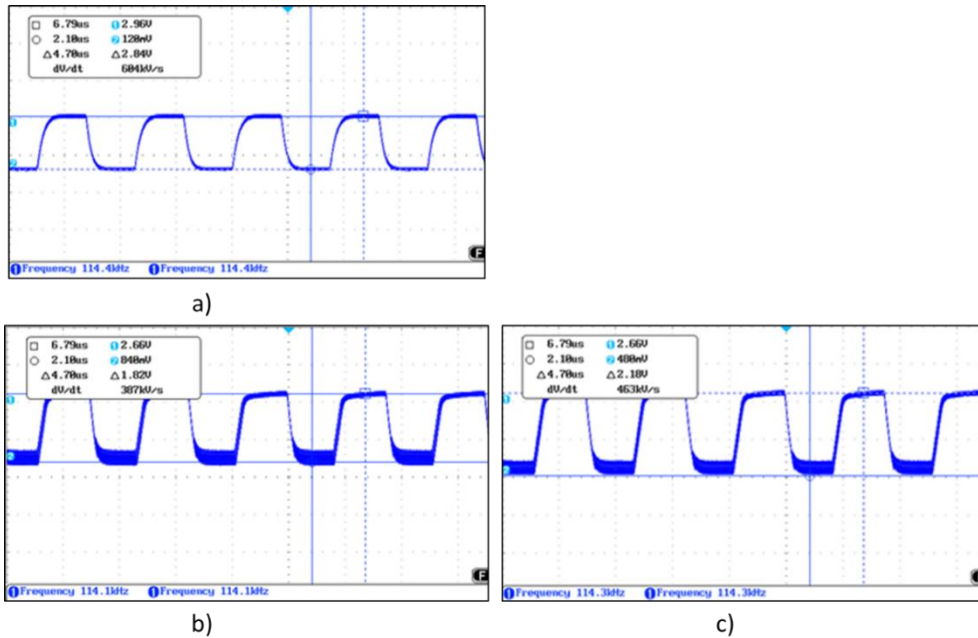


Figure 47. (a) Waveform of the transmission signal, (b) the received Rx signal with no object modifying the field lines, (c) the received Rx signal with an object modifying the field lines.

4.2.3. Textile 3D Gesture Sensor Design

Starting from the design data for the sensitive electrodes from Microchip, several of our own designs have been developed based on textile substrates. A similar design to Microchip PCB has been made but using the textile substrate as the dielectric layer.

The manufacturing technology used to implement this type of sensor was based on serigraphic technology of thick film. The screen-printing process consists of forcing pastes of different characteristics over a substrate through some screens using squeegees. Openings in the screen define the pattern that will be printed on the substrate by serigraphy. The final thickness of the pastes can be adjusted by varying the thickness of the screens. In the same way as for a PCB manufacturing, conductive materials and dielectric materials have been employed. Conductive silver ink has been employed to make the electrodes. In the case of the dielectrics, textile, dielectric inks, and polyurethane plastic films have been the materials used.

Different types of textiles have been selected in function of the material used for their manufacturing. The aim is to study their relative permittivity as well as their thickness. Both parameters influence in the value of the associated capacitances as analysed previously.

For each design, type of textile, and inks, measures of their physical and electrical parameters have been taken. The C_{TxRx} , C_{RxGND} and C_{TxGND} capacitances have been measured as well.

The first design made, named 3DS-1, is shown in Figure 13. It consists of a ground plane layer (Figure 48.a), a layer containing the Tx electrode and the connection lines of Rx with MGC3130 (Figure 48.b), a dielectric layer provided with vias that allow the connection between the Rx layer and the Rx connection lines (Figure 48.c), and the Rx electrode layer with 4 perimeter electrodes and one central (Figure 48.d). The dimensions of the sensor are identical to the 95×60 sensor from Microchip explained previously. In this design, the connection lines of the Rx electrodes have been placed on the transmit layer to minimize interferences.

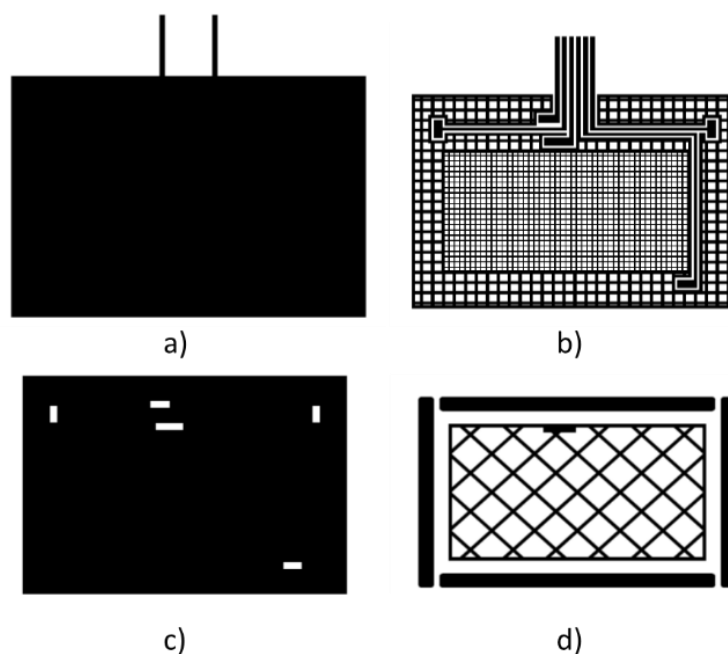


Figure 48. 3DS-1 design with four layers: (a) ground plane layer, (b) transmission Tx electrode, (c) dielectric layer between Rx and Tx layers and vias, (d) Rx electrode layer.

Figure 49 shows the cross-section of the sensor. The complete structure contains 5 layers since the textile substrate is used as a dielectric layer between the ground plane layer and the Tx electrode layer. The different layers, except the substrate, are screen-printed. Silver ink was employed for the conductive materials. Dielectric inks were used in the case of the dielectric layer between the Rx electrode layer and the Tx electrode layer. With this design, high capacitances are obtained out of the range recommended by Microchip for use with MGC3130. In part, this is due to the solution em-

ployed for the dielectric with worse performance than expected. This will be discussed in the Results Section.



Figure 49. Cross-section of the 3DS-1 sensor. In addition to the 4 layers shown in Figure 48 the textile substrate between the ground plane layer and the Tx electrode layer can be observed.

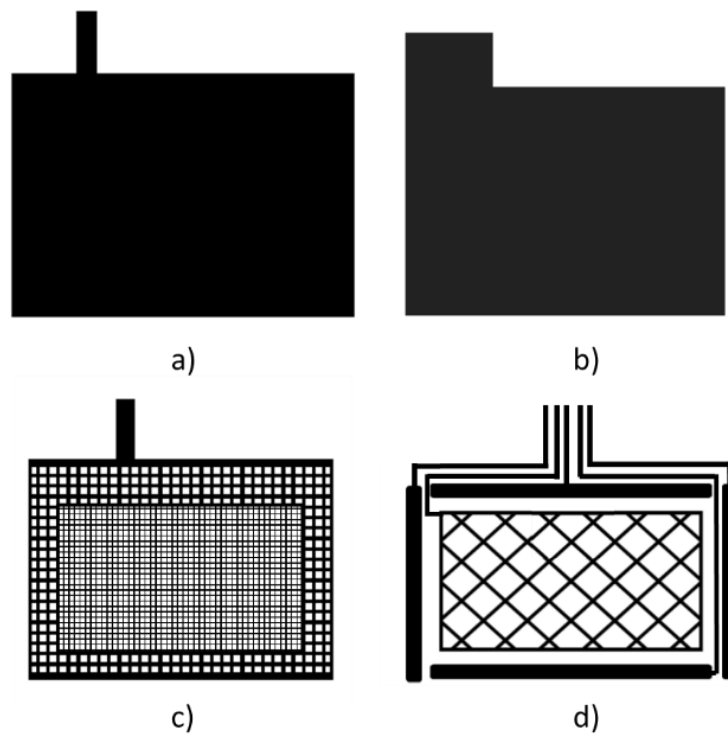


Figure 50. 3DS-2 design with four layers. Ground plane layer (a). Dielectric layer between Tx and ground layer (b). Transmission Tx layer (c). Rx layer (d).

The second design made, named 3DS-2, is shown in Figure 50. It consists of a ground plane layer (Figure 50.a), a dielectric layer between the ground plane layer and the Tx layer (Figure 50.b), a layer containing the transmission Tx electrode (Figure 50.c) and a layer with the reception Rx electrodes (Figure 50.d). The textile substrate acts as a dielectric between Rx and Tx layers. In this case, making the vias on the textile sub-

strate is not viable. Hence, the connection lines between the Rx electrodes and MGC3130 have been made on the same Rx layer. This design allows us to decrease the C_{TxRx} and C_{RxGND} capacitances since it is possible to utilize a textile substrate with a high thickness.

Figure 51 shows the cross-section of the sensor. The complete structure contains 5 layers since the textile substrate is used as a dielectric layer between the Rx electrode layer and the Tx electrode layer. The different layers, except the substrate, are screen-printed employing silver ink for the conductive materials and dielectric inks in the case of the dielectric layer between the Rx electrode layer and the Tx electrode layer. The main problem of this design comes from the alignment of the connection lines. The use of a textile substrate makes it difficult for the correct alignment of the Rx and Tx layers. For this reason, a final design with a different connector position was proposed to solve this problem. The design is shown in Figure 51.



Figure 51. Cross-section of the 3DS-2 sensor. In addition to the 4 layers shown in Figure 50, the textile substrate between the Rx layer and the Tx electrode layer can be observed.

Both designs have been developed with 8 different types of textiles (Table 12 and Table 13). The aim is to determine the influence of the thickness and the relative permittivity of the textiles on the sensor. Each one of the employed textiles have been characterized physically and electrically.

Regarding the inks, one conductive silver ink (Table 14) and three types of dielectric inks have been employed (Table 15). The inks influence noticeably the final capacitance at a thickness level as well as at a relative permittivity level. Heat sealed polyurethanes (

Table 16) have been employed as well in some sensors as substitutes of the dielectric inks.

Once the different sensors were built, they have been characterized electrically by means of the determination of their C_{TxRx} , C_{RxGND} , and C_{TxGND} capacitances. Lastly, the sensitivity of the different sensors has been determined using a graphical user interface software from Microchip, AUREA.

4.3. Materials and Methods

4.3.1. Materials


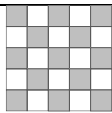
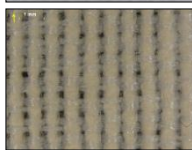
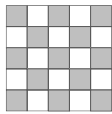
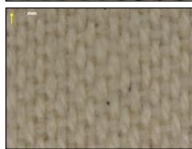
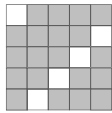

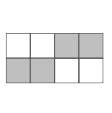
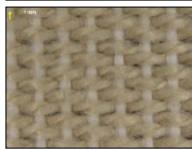
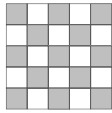
Different cotton, polyester and mixed fabrics with different fabric densities, yarn diameter, and weave have been used. Table 12 and Table 13 show the main characteristics of the fabrics used.

The conductive ink (Table 14) used is silver IPC-603X from INKRON (Kutojantie, Espoo, Finland).

Three dielectric inks (Table 15) with different flexibility and stretchability characteristics have been used. The inks are 127-48D from CREATIVE (Lamesa, Texas, USA), DI-7542 from EMS (Delaware, Ohio, USA) and IPD-670 from INKRON.

Two polyurethane films (Table 16) have been used. The films are EU94DS from DELSTARD and UAF445 from ADHESIVE FILMS.

Table 12. Fabric characteristics (I): composition and ligament.

Fabric	Picture	Weft Material	Warp Material	Ligament
Type A 100% Polyester		Polyester	Polyester	Taffeta 
Type B 50% Cotton 50% Polyester		Cotton	Polyester	Taffeta 
Type C 100% Cotton		Cotton	Cotton	Twill 
Type D 100 % Cotton		Cotton	Cotton	Teleton 
Type E 100% Polyester		Polyester	Polyester	Taffeta 


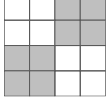
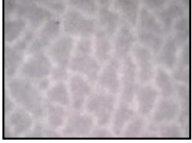

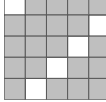

Type F 100 % Cotton		Cotton	Cotton	Teleton	
Type G Polyurethane		Polyurethane	Polyurethane	Non-woven	
Type H 100% Cotton		Cotton	Cotton	Twill	
Type I Polyurethane		Polyurethane	Polyurethane	Non-woven	

Table 13. Fabric characteristics (II): size and weight characteristics.

Fabric	Weft Density (Thread/cm)	Warp Density (Thread/cm)	Fabric Density (Thread/cm ²)	Wire Weft Diameter (μm)	Wire Warp Diameter (μm)	Thickness (μm)	Grammage (g/m ²)
Type A	24	38	62	300	300	110 ± 08	112 ± 4
Type B	13	26	39	450	450	380 ± 07	181 ± 1
Type C	26	34	60	300	300	470 ± 20	235 ± 2
Type D	10	28	38	400	400	530 ± 10	312 ± 5
Type E	10	22	32	350	350	570 ± 11	226 ± 4
Type F	7	24	31	450	450	700 ± 19	324 ± 2
Type G	-	-	-	-	-	720 ± 15	75 ± 1
Type H	20	20	40	360	360	920 ± 11	105 ± 3
Type I	-	-	-	-	-	1300 ± 16	152 ± 5

Table 14. Silver ink characteristics.

INKRON IPC-603X	
Sheet Resistivity(mΩ/sq/mil)	<15
Solids (%)	100
Viscosity (Pas)	16 @0.25 s ⁻¹
Curing	130° C– 15 min

Properties	<ul style="list-style-type: none"> • High Stretchability • Flexible
------------	---

Table 15. Dielectric ink characteristics.

	CREATIVE 127-48D	EMS DI-7542	INKRON IPD-670
Viscosity (Pas)	15–20	7 @0.05 s ⁻¹	32 @2.5 s ⁻¹
Screens polyester [threads/inch]		156-305	
Curing	125° C – 60 min	0.5 J/cm ²	130° C–15 min
Properties	<ul style="list-style-type: none"> • Flexible 	<ul style="list-style-type: none"> • Flexible • UV-Cure 	<ul style="list-style-type: none"> • Stretchable

Table 16. Polyurethane characteristics.

	DELSTAR EU94DS	ADHESIVE FIMS UAF-445
Thickness (µm)	80	120
Weight (g/m ²)	94	-
MVTR* upright (g/m ² /24 h)@37° C	400	-
Tensile Strength MD** (gf/cm)	3000	-
Elongation at break MD** (%)	700	450

* Moisture vapor transmission rate (MVTR), **Machine direction (MD).

4.3.2. Sensor Development

Manufacturing technology used was based on serigraphic technology of thick film. The screen-printing process consists of forcing pastes of different characteristics over a substrate through some screens using squeegees. Openings in the screen define the pattern that will be printed on the substrate by serigraphy. The final thickness of the pastes can be adjusted by varying the thickness of the screens. When screen-printing technology is used, it is necessary to manufacture frames with screen mesh for the design.

The screen for the conductors was a 230 mesh polyester material (PET 1500 90/230-48 from Sefar) and the screen for dielectric layer was a 76 mesh polyester material (PET 1500 30/76-120 PW from Sefar). Afterwards, to transfer the pattern to screen mesh, a UV film Dirasol 132 from Fujifilm was used. The final screen thickness was 74 µm for the screen for conductors and 217 µm for the screen for the dielectric. The patterns were transferred to the screen by using a UV light source unit IC-5000 from BCB.

Printing was carried out by using E2XL from EKRA screen-printer with a shore 75° hardness squeegee, 60° squeegee angle, 1 mm snap-off, 3.5 bar force, and 100 mm/s.

After the deposition of the inks, these were cured in an air oven FED-115 from BINDER at 130° C for 15 min in order to use the same curing characteristics for all inks. In the case of DI-7542 from EMS a UV oven Ncure-Lab/Static 120 from EneMaq was used with 0.5 J/cm².

The polyurethanes have been heat sealed on the fabrics with a DCH-100 heatpress from Microtec at 130° C for 60 s.

4.3.3. Measurements

The capacitance between electrodes was measured at 100 kHz with a KEYSIGHT U1733C LCR meter.

The relative permittivity (ϵ_r) measures were carried out with a Hewlett Packard 4263A LCR meter. The following measurement accessories were used: Hewlett Packard 16089B Kelvin Clips Leads and a Yokogama-Hewlett Packard 16451A Dielectric Test Adaptor. The LCR meter was configured to measure a tension level of 1V, with an average of 64 samples and a low read rate (Level = 1 V, Avg = 64, Meas Time= Low). The measurement mode was Cp and D (parallel capacity and loss tangent). The capacity measurements were taken at three different parts of the fabric with a 4-frequency scan (0.1 kHz, 1 kHz, 10 kHz, and 100 kHz). The ϵ_r value was obtained directly from the Cp value.

The measurements of the thickness of the fabric were taken at 4 different points using a Mitutoyo CP calibre CD-6" with a 10 μ m resolution.

Macroscopic images were taken with a LEICA MZ APO stereomicroscope.

4.4. Results and Discussion

In the 3DS-1 design, the dielectric layer between the Rx electrodes and the Tx electrode must mandatorily be a screen-printed layer of dielectric ink, since this layer contains the connection traces. Implementing these traces with vias in a layer made with textile is practically impossible. Thus, in this design, the substrate textile can be used as the dielectric layer between Tx layer and GND layer (Figure 52.a). The textile provides its physical and electrical characteristics, or it can only be utilized as the base substrate (Figure 52.b) where it only contributes with its physical characteristics. Figure 53 shows the final sensor, the appearance being the same in both of the implemented structures.

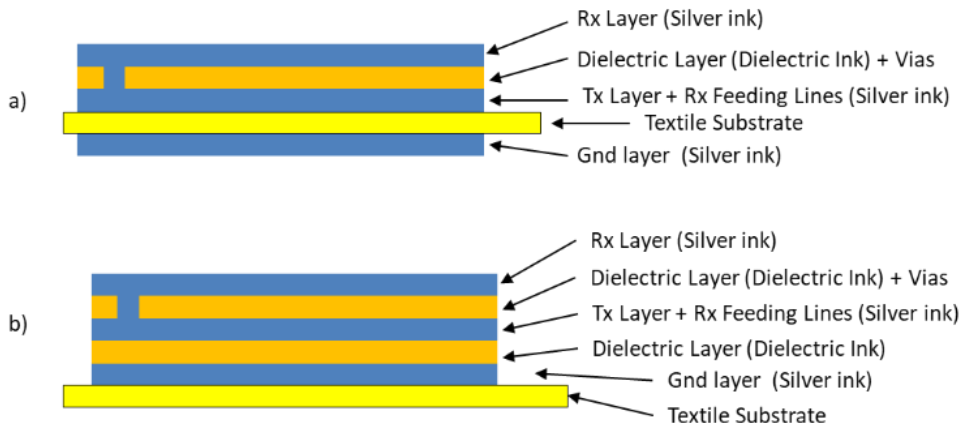


Figure 52. 3DS-1 Design with two construction structures: (a) the textile substrate acting as a dielectric between the Tx electrode and the ground plane (sensor name 3DS_1a) and (b) the textile substrate acting as a mere base (sensor name 3DS_1b).

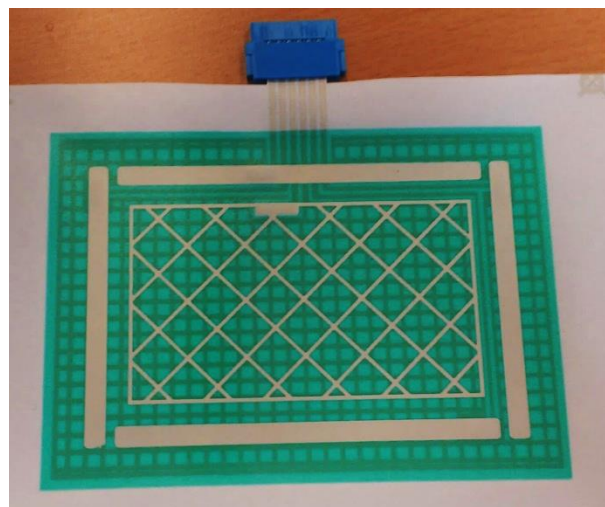


Figure 53. 3DS-1 Sensor.

As aforementioned, the C_{RXTx} , C_{TxG} , and C_{RxG} capacitances must be of a low value and within a very concrete range. Once the dimensions of the areas of these capacitors are fixed, there are only two parameters to be modified to achieve a low capacitance. These parameters are the layer thickness and the relative permittivity. For this reason, the three selected dielectrics have been characterized looking for the one with the lowest relative permittivity. Regarding the layer thickness, a large thickness would be desirable. To increment the thickness, the physical parameters of the screen-printing must be

varied. The mesh must be low in the screen to augment the quantity of ink to be printed and several layers must be screen-printed successively to increase the thickness. Table 17 shows the relative permittivities of the three available inks, where CREATIVE 12-48D presents the lowest relative permittivity. The right column shows the minimum thickness recommended by Microchip to achieve an appropriate value of C_{RxTx} . These large values of thicknesses cannot be obtained using screen-print techniques.

Table 17. Relative permittivity of the dielectric inks ϵ_r @100 kHz.

Dielectric	Relative Permittivity	$t > \epsilon_r/5$ (μm)
CREATIVE 127-48D	1.72	344
EMS DI-7542	5.68	1136
INKRON IPD-670	4.20	840

A first prototype with type A substrate was implemented to characterize the sensor. Two sensors were implemented: a sensor named 3DS-1a-TA and another one named 3DS-1b-TA. To be able to estimate the capacitances using theoretical calculus, the value of the relative permittivity of the textiles is needed. Table 18 shows the determined values. The right column shows the minimum thickness recommended by Microchip to achieve an appropriate value of C_{RxTx} , considering the permittivity obtained from the textiles. Type A textile is located well below the limit; Type C textile is located below as well, and the rest are on the limit or exceed it widely.

Table 18. Relative permittivity of fabrics ϵ_r @100 kHz.

Fabric	Relative Permittivity	Thickness (μm)	$t > \epsilon_r/5$ (μm)
Type A	2.37	110 ± 8	474
Type B	1.93	380 ± 7	386
Type C	2.58	470 ± 20	516
Type D	2.64	530 ± 10	528
Type E	1.37	570 ± 11	274
Type F	2.65	700 ± 19	530
Type G	1.42	720 ± 15	284
Type H	3.41	920 ± 11	680
Type I	1.64	1300 ± 16	328

Table 19 shows the different values obtained from 3DS-1a-TA for C_{TxRx} , C_{RxGND} , and C_{TxGND} . The average dielectric thickness obtained between the Rx and Tx layers is 20 μm . Type A textile has an average thickness of 110 μm . The average thickness between Rx and GND is 135 μm .

Table 19. Capacitance values of 3DS-1a-TA (pF).

C_{TxRxN}	229.6 ± 14.6
C_{TxRxS}	261.9 ± 15.2
C_{TxRxE}	210.1 ± 14.2

C_{TxRxW}	254.3 ± 15.1
C_{TxRxC}	554.9 ± 21.1
C_{RxNGND}	219.7 ± 14.4
C_{RxSGND}	258.8 ± 15.2
C_{RxEGND}	202.8 ± 14.0
C_{RxWGND}	242.4 ± 14.8
C_{RxCGND}	449.6 ± 19.9
C_{TxGND}	1990.0 ± 13.9

Table 20 shows the different values obtained from 3DS-1b-TA for C_{TxRx} , C_{RxGND} , and C_{TxGND} . The average dielectric thickness obtained between Rx and Tx layers is 40 μm . The average thickness between Tx layer and GND is 60 μm . The average thickness between Rx layer and GND is 100 μm .

Table 20. Capacitance values of 3DS-1b-TA (pF).

C_{TxRxN}	301.0 ± 16.0
C_{TxRxS}	354.6 ± 17.1
C_{TxRxE}	276.0 ± 15.5
C_{TxRxW}	326.2 ± 16.5
C_{TxRxC}	716.2 ± 24.3
C_{RxNGND}	296.4 ± 15.9
C_{RxSGND}	357.2 ± 17.1
C_{RxEGND}	274.1 ± 15.5
C_{RxWGND}	317.9 ± 16.3
C_{RxCGND}	671.8 ± 23.4
C_{TxGND}	3430.0 ± 16.9

The capacitances obtained with the 3DS-1a-TA sensor as well as with 3DS-1b-TA, widely exceed the margins recommended by Microchip. This is fundamentally due to the fact that the reached thicknesses with the screen-printed dielectric layers do not achieve the minimum values recommended by Microchip. These high capacitance values affect the input and output signals from/to the controller. Figure 54 shows the waveforms from the 3DS-1a-TA sensor. The transmission signal (Figure 54.a) presents a deformation due to a capacitance of $C_{TxGND} > 1\text{nF}$. If a buffer operational amplifier is coupled between the Tx pin and the Tx electrode, a regenerated signal is obtained (Figure 54.b). Figure 54.c shows the receiving Rx signal with direct connection between the Tx pin and the Tx electrode. Figure 54.d shows the receiving Rx signal with an AO between the Tx pin and the Tx electrode. The results obtained with the 3DS-1b-TA sensor are very similar to those obtained with the PCB reference sensor (Figure 47).

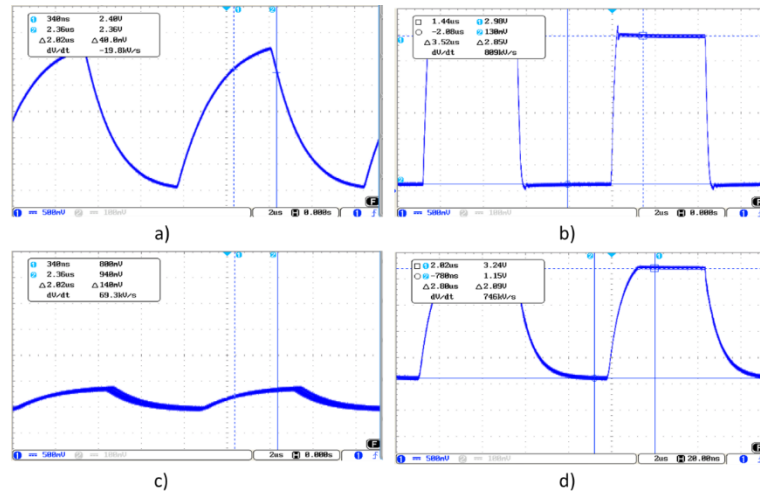


Figure 54. Transmission signal waveform (a), a signal deformation can be observed due to a capacitance of $C_{TxGND} > 1nF$. Regenerated signal obtained coupling an AO between the Tx pin and the Tx electrode (b). Receiving Rx signal with direct connection (c) between the Tx pin and the Tx electrode. Receiving Rx signal with AO (d) between the Tx pin and the Tx electrode.

These capacitance values out of the recommended range have forced the use of the 3DS-2 sensor. This sensor allows us to modify the thickness as well as the relative permittivity of the dielectric Rx-Tx since the textile substrate is used as dielectric (Figure 51). When studying the response using the same textile substrate (Type A) but in 3DS-2 configuration, a significant reduction of the capacitance values is observed (Table 21), although the values are still out of the range recommended by Microchip. This high value out of the range comes from the yet insufficient dielectric thickness, since the type A textile has a thickness of 110 µm. For this reason, textiles with a noticeably higher thicknesses have been employed, between 380 and 1300 µm. In this design, the connection lines of the Rx electrodes with the connector are located on the same layer as the Rx electrodes. Thus, the lines influence the total capacitance. In the case of the North electrode, the connection line is out of the sensitive area and has least influence, getting a lower capacitance with respect to the rest.

Table 21 . Capacitance values of 3DS-2-TA (pF).

C_{TxRxN}	97.2 ± 11.9
C_{TxRxS}	132.4 ± 12.6
C_{TxRxE}	114.5 ± 12.2
C_{TxRxW}	110.9 ± 12.2
C_{TxRxC}	188.1 ± 13.7
C_{RxNGND}	95.1 ± 11.9
C_{RxSGND}	129.0 ± 12.5
C_{RxEGND}	111.6 ± 12.2
C_{RxWGND}	108.5 ± 12.1
C_{RxCGND}	178.6 ± 13.5
C_{TxGND}	1915.0 ± 48.3

The rest of the textiles were fabrics with large thicknesses and presented much roughness. This led to problems with the printing of the conductive and dielectric inks. A couple of samples are presented in Figure 55. On the left, a printing on a type D textile can be observed, and, on the right, a printing on a type E textile. In both textiles, the conductive ink is not uniformly distributed on the textile, leading to very high resistance values, or even infinite, i.e., open circuits or with no electrical continuity. This problem appears on Type B, C, D, E, and F textiles, but on the contrary, in Type G, H, and I, it is possible to screen print the conductive silver ink with no errors of continuity.

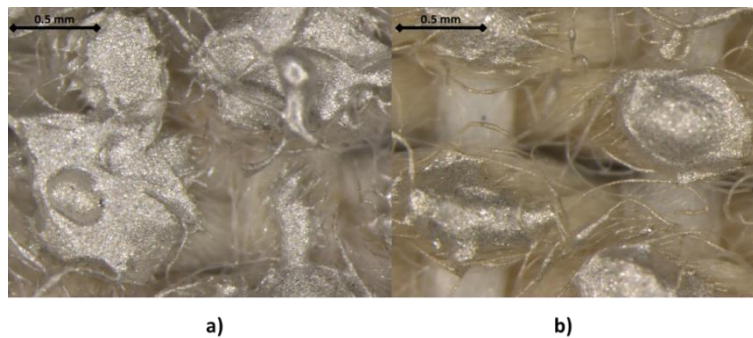


Figure 55. 25× Magnified view of the printing of the conductive ink on the Type D textile (a) and on the Type E textile (b).

This problem can be solved modifying the surface of the textile to soften the roughness. The modification consists of the printing of a dielectric layer on the textile or the heat sealing of a polyurethane film. In the case of the printing of a dielectric layer, the three available dielectrics have been used on each one of the textiles. Later, a conductive silver ink layer was printed to check if there is any improvement in the result of the printing. Figure 56 shows the result of the printing of the different dielectric inks: (a) Type D textile with dielectric Creative 127-48D and a layer of silver ink, (b) Type D

textile with dielectric EMS DI-7542 and a layer of silver ink, (c) Type D textile with dielectric INKRON IPD-670 and a layer of silver ink, (d) Type E textile with dielectric Creative 127-48D and a layer of silver ink, (e) Type E textile with dielectric EMS DI-7542 and a layer of silver ink and (f) Type D textile with dielectric IPD-670 and a layer of silver ink.

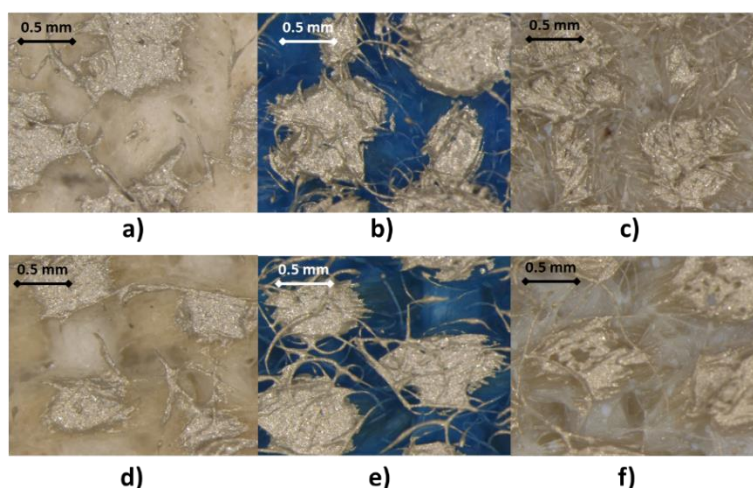


Figure 56. 25× Magnified view of the printing of the dielectric and conductive inks on: (a) Type D textile with dielectric Creative 127-48D and a layer of silver ink, (b) Type D textile with dielectric EMS DI-7542 and a layer of silver ink, (c) Type D textile with dielectric INKRON IPD-670 and a layer of silver ink, (d) Type E textile with dielectric Creative 127-48D and a layer of silver ink, (e) Type E textile with dielectric EMS DI-7542 and a layer of silver ink and (f) Type D textile with dielectric IPD-670 and a layer of silver ink.

The problem of the lack of continuity in the conductive tracks could not be solved with the dielectrics. This led to the use of heat sealable polyurethanes on the different textiles. Specifically, EU94DS from Delstar Inc., and UAF-445 from Adhesive Films. These polyurethanes (Table 16) can help to improve the capacities of the sensor providing a larger layer thickness (80 μm in the case of EU94DS and 120 μm the case of UAF-445). In addition, they can improve the relative permittivity. Table 22 shows the permittivities measured for each one of the used polyurethanes. The printing of the conductive ink on the textiles covered with polyurethanes is perfect.

Table 22. Relative permittivity of the polyurethanes.

	DELSTAR EU94DS	ADHESIVE FILMS UAF-445
ϵ_r @100 kHz	1.46	1.86

With the employment of the polyurethanes, the structure of the 3DS-2 sensor changes depending on the textiles. For Type G, H, and I textiles, the structure of Figure 57.a (named 3SD_2a) has been employed and for Type B, C, D, E, and F textiles, the structure of Figure 57.b (named 3SD_2b) has been employed.

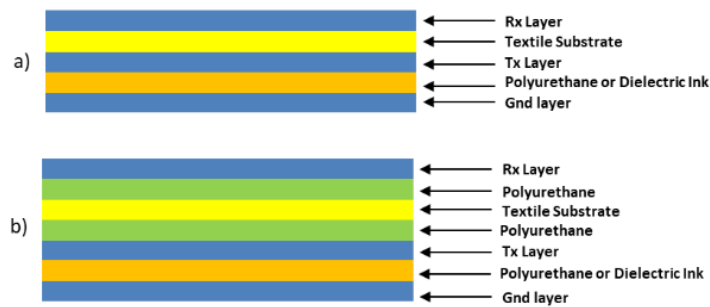


Figure 57. 3DS-2 Design with two construction structures: (a) the textile substrate acting as a dielectric between the Tx electrode and Rx electrode (sensor named 3SD_2a) and (b) the textile substrate covered with polyurethane (sensor named 3SD_2b).

Figure 58 shows the final aspect of one of the sensors made, concretely the 3DS-2a sensor with Type I textile (named 3DS-2a-TI).

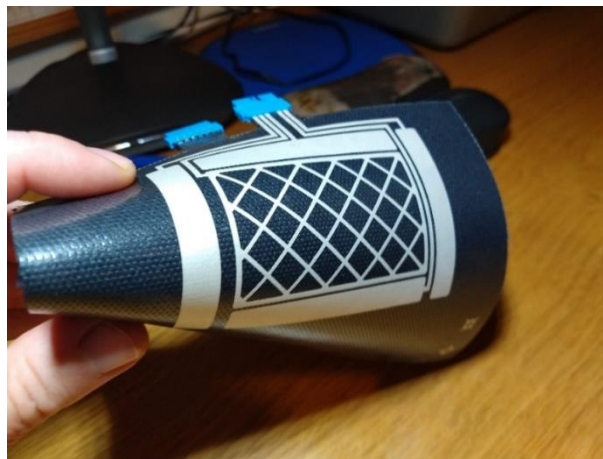


Figure 58. Sensor 3DS-2a.

Table 23 shows the values of the capacitances associated to each one of the types of developed sensors. A remarkable decrease of the capacitance values can be noticed. This is due to the increase of the thickness of the substrates and the values of the relative permittivities. The sensor that most met expectations was 3DS-2a-TI with very low

values of C_{TxRx} and C_{RxGND} capacitances, far below the recommended limit by Microchip. Regarding the value of the C_{TxGND} capacitance, it is situated above the recommended value ($<1nF$). It can be solved inserting an op-amp between the Tx pin and the Tx electrode as recommended by Microchip.

Table 23. Capacitance values of 3DS-2a and 3DS-2b (pF).

	3DS-2b-TB	3DS-2b-TC	3DS-2b-TD	3DS-2b-TE	3DS-2b-TF	3DS-2a-TG	3DS-2a-TH	3DS-2a-TI
C_{TxRxN}	37.4 ± 10.7	38.4 ± 10.7	32.1 ± 10.6	37.4 ± 10.7	29.4 ± 10.6	30.8 ± 10.6	28.9 ± 10.6	15.1 ± 10.3
C_{TxRs}	48.1 ± 10.9	46.0 ± 10.9	40.3 ± 10.8	48.2 ± 10.9	37.8 ± 10.7	43.3 ± 10.9	39.7 ± 10.8	19.3 ± 10.4
C_{TxRe}	39.2 ± 10.7	38.4 ± 10.7	32.9 ± 10.6	38.4 ± 10.7	31.5 ± 10.6	34.1 ± 10.7	32.2 ± 10.6	15.1 ± 10.3
C_{TxRw}	39.6 ± 10.7	36.4 ± 10.7	33.1 ± 10.6	41.4 ± 10.8	29.6 ± 10.5	36.7 ± 10.7	29.6 ± 10.6	16.1 ± 10.3
C_{TxRc}	77.6 ± 11.5	76.4 ± 11.5	63.5 ± 11.2	83.5 ± 11.6	62.8 ± 11.2	64.9 ± 11.3	62.1 ± 11.2	34.7 ± 10.7
C_{RnGND}	37.2 ± 10.7	34.4 ± 10.6	30.6 ± 10.6	37.2 ± 10.7	27.2 ± 10.5	30.6 ± 10.6	28.5 ± 10.6	15.1 ± 10.3
C_{RsgND}	47.7 ± 10.9	52.1 ± 11.0	41.2 ± 10.8	45.8 ± 10.9	35.4 ± 10.7	42.8 ± 10.9	36.8 ± 10.7	19.5 ± 10.4
C_{ReGND}	39.0 ± 10.7	44.3 ± 10.8	32.6 ± 10.6	38.0 ± 10.7	29.1 ± 10.5	33.8 ± 10.7	30.1 ± 10.6	15.1 ± 10.3
C_{RwGND}	39.4 ± 10.7	36.4 ± 10.7	32.0 ± 10.6	42.6 ± 10.8	28.6 ± 10.5	36.4 ± 10.7	29.3 ± 10.6	16.1 ± 10.3
C_{RcGND}	76.8 ± 11.5	71.5 ± 11.4	61.4 ± 11.2	80.2 ± 11.6	60.1 ± 11.2	63.8 ± 11.3	61.8 ± 11.2	34.5 ± 10.7
C_{TxGND}	2488.1 ± 59.8	2595.2 ± 61.9	1842.2 ± 46.8	2137.0 ± 52.7	2590.0 ± 61.8	1553.1 ± 41.1	2122.0 ± 52.4	2327.0 ± 56.5

Figure 59 shows the waveform of the 3DS-2a-TI sensor. Figure 59.a shows the Tx signal with a buffer OA inserted between the Tx pin and the Tx electrode due to the value of C_{TxGND} , greater than 1 nF. Figure 59.b shows the signal in one of the Rx electrodes when there is no object modifying the electrical field. The Tx signal was the original with no buffer. Figure 59.c shows the same Rx signal after inserting the buffer in the path of the Tx signal.

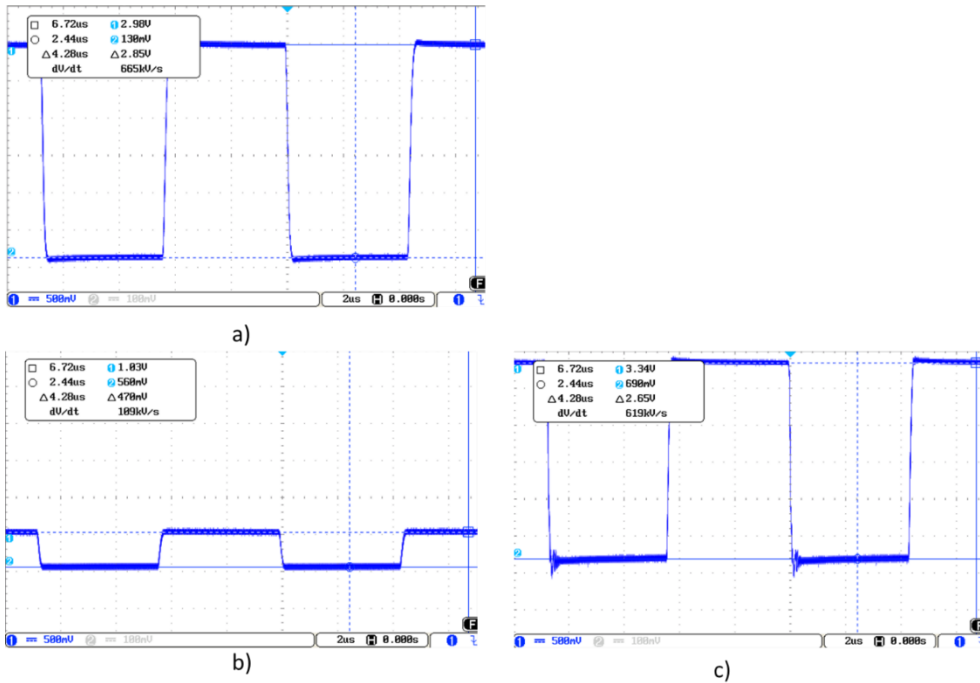


Figure 59. Waveform of the transmission signal (a) with buffer due to the capacitance $C_{TXND} > 1nF$, (b) receiving RX signal with direct connection between the Tx pin and the Tx electrode and (c) receiving RX signal with op-amp between the Tx pin and the Tx electrode.

Microchip provides the AUREA graphical user interface that allows for characterizing the sensors. The sensitivity is, maybe, the most important parameter of these sensors. Microchip [43] provides an “artificial hand”, a $40 \times 40 \times 70$ mm styrofoam ($\epsilon_r \approx 1$) cube covered with an adhesive copper sheet. This block must be connected to ground to simulate the conditions of the human body. To determine the sensitivity, the block is placed at different distances from the surface of the sensor using blocks of styrofoam of different thicknesses (1, 2, ... cm) (Figure 25). AUREA allows us to read the obtained data. Figure 26 shows a representation of the data. It can be observed that as the associated capacitances increase, the signal deviation decreases for the same distance to the surface. The 3DS-2a-TI sensor presents the best sensitivity. The sensitivity is even better than the one of the PCB’s sensor from Microchip, due to the low value of their associated capacitances.

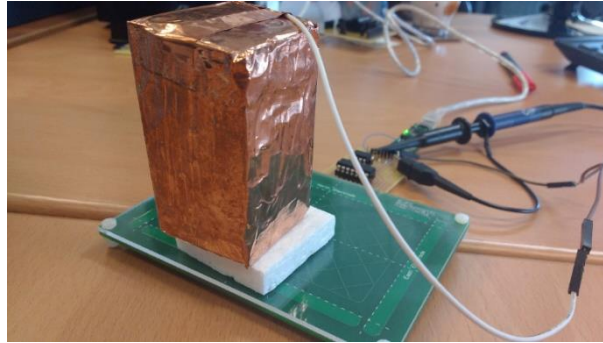


Figure 60. “Artificial hand” provided by Microchip. It is made of styrofoam covered by copper and connected to ground. Some blocks of styrofoam with no covering allow to move the “artificial hand” away from the sensor.

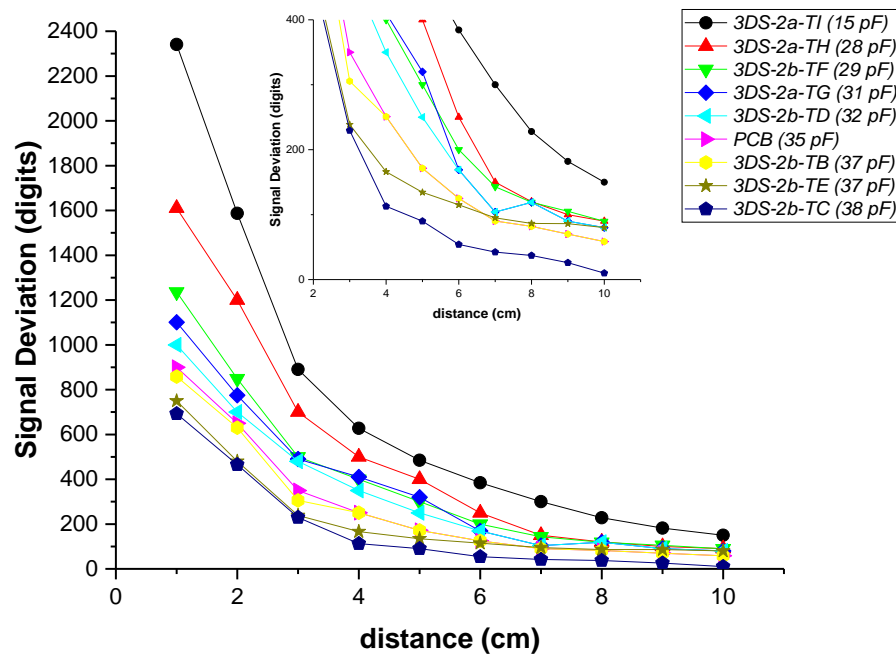


Figure 61. Signal Deviation of the different sensors in function of the distance of the hand from the surface of the sensor. The C_{TxRxN} value, in brackets in the legend, has been included as a reference to assess the relationship between capacitance and sensitivity. This relationship is the same in any of the associated capacities.

It would be convenient to be able to determine the value of the associated sensor capacities prior to their manufacturing. Thus, only those textiles that achieve capacities below 30 pF would be utilized in the sensors.

Two theoretical values have been calculated, the nominal theoretical value (C_n) calculated with Equation 1 and the edge effect capacitance value (C_{edge}). This latter value considers the effect of the field lines around the edges of the capacitor and can be calculated according to Equations 2 and 3.

$$C = \varepsilon_r \cdot \varepsilon_0 \frac{L \cdot w}{t} \quad (1)$$

$$C = \frac{\varepsilon_0 \cdot \varepsilon_r \cdot (L + \Delta f) \cdot (w + \Delta f)}{t} \quad (2)$$

$$\Delta f = t + \frac{\varepsilon_0 \cdot t \cdot 10 \cdot \ln((L + w) + 1)}{\pi} \quad (3)$$

where C is the value of the capacitance in pF, L is the length in cm, w is the width in cm, t is the thickness in cm, ε_r is the relative permittivity, and ε_0 is the vacuum permittivity (8.85×10^{-12} F/m).

A comparative study has been made with the North electrode. This electrode is the one with less influence of the capacitances associated to the Rx conduction lines to the connector. Table 24 shows the values of the theoretical capacities and the real C_{TxRx} value measured with an LCR meter. In general, the theoretical results are validated by the real ones. The C_{edge} value is very close to the real one in all the cases. Thus, it is possible, knowing the relative permittivity of each textile and its thickness, to deduct the value of its associated capacitances prior to the sensor manufacturing.

Table 24. Values of C_{TxRx} : theoretical nominal capacity (C_n), with Edge effect (C_{edge}) and real values (C_{real}) (pF).

	C_n	C_{edge}	C_{real}
3DS-2b -TB	32.4	35.7	37.4 ± 10.7
3DS-2b -TC	30.3	33.7	38.4 ± 10.7
3DS-2b -TD	25.2	28.7	32.1 ± 10.6
3DS-2b -TE	23.0	25.6	37.4 ± 10.7
3DS-2b -TF	17.7	20.5	29.4 ± 10.6
3DS-2a -TG	27.1	30.7	30.9 ± 10.6
3DS-2a -TH	29.3	33.3	28.9 ± 10.6
3DS-2a -TI	8.9	10.9	15.1 ± 10.3

The following figures show the frames of a video with some gestures that the controller can recognize: Figure 62. Approach detection, Figure 63. Flick north to south, Figure 64. Flick west to east and Figure 65. Airwheel.

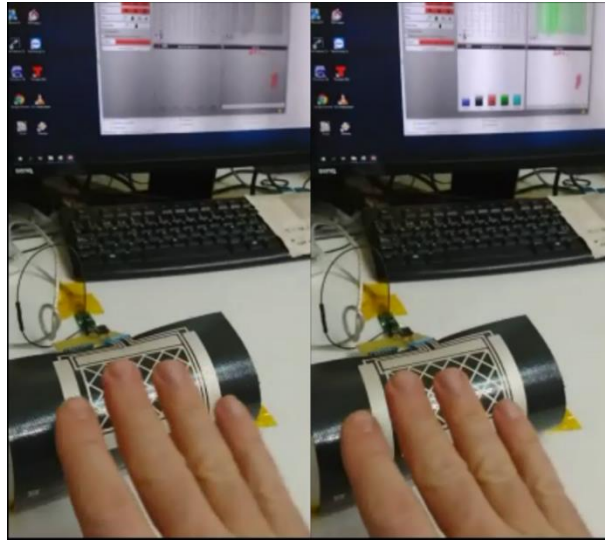


Figure 62. Approach detection.



Figure 63. Flick north to south.

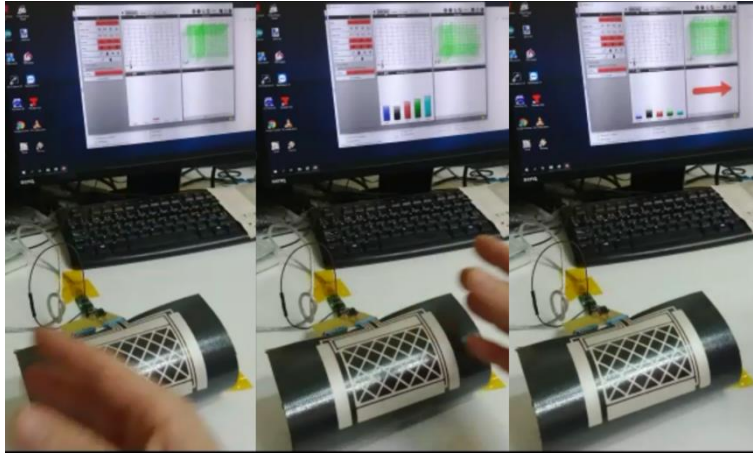


Figure 64. Flick west to east.

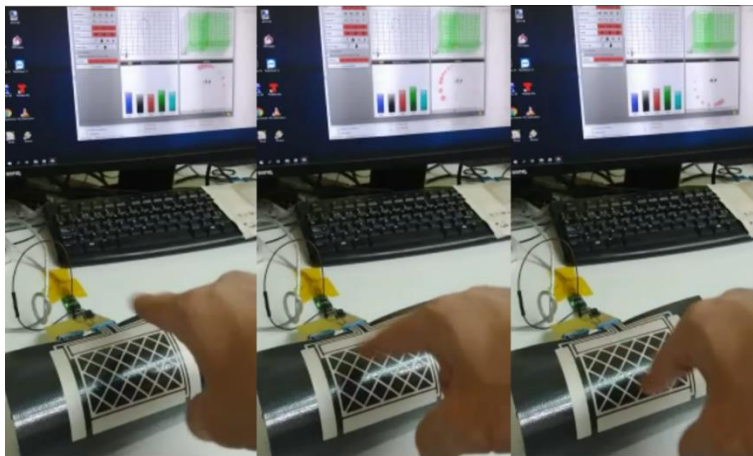


Figure 65. Airwheel.

A Bluetooth portable system has been developed to be used with mobile devices (Figure 66). The system is configured with the AUREA application and the configuration parameters are saved in the portable device. To check the functioning, it is connected to an Android device as wireless mouse as shown in Figure 67.

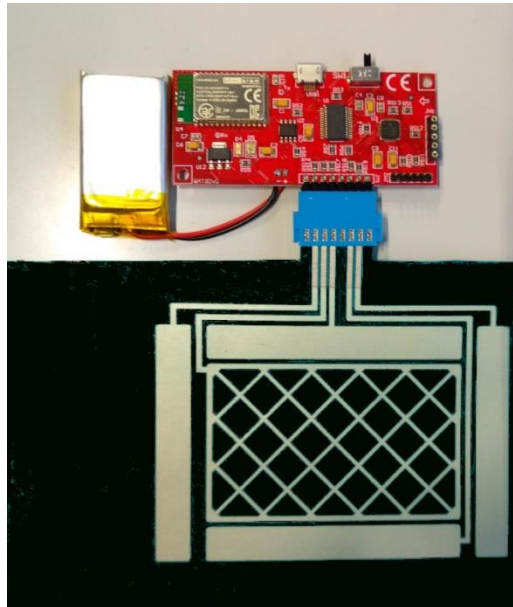


Figure 66. Complete portable system.

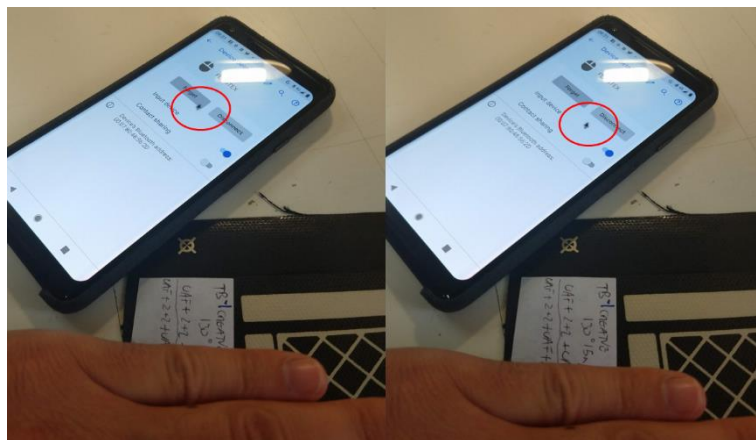


Figure 67. 3D Sensor used as a Wireless mouse with a mobile phone.

4.5. Conclusions

The aim of this research was to obtain a wearable textile 3D gesture recognition sensor based on the Microchip 3D GestIC® sensor design. The fundamental parameters of that sensor design are the capacitance between transmission and reception electrodes. The value of this capacitance depends fundamentally on the thickness of the substrate

and its relative permittivity. Therefore, the key to the design is to look for the best textile substrate materials. But the best textile material is not always the best material to be used with screen-printed technology. For this reason, a large proportion of the research has consisted of trying different fabrics. Fabrics are composed of different materials and, therefore, with different thickness and relative permittivity but also with different behaviour regarding silver and dielectrics inks. A flexible textile 3D sensor was developed after studying all these parameters.

That sensor was characterized in relation to its electrical parameters, namely its capacitances between electrodes, its thickness, and its sensitivity to the presence of a hand. The characteristics obtained were better than Microchip's PCB design and with the further advantage of its flexibility. The Microchip driver (MGC3XXX) incorporates a calibration procedure that can be programmed, for example, on stand-by periods. This allows the driver to adjust to the base signal according to the bending angle. This feature maximizes the advantage of using a flexible sensor.

We are currently working on the study of the variation of two important features of textiles, such as softness or permeability. The use of soft polyurethane films guarantees softness. Regarding the permeability, the addition of different layers reduces it. We are currently exploring different solutions such as microperforations and hole patterns. Lastly, we are preparing some experiments to determine the washing capacity of the sensor, due to the importance of washing in the textile area.

In conclusion, a 3D gesture sensor based on E-field change technologies has been developed to be used with textile substrates using a low cost and common textile industry printing technique: screen-printing. The system works on both flat and curved surfaces, which allows it to be used in several areas: clothes, automobile industry, healthcare, etc.

References

- 1 Chakraborty, B.K.; Sarma, D.; Bhuyan, M.K.; MacDorman, K.F. Review of constraints on vision-based gesture recognition for human-computer interaction. *IET Comput. Vis.* **2018**, *12*, 3–15.
- 2 Zhang, Z. Microsoft kinect sensor and its effect. *IEEE Multimed.* **2012**, *19*, 4–10.
- 3 Malinverni, L.; Pares, N. Learning of Abstract Concepts through Full-Body Interaction: A Systematic Review. *Educ. Technol. Soc.* **2014**, *17*, 100–116.
- 4 Lai, H.Y.; Ke, H.Y.; Hsu, Y.C. Real-time Hand Gesture Recognition System and Application. *Sens. Mater.* **2018**, *30*, 869–884.
- 5 Karim, R.A.; Zakaria, N.F.; Zulkifley, M.A.; Mustafa, M.M.; Sagap, I.; Latar, N.H.M. Telepointer technology in telemedicine: A review. *Biomed. Eng. Online* **2013**, *12*, 21.
- 6 Santos, L.; Carbonaro, N.; Tognetti, A.; González, J.; de la Fuente, E.; Fraile, J.; Pérez-Turiel, J. Dynamic gesture recognition using a smart glove in hand-assisted laparoscopic surgery. *Technologies* **2018**, *6*, 8.
- 7 Singh, A.; Buonassisi, J.; Jain, S. Autonomous Multiple Gesture Recognition System for Disabled People. *Int. J. Image Graph. Signal Process.* **2014**, *6*, 39–45.
- 8 Tan, C.W.; Chin, S.W.; Lim, W.X. Game-based human computer interaction using gesture recognition for rehabilitation. *Proc. - 2013 IEEE Int. Conf. Control Syst. Comput. Eng. ICCSCE 2013* **2013**, 344–349.
- 9 Rautaray, S.S.; Agrawal, A. Interaction with virtual game through hand gesture recognition. *Int. Conf. Multimedia, Signal Process. Commun. Technol. IMPACT 2011*, **2011**, 244–247.
- 10 Huang, Y.A.; Chen, P.; Chen, Y.; Tsau, S.; Wu, K. Employ Gesture Recognition Interface to Screen Operation in Cooking Scenario. *International Association of Societies of Design Research*, **2013**, 3973–3981.
- 11 Lavanya, K.N.; Shree, D.R.; Nischitha, B.R.; Asha, T.; Gururaj, C. Gesture controlled robot. *Int. Conf. Electr. Electron. Commun. Comput. Technol. Optim. Tech. ICECCOT 2017*, **2018**, 2018-Janua, 465–469.
- 12 Bach, K.M.; Jaeger, M.G.; Skov, M.B.; Thomassen, N.G. You can touch, but you can't look: Interactina with in-vehicle systems. *Conf. Hum. Factors Comput. Syst. - Proc.* **2008**, 1139–1148.

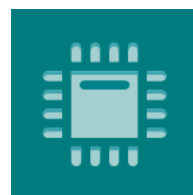
- 13 Ohn-Bar, E.; Trivedi, M.M. Hand gesture recognition in real time for automotive interfaces: A multimodal vision-based approach and evaluations. *IEEE Trans. Intell. Transp. Syst.* **2014**, *15*, 2368–2377.
- 14 Elliott, L.R.; Hill, S.G.; Barnes, M. Gesture-Based Controls for Robots: Overview and Implications for Use by Soldiers. *US Army Research Laboratory Aberdeen Proving Ground United States*, **2016**.
- 15 Khan, R.Z.; Ibraheem, N.A. Hand gesture recognition: A literature review. *Int. J. Artif. Intell. Appl.* **2012**, *3*, 161.
- 16 Shen, Z.; Yi, J.; Li, X.; Mark, L.H.P.; Hu, Y.; Wang, Z. A soft stretchable bending sensor and data glove applications. *2016 IEEE Int. Conf. Real-Time Comput. Robot. RCAR 2016* **2016**, 88–93.
- 17 Ferrane, A.; Jiang, X.; Maiolo, L.; Pecora, A.; Colace, L.; Menon, C. A fabric-based wearable band for hand gesture recognition based on filament strain sensors: A preliminary investigation. *2016 IEEE Healthc. Innov. Point-of-Care Technol. Conf. HI-POCT 2016* **2016**, 113–116.
- 18 Abraham, L.; Urru, A.; Normani, N.; Wilk, M.P.; Walsh, M.; O’Flynn, B. Hand tracking and gesture recognition using lensless smart sensors. *Sensors*, **2018**, *18*, 2834.
- 19 Zhang, Y.; Harrison, C. Tomo: Wearable, low-cost, electrical impedance tomography for hand gesture recognition. *UIST 2015 - Proc. 28th Annu. ACM Symp. User Interface Softw. Technol.* **2015**, 167–173.
- 20 Zeng, Q.; Kuang, Z.; Wu, S.; Yang, J. A method of ultrasonic finger gesture recognition based on the micro-doppler effect. *Appl. Sci.* **2019**, *9*, 2314.
- 21 Lien, J.; Gillian, N.; Karagozler, M.E.; Amihod, P.; Schwesig, C.; Olson, E.; Raja, H.; Poupyrev, I. Soli: Ubiquitous gesture sensing with millimeter wave radar. *ACM Trans. Graph.* **2016**, *35*, 142.
- 22 Sang, Y.; Shi, L.; Liu, Y. Micro hand gesture recognition system using ultrasonic active sensing. *IEEE Access* **2018**, *6*, 49339–49347.
- 23 Wang, W. Device-Free Gesture Tracking Using Acoustic Signals Motivation It is difficult to input on smart watches. *In Proceedings of the 22nd Annual International Conference on Mobile Computing and Networking*, **2016**, 82–94.

- 24 Nandakumar, R.; Iyer, V.; Tan, D.; Gollakota, S. Fingerio: Using active sonar for fine-grained finger tracking. *In Proceedings of the 2016 CHI Conference on Human Factors in Computing Systems*, **2016**, 1515–1525.
- 25 Ferri, J.; Lidón-Roger, J.; Moreno, J.; Martínez, G.; García-Breijo, E. A Wearable Textile 2D Touchpad Sensor Based on Screen-Printing Technology. *Materials* **2017**, *10*, 1450.
- 26 Nunes, J.S.; Castro, N.; Gonçalves, S.; Pereira, N.; Correia, V.; Lanceros-Mendez, S. Marked object recognition multitouch screen printed touchpad for interactive applications. *Sensors* **2017**, *17*, 2786.
- 27 Steiner, E. Fully Printed Transparent Capacitive Touchpads from PEDOT: PSS e. g. for Touchscreens—A Project of the HdM Stuttgart, Germany. *Int. Circ. Graph. Educ. Res.* **2016**, *9*, 18–26.
- 28 Ferri, J.; Fuster, C.P.; Llopis, R.L.; Moreno, J.; García-Breijo, E. Integration of a 2D touch sensor with an electroluminescent display by using a screen-printing technology on textile substrate. *Sensors* **2018**, *18*, 3313.
- 29 Cronin, S.; Doherty, G. Touchless computer interfaces in hospitals: A review. *Health Inform. J.* **2018**, *25*(4), 1325–1342.
- 30 Pitts, M.J.; Skrypchuk, L.; Attridge, A.; Williams, M.A. Comparing the user experience of touchscreen technologies in an automotive application. *AutomotiveUI 2014 - 6th Int. Conf. Automot. User Interfaces Interact. Veh. Appl. Coop. with ACM SIGCHI - Proc.* **2014**.
- 31 Aezinia, F.; Wang, Y.F.; Bahreyni, B. Touchless capacitive sensor for hand gesture detection. *Proc. IEEE Sensors* **2011**, 546–549.
- 32 Haslinger, L.; Wasserthal, S.; Zagar, B. A capacitive measurement system for gesture recognition. *Proc. Sens.* **2017**, 616–620.
- 33 Wimmer, R.; Holleis, P.; Kranz, M.; Schmidt, A. Thracker - Using capacitive sensing for gesture recognition. *Proc. - Int. Conf. Distrib. Comput. Syst.* **2006**.
- 34 Grosse-Puppendahl, T.; Holz, C.; Cohn, G.; Wimmer, R.; Bechtold, O.; Hodges, S.; Smith, J.R. Finding common ground: A survey of capacitive sensing in human-computer interaction. *In Proceedings of the 2017 CHI Conference on Human Factors in Computing Systems*, **2017**, 3293–3315.

- 35 Gotsch, D.; Zhang, X.; Burstyn, J.; Vertegaal, R. HoloFlex: A flexible holographic smartphone with bend input. *In Proceedings of the 2016 CHI Conference Extended Abstracts on Human Factors in Computing Systems*, **2016**, 3675–3678.
- 36 Han, J.; Gu, J.; Lee, G. Trampoline: A double-sided elastic touch device for creating reliefs. *In Proceedings of the 27th Annual ACM Symposium on User Interface Software and Technology*, **2014**, 383–388.
- 37 Cherenack, K.; Van Pieteron, L. Smart textiles: Challenges and opportunities. *J. Appl. Phys.* **2012**, 112.
- 38 Lymberis, A.; Paradiso, R. Smart fabrics and interactive textile enabling wearable personal applications: R&D state of the art and future challenges. *In Proceedings of the 2008 30th Annual International Conference of the IEEE Engineering in Medicine and Biology Society*, **2008**, 5270–5273.
- 39 Al-huda Hamdan, N.; Heller, F.; Wacharamanatham, C.; Thar, J.; Borchers, J. Grabrics: A Foldable Two-Dimensional Textile Input Controller. *In Proceedings of the 2016 CHI Conference Extended Abstracts on Human Factors in Computing Systems*, **2016**, 2497–2503.
- 40 Microchip. GestIC® Design Guide; DS40001716C; 2016; ISBN 978-1-5224-0477-4. Available online: <http://ww1.microchip.com/downloads/en/devicedoc/40001716c.pdf> (accessed on **2018**).
- 41 Microchip. MGC3030/3130 3D Tracking and Gesture Controller Data Sheet; DS40001667E; 2017; ISBN: 978-1-5224-1910-5. Available online: <http://ww1.microchip.com/downloads/en/DeviceDoc/40001667E.pdf> (accessed on 16 October **2018**).
- 42 Microchip. Programming MGC3030/3130 in Production; DS00001934A; 2015; ISBN 978-1-63277-397-5. Available online: <http://ww1.microchip.com/downloads/en/AppNotes/00001934A.pdf> (accessed on 16 October **2018**).
- 43 Microchip. Aurea Graphical User Interface User's Guide, DS40001681D; 2015; ISBN 978-1-63276-972-5. Available online: <http://ww1.microchip.com/downloads/en/DeviceDoc/40001681D.pdf> (accessed on 16 October **2018**).

Chapter 5

A Boosted Textile 3D Gesture Recognition Textile Sensor



sensors

Impact factor (2018): 3.031

Q1-Instruments & Instrumentation (2018)

5.1. Introduction

Textiles are everywhere; used as decoration, worn as protection, assembled as interior components in cars, or structural elements in constructions among others. Although normally, Textile Industry is considered a traditional sector, the new market demands innovations to distinguish it from the other competitors and meet the new requests of the market [1]. The evolution of Electronics and textile technologies have enabled the combination of their strengths, increasing computing speed, reducing chip size, improving energy autonomies and offering flexible surfaces. There exists an interest in new wearable solutions that can be directly worn on the curved human body or integrated in daily objects. Textiles offer some features appropriate to the human body, such as softness, comfortability and flexibility, and others that make them suitable to include electronics, since they can be stretched, compressed, twisted and deformed arbitrarily. In addition, they offer excellent integrity and structural behavior during daily wearing and washing.

One of the most challenging applications of electronic textiles is to analyze postures and gestures for different purposes. The corresponding posture and gesture sensors can be utilized for many applications, such as rehabilitation [2-4], sign language recognition [5,6], remote control [7] or medical applications [8] among others.

Many researchers have developed sensing technologies to meet the need of soft wearable devices. Some of them are focused on soft bending sensors based on specific materials to accommodate the flexible and deformable nature of the human body [9]. Elastic conductive webbing solutions [10] or highly flexible fabrics [11] have drawn some interest. These solutions are normally used as small pieces of material attached to cloths in a specific position. Other group of solutions are embedded in the fabric. These sensors combine different layers of both conductive and non-conductive textiles such as smart sleeves. These smart sleeves with deformable textiles enable the detection of a wide range of deformable gestures [12]. Other approaches present microfiber sensors by means of using fibers, such as dual-core conductive fibers working as a capacitive strain sensor, which can be sewed in a bandage or gloves [13], or more complex materials such as piezoelectric [14,15] or triboelectric [16,17] materials to create fiber strain sensors that can detect bending and torsion deformations. There are also solutions based on stretchable conductive threads that measure variations of resistance using materials such as reduced graphene oxide [18] or PEDOT [19] among others. All these previous solutions need to be attached to cloths or gloves to locate the sensors in specific positions to detect bending movements that sometimes could be obtrusive. As alternative solutions, some authors place the sensor on other external surfaces, obtaining touchless textile sensors used as an input to environmental control for individuals with upper-extremity mobility impairments [20] or multi electrode capacitive sensors that detect simple control gestures [21] by means of contactless sensing.

Some existing research in textile sensors focuses on the use of capacitive sensors. Textile capacitors can be made combining conductive materials that are acting as conduc-

tive plates separated by dielectrics. The conductive plates can be woven, sewn, and embroidered with conductive thread/fabrics, or they can be painted, printed, sputtered, or screened with conductive inks, or conductive polymers. The dielectrics used are typically foams, fabric spacers or non-conductive polymers [22,23]. Some works have achieved capacitive embroidered interdigitated structure used as moisture sensor [24], or conductive-knit fabric used as strain sensors [25]. Recently RFID antennas has been implemented using embroidery [26]. Other investigation studies the impact of the human body on a capacitive textile sensor concluding how the movement of the body can affect the capacitance [27].

Regarding capacitive textile sensors for gesture recognition, few references can be found in the literature. In [20], 12 textile conductive plates sewn in a fabric implement a textile touchless capacitive sensor. In our previous work, two capacitive sensors for the purpose of gesture recognition were presented [28]. In addition, the behavior and influence of different e-textile materials in the textile sensor were shown. The electrodes that conformed the structure of the standard sensor were printed on textiles substrates using screen printing technology. The different smart textiles prototypes presented were compared with a reference sensor.

In the present paper, an own boosted sensor design on a textile substrate is developed. It is based on the design recommended by Microchip. This boosted design presents fewer conductive layers and better performance than the standard one [29]. Although the boosted design needs higher voltage and more power than standard one, it is also sensitive to greater distance between the hand and the surface of the sensor. Three textile manufacturing technologies are used to implement this type of sensor with satisfactory results. A characterization of the sensors using a static artificial hand was performed. Subsequently, a validation was carried out with different subjects, measuring the detection rate after several gesture repetitions. The obtained prototypes present some features such as flexibility that makes them suitable to be attached into clothing or textiles surfaces such as armchairs, curtains or automotive upholstery.

5.2. Materials and Methods

The research is divided into two main parts, one corresponding to the design and working principles and the other one focusing on the development of the prototypes and the obtained results. Four resulting sensors were made considering the design recommendations of Microchip. The corresponding materials and technologies used are conductive ink screen printed, conductive thread embroidered, conductive fabric thermosealed and conventional PCB (printed circuit board) using a milling machine. The expected theoretical value of the associated capacities is studied considering the permittivity of the materials to be used as dielectric layers. Furthermore, the real capacitance values obtained for each individual electrode are presented and compared with the theoretical ones. Afterward, the sensitivity of each individual development is measured and compared with the standard versions. Next, a characterization of the sensors and a user

validation stage was carried out to assess their functioning. Moreover, an additional study of the response considering variations of temperature and humidity is presented. Finally, a complementary study of washability is given.

5.2.1. Electronic Design

Microchip Technology Inc. has developed a new technology for gesture recognition [23]. This feature is carried out by means of some specific devices, named MGC3130 and MGC3030, capable of sensing a series of hand or finger movements. These devices, in combination with some sensing electrodes and a gesture recognition algorithm, compose the GestIC® sensor. This sensor utilizes an electric field for advanced proximity sensing. Usually, this sensor is implemented using a PCB (Printed Circuit Board) technology on a rigid or flexible substrate, normally of polymer materials. The signals provided by the sensor are processed by the MGC3XXX devices. These devices utilize an algorithm to detect the position of the hand respect the sensor and the following gestures: approach detection, position tracking in 3D, sensor touch (touch, multitouch, tap and double tap), flick gestures, circle gestures, and airwheel.

The basic sensor design consists of 4 or 5 receiving electrodes (Rx) connected to the MGC3XXX Rx pins, 1 transmitting electrode (Tx) connected to the MGC3XXX Tx pin, and an isolation layer between Rx and Tx electrodes. Both electrodes, Rx and Tx, are implemented with conductive material such as copper, silver, etc. Regarding the isolation layer, it is made of any non-conductive material (FR4, glass, PET, etc.).

The sensor is based on the use of an electric field to sense proximity. The lines of the electric field are distorted when a hand or finger is placed in the free space above the sensor (Figure 68): The registered variation allows the system to detect, track or classify the motion resulting in a gesture visualized in a user interface application. The electrical field is generated by the application of an alternating signal conducted by an electrode that acts as an antenna. This produces an electrical field that propagates three-dimensionally around the surface. This electrode is named transmission electrode or Tx electrode. Its geometry is much smaller than the used wavelength, forcing the magnetic component to be practically zero with no wave propagation. Thus, quasi-static electrical near field is found, allowing the system to sense conductive objects, such as the human body. When a person places a finger on the sensor, it intrudes into the electrical field. The field lines are drawn to the finger and shunted to the ground using the intrinsic conductivity of the human body. This produces a distortion of the electrical field that is detected using some reception electrodes named Rx electrodes. Different Rx electrodes at different positions enable one to determine the origin of the perturbation and its value.

Microchip proposes two designs for the GestIC® sensors (Figure 68):

1. Standard sensor (Tx signal amplitude of 2.85 V). It is used in small or medium-sized devices (between 20 and 140 mm of width or length of the sensor). It is mandatory for devices with a weak connection to ground, that is, with bat-

tery. This Standard sensor consists of a top layer where four Rx electrodes are located on each of the cardinal points as well as a central Rx electrode. This layer is separated from the bottom layer, that contains the Tx electrode, by a dielectric. The ground plane layer is optional and would be located below the Tx electrode layer.

2. Boosted sensor (Tx signal amplitude between 5 and 18 V). It is used in systems with a large sensor size (even more than 200 mm of width or length of the sensor). In this case, the system must necessarily be grounded. This Boosted sensor consists of a top layer where four Rx electrodes are located on each of the cardinal points and a central Tx electrode. This layer is separated from the bottom layer that contains the GND plane by a dielectric. The sensitive area is just delimited by the four perimeter Rx sensors.

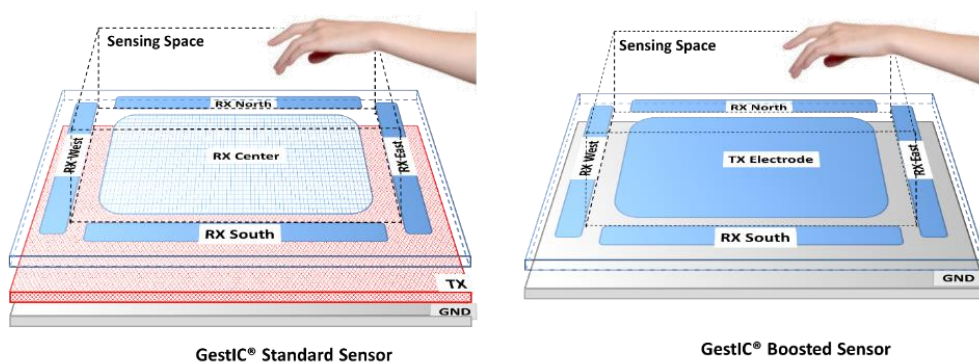


Figure 68. Standard (left) and Boosted (right) sensors used by Microchip. The standard version consists of 5 RX electrodes on top layer plus a TX electrode on an inner layer. The boosted version has 4 RX and 1 TX electrodes on the top layer. The sensing space is the same in terms of area but is lower in volume in the case of the standard version. Source: Microchip Technology Inc.

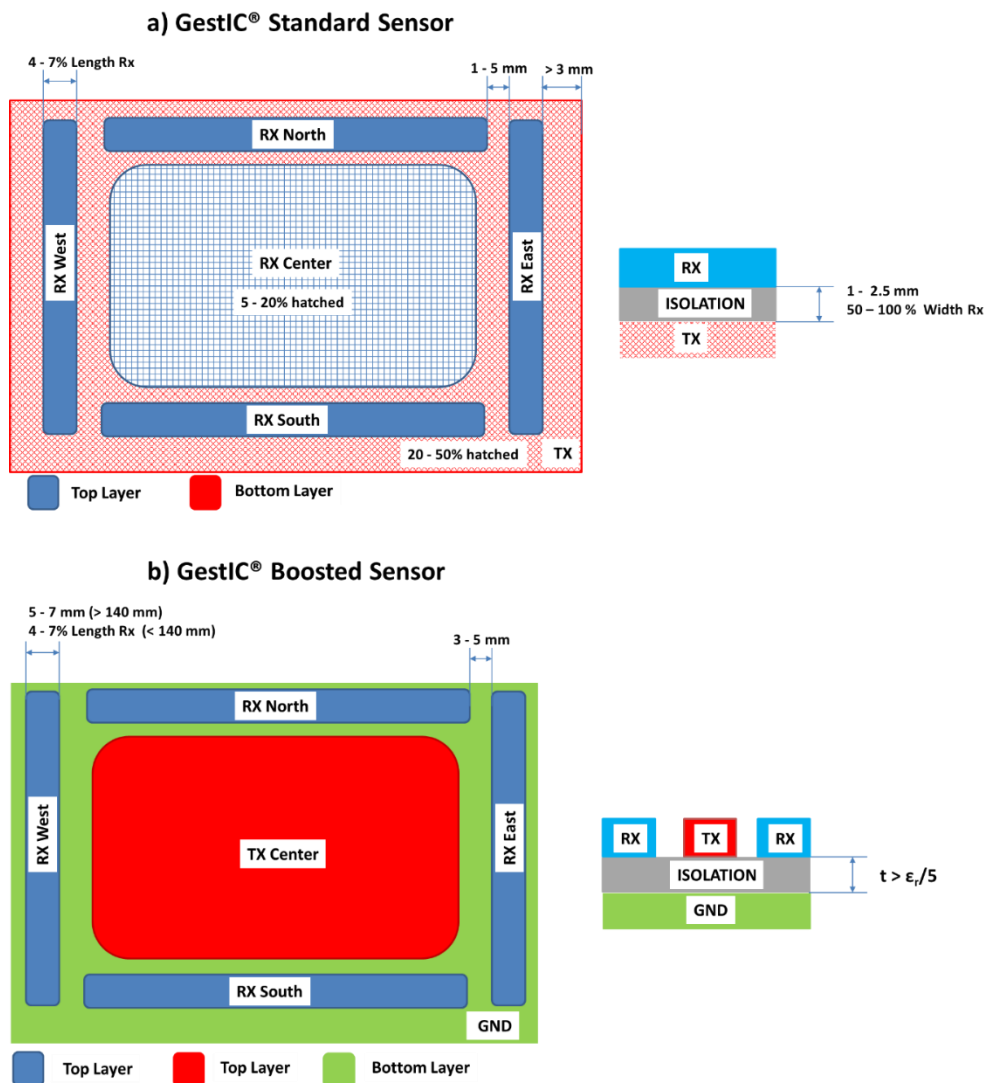
The design of the boosted sensor is based on the structure of the Standard sensor with some modifications (Figure 69). More information on the working principle and the design of the Standard sensor can be found in J. Ferri [28].

The main difference between the standard and the boosted sensor consists of the location of the Tx electrode. Boosted Tx electrodes are not placed underneath the Rx electrodes. Instead, the Tx electrode is laid out in the same layer as the Rx electrodes, substituting the central Rx electrode. Microchip recommends placing a GND plane in the bottom layer.

The design of the Rx electrodes is identical to the corresponding to the Standard sensor. For a sensor length < 140 mm, the electrode's width must be between 4 and 7 % of its electrode's length whereas for a sensor length > 140 mm, it is recommended to use a

width between 5 and 7 mm. As aforementioned, there is no Rx center electrode, since the center is dedicated to the Tx electrode.

Regarding the Tx electrode, it is not placed on another layer, but in the center of the Rx frame. This change with respect to the standard design forces a minimum distance between the Rx and Tx electrodes to limit the noise coupling between them. This distance is about 3 and 5 mm.



The Rx feeding lines must be kept apart from the Tx electrode. They must be routed next to the Rx electrodes or inside the GND plane. In addition, it is necessary to keep a distance of about 0.3 or 0.5 mm between GND and the Rx feeding lines.

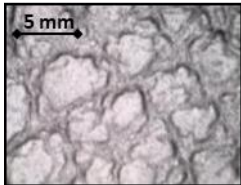
Regarding the number of layers, the Standard sensor can be designed with a 2 or 3 layer stack, usually with 3 layers. On the other hand, the Boosted sensor consists of a 2-layer stack, a top layer with the Rx and Tx electrodes and a bottom layer with the GND plane. The optimum distance between these two layers (t) will depend on the relative permittivity (ϵ_r) of the isolation material between both layers. Microchip recommends $t > \epsilon_r/5$. Hence, for an FR4 material (glass-reinforced epoxy laminate material with $\epsilon_r = 5$), the thickness can be of 1 mm, whereas for plastic ($\epsilon_r = 3$) it can be of 0.6 mm.

With respect to the circuitry for the boosted sensor, it is necessary a Tx level shifter since the Tx output voltage from MGC3XXX is 2.85 V. Microchip recommends the use of an MCP1416 power driver which allows one to increase the amplitude to values of up to 18 V. Hence, an additional DC input voltage must be used, or it must be generated by a DC-DC boost converter such as the MCP1661 converter.

5.2.2. Materials

With the aim of finding a textile with good characteristics to obtain capacitances of the order of 20 pF (capacitance recommended by Microchip), different cotton, polyester and mixed fabrics with different fabric densities, yarn diameter and weave were studied in J. Ferri [28,30]. According to these studies, a polyurethane fabric with excellent characteristics was found. Table 25 shows the main characteristics of that fabric.

Table 25. Fabric characteristics.

Fabric	Polyurethane
Picture	
Weft Material	Polyurethane
Warp Material	Polyurethane
Ligament	Non-woven
Thickness (μm)	1300 \pm 16
Grammage (g/m^2)	152 \pm 5

The conductive ink used was nano-silver DGP-NO from ANP (Table 26) for screen-printing technology, silver-coated polyamide/polyester hybrid thread (Silver-Tech 120) from AMANN Group (Table 27) for E-broidery and conductive woven fabric plain

Shieldex® Zell from STATEX (Table 28) for the direct application of conductive textiles.

Table 26. Silver ink characteristics.

	DGP-NO
Specific Resistivity ($\mu\Omega\cdot\text{cm}$)	10 ~ 50
Solids (%)	70 ~ 80
Viscosity (cps)	50 ~ 150
Curing	120 °C ~ 150 °C
Properties	Silver Nanoparticles

Table 27. Embroidery thread silver characteristics.

	Silvertex 120
Resistance per unit length (Ω/m)	<530
Tex no.	28
Needle size (in No.)	11 ~ 14
Materials	Polyamide/polyester covered of silver
Properties	<ul style="list-style-type: none"> • Skin friendly • Biocompatible • Antibacterial • Antistatic

Table 28. Conductive fabric plain characteristics

	Zell RS
Grammage (g/m^2)	77±15%
Thickness (μm)	110±15%
Width (mm)	1300±3%
Fabric Density ($\text{thread}/\text{cm}^2$)	84±2
Sheet Resistivity (Ω/sq)	≤0.02
Materials	Tin copper silver plated nylon fabric
Properties	Washable

5.2.3. Manufacturing

In this research, an own boosted sensor design has been developed to be applied on a textile substrate. It is based on the design recommended by Microchip and applied to different manufacturing technologies, such as screen-printing technology, E-broidery and direct application of conductive textiles:

- The screen-printing process consists of forcing pastes of different characteristics over a substrate through some screens using squeegees. Openings in the screen define the pattern that will be printed on the substrate by se-

igraphy. Conductive silver ink has been employed to make the electrodes and the GND plane.

- E-broidery consists of patterning of conductive textiles by numerically controlled sewing or weaving processes. Conductive silver-coated threads have been used to embroider the electrodes and the GND plane.
- Direct application of conductive textiles consists of adhering conductive textiles on the textile to create the electrodes and the GND plane.

The capacitances associated with the architecture design are fundamental in the operation of the sensor and, therefore, in its design. The C_{TxRx} (capacitance between the Tx and the Rx electrodes), C_{RxGND} (capacitance between the Rx electrodes and GND) and C_{TxGND} (capacitance between the Tx electrodes and GND) associated capacitances are the ones that must be considered for the design. More information about these capacitances can be found in J. Ferri [28]. Microchip recommends a value lower than 20 pF for the C_{TxRx} and C_{RxGND} capacitances, and lower than 1 pF for the C_{TxGND} capacitance in the case of Standard sensor, whereas for a Boosted sensor, the values will depend on the booster driving circuit capabilities.

The proposed design is shown in Figure 70. It consists of a ground plane layer (Figure 70.a) and a layer containing the Tx electrode, the four Rx electrodes and their connection lines with the MGC3XXX device (Figure 70.b). The dimensions are shown in the same Figure. The electrode size is 80 x 80 mm and the sensing area is 66 x 66 mm. Figure 76 shows the resulting sensor after the manufacturing process for the case of the E-broidery technology.

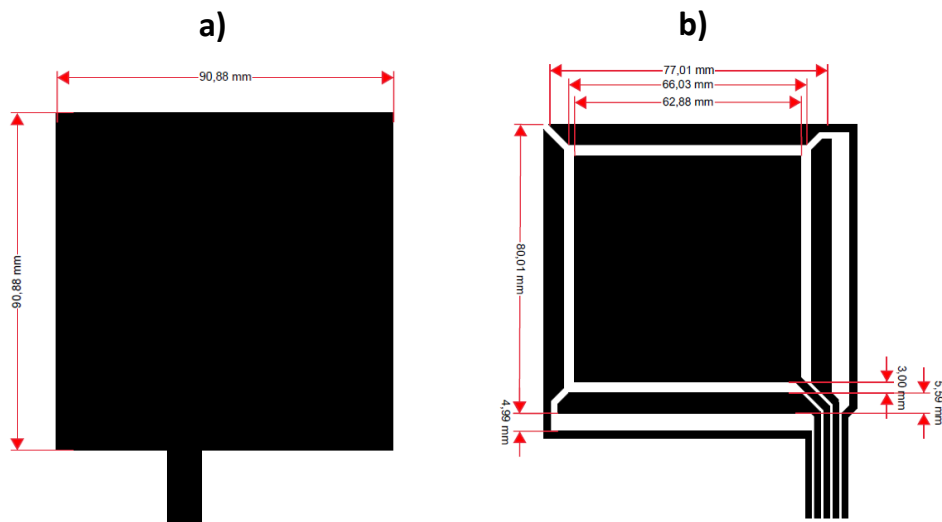


Figure 70. Boosted sensor design: Ground plane layer (a) and Tx-Rx electrodes (b).

The resulting sensors have been named as 3DBS_Screen, 3DBS_Embroidery and 3DBS_Fabric in the case of those made with the aforementioned E-textile technologies. For comparison purposes, a fourth boosted sensor made with a PCB technology, named 3DBS_PCB, was made. Moreover, two additional Standard sensors have also been analyzed in order to compare the standard and the boosted response. These standard sensors can be found in J. Ferri [28]. The names used for them in the paper are 3DS_Screen and 3DS_PCB.

5.2.4. Sensor Development

The same pattern design (Figure 70) has been applied to the three E-textile technologies and, in addition, to a PCB sensor in order to be able to carry out a comparison (Figure 71).

Screen-Printing technology (Figure 71.a): as previously mentioned, screen-printing technology uses a mesh to transfer ink onto a substrate, openings in the screen defining the pattern that will be printed on the substrate. The rest of the screen is made impermeable to the ink by a blocking stencil. The thickness of the screen, among other parameters, defines the final thickness of the ink. When screen-printing technology is used, it is necessary to manufacture frames with the screen mesh for the design. The screen for the conductors was a 230 mesh polyester material (PET 1500 90/230-48 from Sefar). Afterwards, to transfer the pattern to a screen mesh, a UV film Dirasol 132 from Fujifilm was used. The final screen thickness was 74 μm for the screen for conductors. The patterns were transferred to the screen by using a UV light source unit IC-5000 from BCB. Printing was carried out by using E2XL from EKRA screen-printer with a shore 75° hardness squeegee, 60° squeegee angle, 1 mm snap-off, 3.5 bar force and 100 mm/s. After the deposition of the inks, these were cured in an air oven FED-115 from BINDER at 130° C for 15 min.

E-broidery technology (Figure 71.b): An embroidery process whereby an embroidery machine is used to create electrical patterns on textiles. One type of silver-coated polyamide/polyester hybrid threads was used with 28 Tex properties on the textile substrate selected. An Embroidery machine was preferred instead of a normal stitching machine due to the fact that it has a better stitch quality and a vast range of design possibilities. The process was carried out by using an embroidery machine from ZSK with an F Head, with a 1.5 mm/stitch configuration. The conductive design has been accomplished with 7350 stitches in all.

Direct application of conductive textiles technology (Figure 71.c): The textile conductor Shieldex® Zell was placed on a MACbond 0.5 mil PET double-sided coated adhesive tape from MACTAC. A desktop cutting machine Cameo3 from SILHOUETTE was used to make the pattern cut. Subsequently, the different parts of the electrode were peeled off and adhered onto the fabric using the other adhesive side of the film.

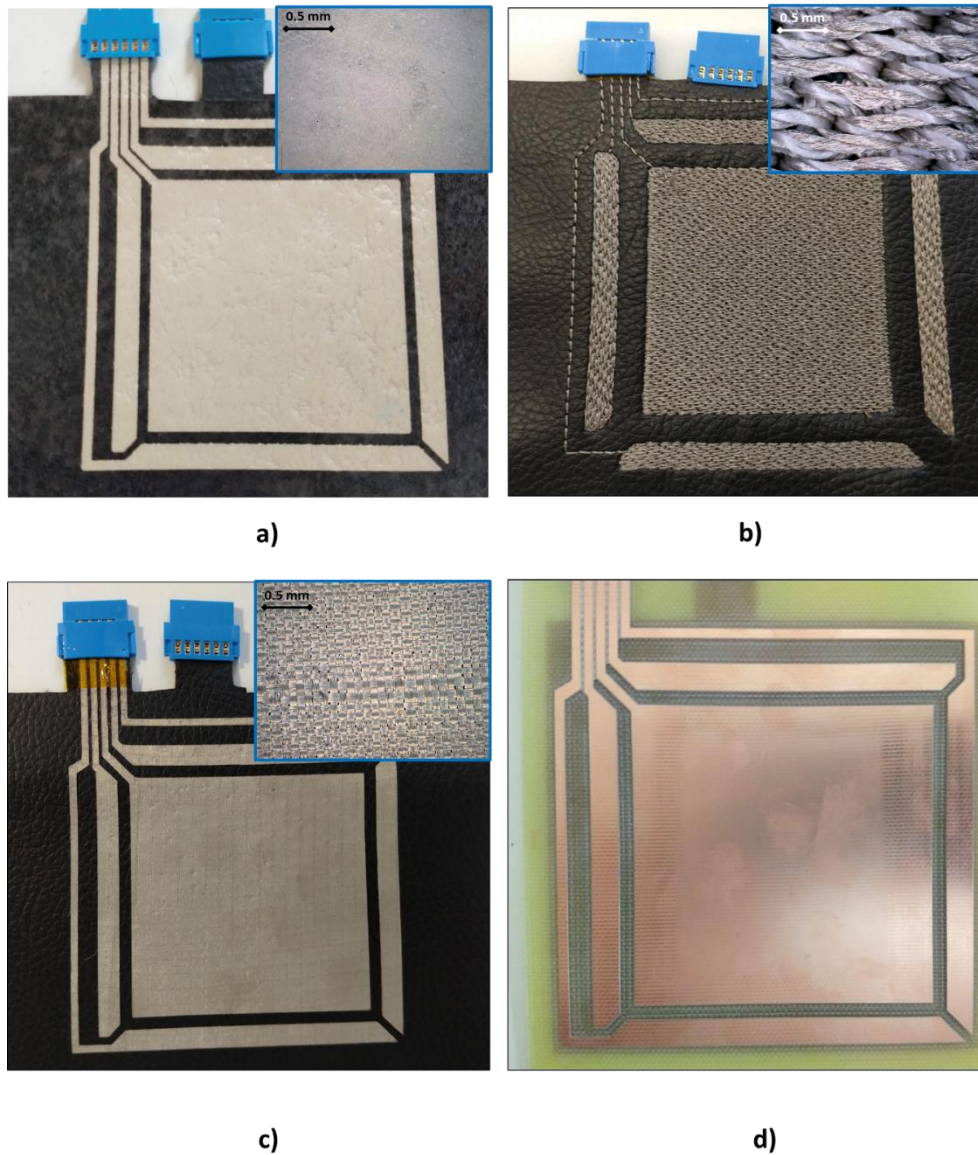


Figure 71. 3D gesture sensor developments with the three E-textile technologies: (a) screen-printing, (b) embroidery and, (c) direct application of conductive textile, and with the PCB material (d).

PCB technology (Figure 71.d): A double-side PCB was made with a ProtoMat S63 from LPKF. The main characteristics of the PCB are 1.6 mm of thickness, 15 μm of copper thickness and the use of FR4 as the isolation material.

5.2.5. Measurement

The relative permittivity measures were carried out with a BK PRECISION 895 LCR meter. The following measurement accessories were used: BK PRECISION TL89K1 Kelvin Clips Leads and a Yokogawa-Hewlett Packard 16451A Dielectric Test Adaptor. The LCR meter was configured to measure a tension level of 1V, with an average of 64 samples and a low read rate (Level = 1 V, Avg = 64, Meas Time= Low). The measurement mode was Cp and D (parallel capacitance and loss tangent). The capacitance measurements were taken at three different parts of the fabric with a 5-frequency scan (0.1 kHz, 1 kHz, 10 kHz, 100 kHz and 1000 kHz). The ϵ_r value was obtained directly from the Cp value.

The capacitance values were measured with the same equipment but in mode Cp-Rp (parallel capacitance and resistance) and Z-d (impedance and phase). The capacitance measurements were taken at three different parts of the fabric with a 9-frequency scan (0.1 kHz, 0.5 kHz, 1 kHz, 5 kHz, 10 kHz, 50 kHz, 100 kHz, 500 kHz and 100 kHz).

5.3. Results and discussion

Figure 72 shows the relative permittivity values (ϵ_r) of the fabric which acts as a dielectric of the capacitor. This value is important since it defines the values of the capacitances of the electrodes. As it can be seen, its value remains stable from 104 Hz. Since the working frequency of MGC3XXX is situated between 40 kHz and 100 kHz, the relative permittivity remains constant and does not contribute to a variation of the capacity value in this working range [30].

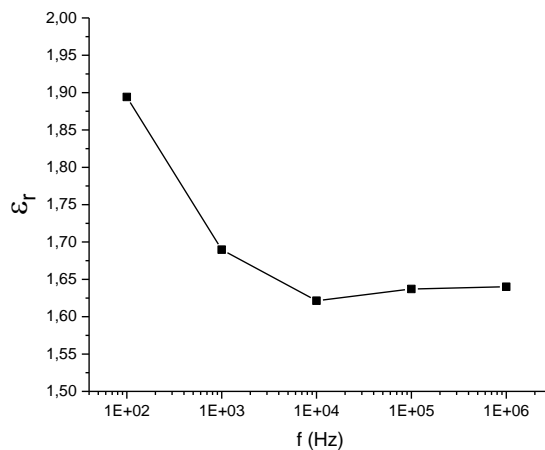


Figure 72. Frequency response of fabric relative permittivity.

The relative permittivity allows one to calculate the expected theoretical value of the associated capacities. The edge effect capacitance value (C_{edge}) has been taken as the theoretical value since it considers the effect of the field lines around the edges of the capacitor. It is estimated using Equation 1 and Equation 2:

$$C_{edge} = \frac{\epsilon_0 \cdot \epsilon_r \cdot (L + \Delta f) \cdot (w + \Delta f)}{t} \quad (1)$$

$$\Delta f = t + \frac{\epsilon_0 \cdot t \cdot 10 \cdot \ln((L + w) + 1)}{\pi} \quad (2)$$

where C_{edge} is the value of the capacitance in pF, L is the length in cm, w is the width in cm, t is the thickness in cm, ϵ_r is the relative permittivity, and ϵ_0 is the vacuum permittivity (8.85×10^{-12} F/m). The capacitance value (C_{RxGND}) of the North electrode has been calculated since this electrode is the one with less influence of the capacitances associated with the Rx conduction lines to the connector. The calculated value is 10.9 pF at 104 Hz.

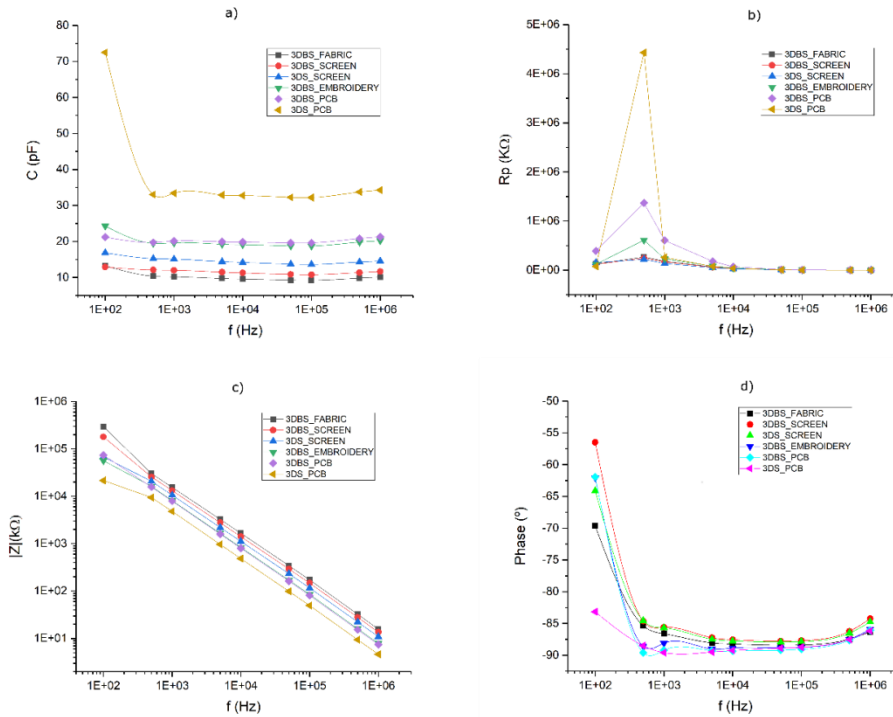


Figure 73. Values of the equivalent capacitor circuit: a) parallel capacitance C_p , b) parallel resistance R_p , c) impedance and d) phase value.

For each manufacturing technology and type of textile, the following measures of their electrical parameters have been taken: the C_{TxRx} , C_{RxGND} and C_{TxGND} capacitances. Figure 73 shows the Cp and Rp values of the parallel equivalent circuit as well as the impedance and phase values. The frequency response of the capacity value remains constant in the working range of MGC3XXX, ensuring the correct configuration of the device regardless of the frequency value. The Rp value is low enough to not have significant loss current. The impedance and phase correspond to the expected ones in a pure capacitor and there is no resonance up to the studied frequency (106 kHz).

Table 29 shows only the values of the capacitances (Cp) associated with each one of the types of developed sensors. All the boosted sensors have a capacitance lower or close to 20 pF. 3DBS_Fabric presents the lowest capacitances, followed by 3DBS_Screen. 3DBS_Embroidery and 3DBS_PCB have capacitances around 20 pF and a C_{TxGND} noticeably greater than 3DBS_Fabric and 3DBS_Screen; this difference may be what leads to a different sensitivity of these sensors can be seen in Figure 75. In the case of the standard versions, 3DS_Screen presents a capacitance lower than 20 pF, except in the case of C_{TxGND} . For this reason, an operational amplifier (op-amp) must be inserted between the Tx pin and the Tx electrode as Microchip recommends. Finally, 3DS_PCB presents the greatest capacitances, above 20 pF.

Table 29. Capacitance values (pF) at 104 Hz.

	3DBS_Screen	3DBS_Embroider	3DBS_Fabri	3DBS_PC	3DS_Screen	3DS_PC
	n	y	c	B	n	B
C_{TxRxN}	11.7±0.1	18.6±0.5	8.9±0.4	18.5±0.4	15.1±10.3	33.9±10.7
C_{TxRxS}	13.5±1.0	18.1±0.1	9.8±0.3	24.1±0.4	19.3±10.4	34.6±10.7
C_{TxRxE}	13.5±0.6	19.8±0.1	11.6±0.6	22.3±0.8	15.1±10.3	30.1±10.6
C_{TxRxW}	11.6±0.8	16.6±0.5	8.2±0.1	18.9±0.3	16.1±10.3	30.6±10.6
C_{RxNGN}	12.5±0.9	22.7±1.1	9.9±0.1	20.7±1.1	15.1±10.3	34.3±10.7
D						
C_{RxSGND}	16.6±0.8	21.8±0.9	11.3±0.2	29.3±1.0	19.5±10.4	33.2±10.7
C_{RxEGND}	16.1±0.5	24.1±1.2	12.5±0.2	27.7±0.9	15.1±10.3	30.3±10.6
C_{RxWGN}	13.0±0.4	19.5±0.7	10.2±0.1	21.4±1.2	16.1±10.3	30.2±10.6
D						
C_{TxGND}	56.2±0.5	112.6±2.3	38.1±1.1	130.8±5.7	2327.0±56.5	635.0±22.7

When comparing the theoretical C_{RxGND_North} value (10.9 pF) with the real one ($C_{RxGND_Screen} = 12.5±0.9$ pF, $C_{RxGND_Embroidery} = 22.7±1.1$ pF and $C_{RxGND_Fabric} = 9.9±0.1$ pF), it can be observed that the theoretical approximation is very reliable. It is practically identical in the case of using fabric, very approximate in the case of using ink and it moves away significantly in the case of using Embroidery. In the latter case, it can be considered that there is an added effect in the dielectric caused by the air that exists between the fabric and the threads and among the threads themselves.

The sensitivity was measured with software provided by Microchip, the AUREA graphical user interface. The sensitivity allows one to characterize the sensors, being, maybe, the most important parameter of these sensors. Microchip [31] provides an “artificial hand”, a 40 x 40 x 70 mm styrofoam ($\epsilon_r \approx 1$) cube covered with an adhesive copper sheet (Figure 74). This block must be connected to the ground to simulate the conditions of the human body. To determine the sensitivity at different heights from the surface of the sensor, the block is placed on blocks of styrofoam (with no copper cover) of different thicknesses (1, 2, ... cm). AUREA allows one to read the obtained data.



Figure 74. “Artificial hand” provided by Microchip made of styrofoam covered by copper and connected to ground.

Figure 75 shows a representation of the sensitivity in terms of the signal deviation. Microchip references the signal deviation obtained in MGC3XXX with respect to the distance of the hand compared with the width of the Rx electrodes. The 3DBS_Screen and 3DBS_Fabric sensors present the best sensitivity with similar capacitances to the 3DBS_Embroidery and 3DBS_PCB sensors. The difference may be due to the fact that in the latter, the C_{TXGND} is greater. The standard version, 3DS_Screen, presents a similar sensitivity to the 3DBS_Embroidery and 3DBS_PCB sensors. However, the 3DS_Screen design manufacturing needs one more layer, which is a disadvantage, despite having similar capacitances. Another factor to consider is that the boosted sensor uses a Tx output voltage increasing the amplitude up to 18V. As expected, The PCB standard version presents the lowest sensitivity.

As aforementioned, the sensor is initially designed to be attached into clothing or textiles surfaces such as armchairs, curtains or automotive upholstery. In this case, the most important textile feature is flexibility. Several bend radiuses were proved and the response was successful up to radiuses lower than 3 cm. The driver had to be calibrated for every test. Figure 76 shows the flexibility of the resulting 3DBS_Embroidery sensor, assessing the flexibility feature of the e-textile sensor.

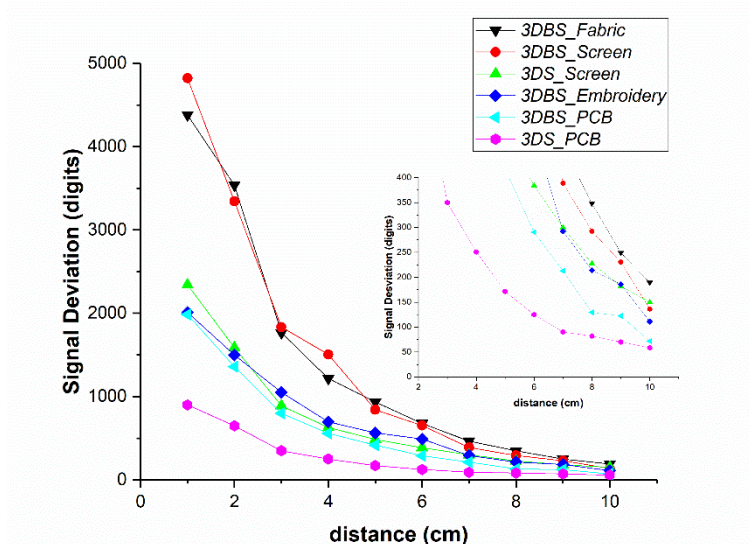


Figure 75. Signal Deviation of the different sensors in function of the distance of the hand from the surface of the sensor. The smallest graph is the magnification of the 10 cm limit.



Figure 76. Flexible 3D Boosted sensor manufactured.

A study of the response of the electrode based on the variation of temperature and humidity has been carried out to determine their influence under different operating conditions with a climatic test chamber CTS C70/300 from Controltecnia-CTS. Figure 77 shows how these variations have a low influence on the associated capacitance.

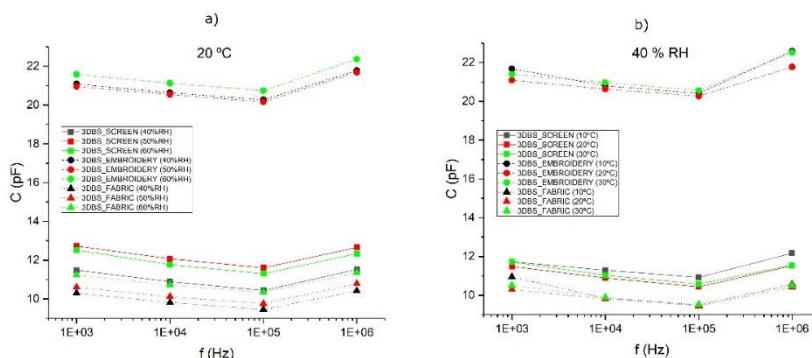


Figure 77. a) Capacitance variation depending on the humidity at a fixed temperature of 20 °C, b) Capacitance variation depending on the temperature at a fixed humidity of 40% RH.

Finally, a study of the variation in conductivity versus washing processes has been carried out. The characteristics of the wash have been one hour of delicate wash at 30 °C with a spin cycle of 700 rpm. Figure 78 shows the result of the normalized resistance variation, from initial resistance value, in a conductor pattern used in the three technologies (fabric, thread and ink).

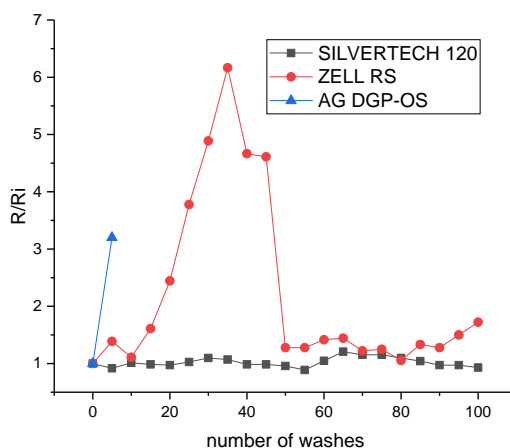


Figure 78. Normalized resistance variation in a conductor pattern used in the three technologies (fabric, thread and ink) versus number of washes.

The best behavior to washing is offered by the conductive thread, maintaining its characteristics after 100 washes, the silver ink deteriorates rapidly after 5 washes losing conductivity (Figure 79) and the conductive fabric supports the 100 washes but its electrical characteristics varied during the process.

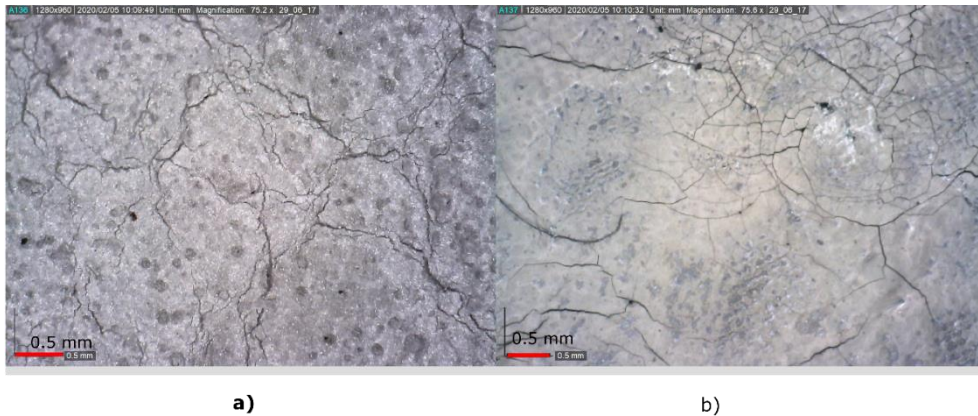


Figure 79. a) appearance of the silver ink before washing and, b) after 5 washes.

For the silver ink case, it could have chosen to cover the sensor with a heat-sealable film, but after the washing test with this type of film, problems of adhesion between the film and the conductors also arise after few washes (Figure 80). With this background, the best option is to use a conductive thread.

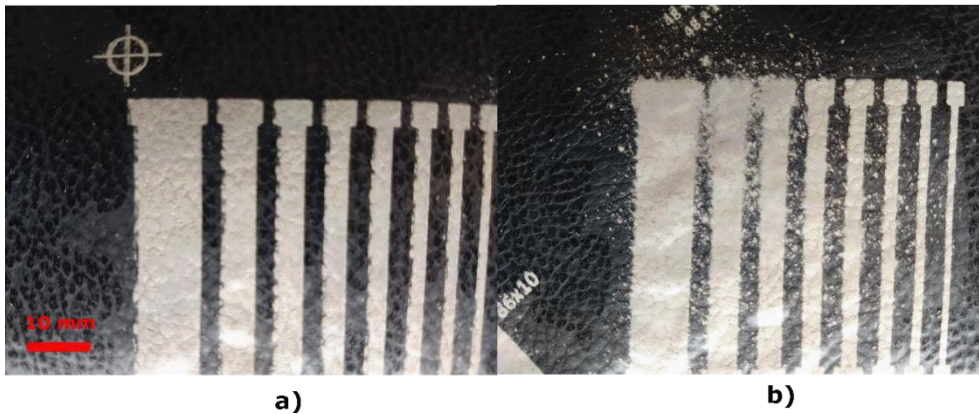


Figure 80. a) Appearance of the silver ink coated with a heat-sealed film before washing and, b) after 5 washes. The bubbles generated between the substrate and the film and the degeneration of the silver ink are observed.

For the characterization of the sensors, the following protocol has been established. An artificial hand has been placed at different positions on the X, Y and Z axis with respect to the center of the sensor. For each position, the signal deviation data provided by the device has been registered. For the sake of simplicity, only the measurements taken from the PCB sensor and the screen-printed sensor (3DBS_Screen) are shown in Figure 81. It shows the curves obtained by moving the artificial hand in the X axis in

the [-5 cm, 5 cm] interval in 1 cm steps for the following values of Z: 1 cm, 3 cm and 5 cm. In all the cases, the value of Y = 0.

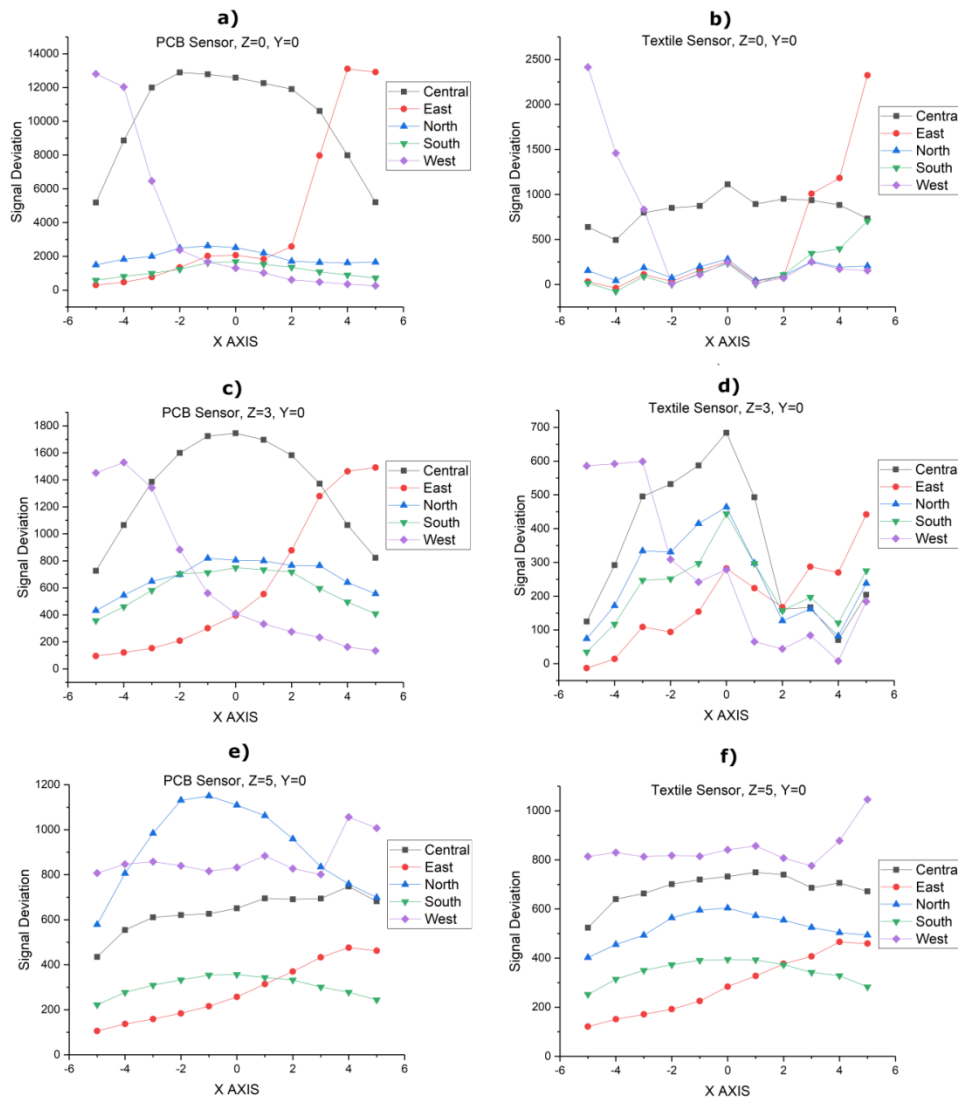


Figure 81. Characterization of the sensors using an artificial hand: a) PCB reference sensor fixing Z = 0 position. b) Textile sensor fixing Z = 0 position. c) PCB reference sensor fixing Z = 3 cm position. d) Textile sensor fixing Z = 3 cm position. e) PCB reference sensor fixing Z = 5 cm position. f) Textile sensor fixing Z = 5 cm position.

As can be seen, the results for the textile sensor are not as smooth as in the PCB sensor due to the textile structure itself. On the other hand, a conductivity variation is observed in the textile sensor, as opposed to the case of the PCB sensor. This behavior is due to the asymmetry of the east and the west sensor. The design of the east sensor tracks is shifted to the left favoring a shorter track for the west sensor. The different tests carried out showed the same behavior. Despite this, the functioning of the gesture recognition is not affected, since the variations are high enough to be detected in the five sensors. The rest of the sensors showed a similar behavior.

Next, a validation of the sensors was carried out with different subjects. The objective was to measure the detection rate of several gestures. Figure 82 shows two of the gestures used in the validation procedure. The software used, AUREA, is supplied by Microchip.

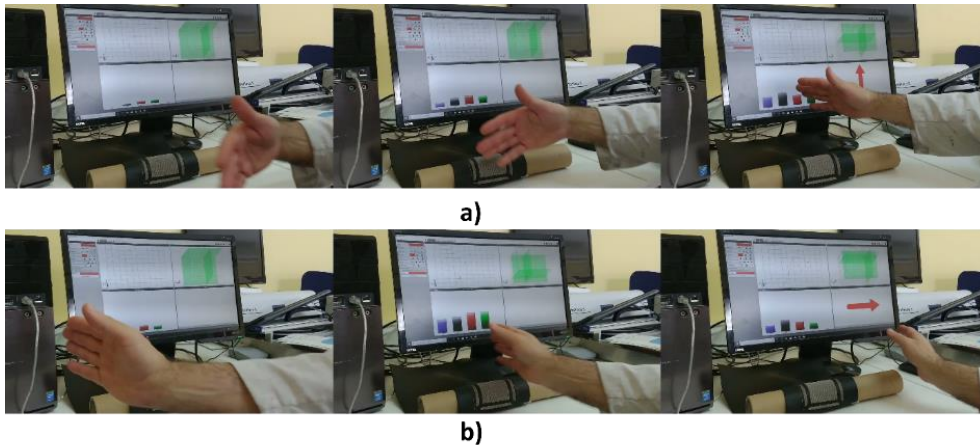


Figure 82. Two of the gestures used in the validation: a) flick from north to south and b) flick from west to east.

In the validation procedure, 10 subjects participated in the experiment. Initially, they were completely unaware of the operation of the sensor. They were allowed to interact with the sensor for 10 minutes. Afterwards, they were asked to perform different gestures detectable by the sensor. After a calibration, the subjects were asked to make 10 repetitions of the following movement types: flick from west to east, flick from east to west, flick from north to south, flick from south to north, clockwise circular and counterclockwise circular. The results of the detection rate for the 3DBS_Screen sensor are shown in Table 30.

Table 30. Gesture conducted tests results for the 3DBS_Screen sensor.

Gesture	S. 0	S. 1	S. 2	S. 3	S. 4	S. 5	S. 6	S. 7	S. 8	S. 9	%
Flick W-E	90%	90%	80%	80%	90%	80%	70%	90%	90%	80%	84%
Flick S-N	80%	100%	80%	100%	60%	80%	70%	80%	70%	70%	79%
Flick N-S	90%	100%	90%	80%	80%	90%	90%	80%	70%	60%	83%
Flick E-W	90%	90%	90%	90%	90%	90%	90%	90%	70%	80%	87%
Counterclockwise	60%	70%	70%	70%	70%	60%	60%	70%	60%	60%	65%
Clockwise	70%	80%	70%	80%	80%	70%	70%	60%	70%	80%	73%

The results show that most of the gestures are detected successfully. All the flick-type gestures were detected with a percentage higher than 75%. In contrast, the clockwise and counterclockwise gestures have a lower detection rate. This is due to the higher complexity of the circular movement. Besides, the counterclockwise is more difficult to detect than the clockwise movement.

Table 31 shows the comparison of the results obtained by the three proposed sensors and the PCB sensor.

Table 31. Comparison between proposed Sensors.

Gesture	3DBS_Fabric	3DBS_Screen	3DBS_Embroidery	PCB
Flick W-E	84%	84.00%	86%	89%
Flick S-N	81%	79.00%	81%	81%
Flick N-S	84%	83.00%	85%	86%
Flick E-W	88%	87.00%	89%	90%
Counterclockwise	59%	65.00%	73%	86%
Clockwise	76%	73.00%	74%	84%

It can be observed that although the three proposed sensors have slightly worst performance than the PCB sensor, most of the gestures were detected successfully. The proposed sensors have better performance with flick gestures rather than with counterclockwise and clockwise gestures. Among the proposed sensors, the 3DBS_Embroidery showed the best performance.

5.4. Conclusion

The aim of this work was to obtain a textile 3D gesture recognition sensor based on the Microchip 3D GestIC® sensor design. A boosted sensor was used allowing greater sensing distances with respect to the standard sensor. Three manufacturing techniques were considered as alternatives: screen printing with conductive ink, embroidery with conductive thread and thermosealing with conductive fabric. The theoretical capacitance study was very reliable when compared with the real measurements. The prototypes were validated with respect to the detection of gestures with successful results. In the base of the studies of sensitivity, response to humidity and temperature, and resistance to washing, it can be concluded that the technique of embroidery with conductive thread is a good solution to incorporate into the e-textile industry.

References

- 1 Cherenack, K.; Van Pieteron, L. Smart textiles: Challenges and opportunities. *J. Appl. Phys.* **2012**, *112*. <https://doi.org/10.1063/1.4742728>.
- 2 Yang, G.; Deng, J.; Pang, G.; Zhang, H.; Li, J.; Deng, B.; Pang, Z.; Xu, J.; Jiang, M.; Liljeberg, P.; et al. An IoT-Enabled Stroke Rehabilitation System Based on Smart Wearable Armband and Machine Learning. *IEEE J. Transl. Eng. Heal. Med.* **2018**, *6*, 1–10. <https://doi.org/10.1109/JTEHM.2018.2822681>.
- 3 Caldani, L.; Pacelli, M.; Farina, D.; Paradiso, R. E-textile platforms for rehabilitation. *2010 Annu. Int. Conf. IEEE Eng. Med. Biol. Soc. EMBC'10* **2010**, 5181–5184. <https://doi.org/10.1109/IEMBS.2010.5626148>.
- 4 Han, S.H.; Ahn, E.J.; Ryu, M.H.; Kim, J.N. Natural hand gesture recognition with an electronic textile goniometer. *Sensors Mater.* **2019**, *31*, 1387–1395. <https://doi.org/10.18494/SAM.2019.2261>.
- 5 Lorussi, F.; Scilingo, E.P.; Tesconi, M.; Tognetti, A.; Rossi, D. De Strain Sensing Fabric for Hand Posture and Gesture Monitoring. **2005**, *9*, 372–381.
- 6 He, T.; Shi, Q.; Wang, H.; Wen, F.; Chen, T.; Ouyang, J.; Lee, C. Beyond energy harvesting - multi-functional triboelectric nanosensors on a textile. *Nano Energy* **2019**, *57*, 338–352. <https://doi.org/10.1016/j.nanoen.2018.12.032>.
- 7 Kundu, A.S.; Mazumder, O.; Lenka, P.K.; Bhaumik, S. Hand Gesture Recognition Based Omnidirectional Wheelchair Control Using IMU and EMG Sensors. *J. Intell. Robot. Syst. Theory Appl.* **2018**, *91*, 529–541. <https://doi.org/10.1007/s10846-017-0725-0>.
- 8 Santos, L.; Carbonaro, N.; Tognetti, A.; González, J.; de la Fuente, E.; Fraile, J.; Pérez-Turiel, J. Dynamic Gesture Recognition Using a Smart Glove in Hand-Assisted Laparoscopic Surgery. *Technologies* **2018**, *6*, 8. <https://doi.org/10.3390/technologies6010008>.
- 9 Shen, Z.; Yi, J.; Li, X.; Mark, L.H.P.; Hu, Y.; Wang, Z. A soft stretchable bending sensor and data glove applications. *2016 IEEE Int. Conf. Real-Time Comput. Robot. RCAR 2016* **2016**, 88–93. <https://doi.org/10.1109/RCAR.2016.7784006>.
- 10 Shyr, T.-W.; Shie, J.-W.; Jiang, C.-H.; Li, J.-J. A Textile-Based Wearable Sensing Device Designed for Monitoring the Flexion Angle of Elbow and Knee Movements. *Sensors* **2014**, *14*, 4050–4059. <https://doi.org/10.3390/s140304050>.

- 11 Huang, Y.; Gao, L.; Zhao, Y.; Guo, X.; Liu, C.; Liu, P. Highly flexible fabric strain sensor based on graphene nanoplatelet–polyaniline nanocomposites for human gesture recognition. *J. Appl. Polym. Sci.* **2017**, *134*, 1–8. <https://doi.org/10.1002/app.45340>.
- 12 Parzer, P.; Sharma, A.; Vogl, A.; Steimle, J.; Olwal, A.; Haller, M. SmartSleeve: Realtime sensing of surface and deformation gestures on flexible, interactive textiles, using a hybrid gesture detection pipeline. *UIST 2017 - Proc. 30th Annu. ACM Symp. User Interface Softw. Technol.* **2017**, 565–577. <https://doi.org/10.1145/3126594.3126652>.
- 13 Yu, L.; Feng, Y.; Yao, L.; Soon, R.H.; Yeo, J.C.; Lim, C.T. Dual-Core Capacitive Microfiber Sensor for Smart Textile Applications. *ACS Appl. Mater. Interfaces* **2019**, *11*, 33347–33355. <https://doi.org/10.1021/acsami.9b10937>.
- 14 Chen, S.; Lou, Z.; Chen, D.; Jiang, K.; Shen, G. Polymer-Enhanced Highly Stretchable Conductive Fiber Strain Sensor Used for Electronic Data Gloves. *Adv. Mater. Technol.* **2016**, *1*, 1–9. <https://doi.org/10.1002/admt.201600136>.
- 15 Li, Y.-Q.; Huang, P.; Zhu, W.-B.; Fu, S.-Y.; Hu, N.; Liao, K. Flexible wire-shaped strain sensor from cotton thread for human health and motion detection. *Sci. Rep.* **2017**, *7*, 45013. <https://doi.org/10.1038/srep45013>.
- 16 Guo, Y.; Zhang, X.S.; Wang, Y.; Gong, W.; Zhang, Q.; Wang, H.; Brugger, J. All-fiber hybrid piezoelectric-enhanced triboelectric nanogenerator for wearable gesture monitoring. *Nano Energy* **2018**, *48*, 152–160. <https://doi.org/10.1016/j.nanoen.2018.03.033>.
- 17 Haque, R.I.; Farine, P.A.; Briand, D. Soft triboelectric generators by use of cost-effective elastomers and simple casting process. *Sensors Actuators, A Phys.* **2018**, *271*, 88–95. <https://doi.org/10.1016/j.sna.2017.12.018>.
- 18 Huang, X.; Wang, Q.; Zang, S.; Wan, J.; Yang, G.; Huang, Y.; Ren, X. Tracing the Motion of Finger Joints for Gesture Recognition via Sewing RGO-Coated Fibers onto a Textile Glove. *IEEE Sens. J.* **2019**, *19*, 9504–9511. <https://doi.org/10.1109/JSEN.2019.2924797>.
- 19 Eom, J.; Jaisutti, R.; Lee, H.; Lee, W.; Heo, J.; Lee, J.; Park, S.K.; Kim, Y. Highly Sensitive Textile Strain Sensors and Wireless User-Interface Devices Using All-Polymeric Conducting Fibers. **2017**. <https://doi.org/10.1021/acsami.7b01771>.
- 20 Nelson, A.; McCombe Waller, S.; Robucci, R.; Patel, C.; Banerjee, N. Evaluating touchless capacitive gesture recognition as an assistive device for upper extremity

- mobility impairment. *J. Rehabil. Assist. Technol. Eng.* **2018**, *5*, 205566831876206. <https://doi.org/10.1177/2055668318762063>.
- 21 Cheng, J.; Bannach, D.; Lukowicz, P. On body capacitive sensing for a simple touchless user interface. Proc. 5th Int. Work. Wearable Implant. Body Sens. Networks, BSN2008, conjunction with 5th Int. Summer Sch. Symp. Med. Devices Biosensors, ISSS-MDBS 2008 **2008**, 113–116. <https://doi.org/10.1109/ISSMDBS.2008.4575031>.
- 22 Gonçalves, C.; da Silva, A.F.; Gomes, J.; Simoes, R. Wearable e-textile technologies: A review on sensors, actuators and control elements. *Inventions* **2018**, *3*, 1–13.
- 23 Mecnika, V.; Hoerr, M.; Krievins, I.; Jockenhoevel, S.; Gries, T. Technical Embroidery for Smart Textiles: Review. *Mater. Sci. Text. Cloth. Technol.* **2015**, *9*, 56.
- 24 Martínez-Estrada, M.; Moradi, B.; Fernández-García, R.; Gil, I. Impact of conductive yarns on an embroidery textile moisture sensor. *Sensors (Switzerland)* **2019**, *19*.
- 25 Atalay, O. Textile-based, interdigital, capacitive, soft-strain sensor for wearable applications. *Materials (Basel)*. **2018**, *11*.
- 26 Liu, Y.; Xu, L.; Li, Y.; Ye, T.T. Textile based embroidery-friendly RFID antenna design techniques. *2019 IEEE Int. Conf. RFID, RFID 2019* **2019**.
- 27 Iliev, I.T.; Nikolov, G.T.; Tabakov, S.D.; Tzaneva, B.R. Experimental Investigation of Textile Planar Capacitive Sensors. *2018 IEEE 27th Int. Sci. Conf. Electron. 2018 - Proc.* **2018**, 1–4.
- 28 Ferri, J., Llopis, R., Moreno, J., Ibañez Civera, J., Garcia-Breijo, E. A Wearable Textile 3D Gesture Recognition Sensor Based on Screen-Printing Technology. *Sensors* **2019**, *19*, 5068. <https://doi.org/10.3390/s19235068>.
- 29 Microchip, GestIC® Design Guide, DS40001716C, **2016**, ISBN 978-1-5224-0477-4, <http://ww1.microchip.com/downloads/en/devicedoc/40001716c.pdf> (accessed: 2018).
- 30 Ferri, J.; Llinares Llopis, R.; Moreno, J.; Vicente Lidón-Roger, J.; Garcia-Breijo, E. An investigation into the fabrication parameters of screen-printed capacitive sensors on e-textiles. *Text. Res. J.* **2020**. <https://doi.org/10.1177/0040517519901016>.

- 31 Microchip, Aurea Graphical User Interface User's Guide, DS40001681D, **2015**, ISBN 978-1-63276-972-5, <http://ww1.microchip.com/downloads/40001681D.pdf> (accessed: October 2018).

Chapter 6

Conclusions

This last chapter summarizes the main conclusions obtained throughout this work and points out some future research lines to carry out during the next years. The novel contributions in the fabrication process of sensors on textiles substrates and stretchable substrates are described. Although the design, manufacture and characterization of each structure was successfully demonstrated, several aspects require further research.

6.1. Conclusions

This thesis is focused on the development and performance evaluation of printed conductive designs on textile substrates to be used as sensors. The main goal was to achieve computer interfaces using arrays of capacitive sensors.

One of the initial challenges in the different developments was to control the capacitances with the selected inks and textiles. The main parameters that affect the capacitance of the capacitors are the size of the electrodes, the distance between the electrodes and the relative permittivity of the dielectric between them. All these parameters must be considered in the design phase according to the requirements. On the other hand, there are some additional parameters that are very difficult to consider in the design and affect the performance considerably. These parameters are the fabric roughness, printing direction, type of fabric used as substrate, curing temperatures, curing time and compatibilities between pairs of materials, among others. During this work, several tests were carried out combining variations of the different parameters in order to obtain conclusions about which strategies give better performances. Part of the investigation revealed that some of them depends on how they are combined. A clear example is found in the combinations between conductive inks and textiles substrates: some of the inks work better with concrete textiles, but other ones work better with textiles totally different.

Another important conclusion found in this work, is that a design made for traditional electronics can be transformed to be produced with Printed Electronics technology. For instance, the copper used in PCB can be substituted by conductive inks. This was shown with both developments, the 2D touchpad sensors and the 3D gesture sensors. In addition, in this work, it is shown that different approaches for the same application can be designed. The different solutions can allow one to reduce the costs of the production or to get better performance.

Another aspect to consider, in comparison with other techniques, is that the use of Printed Electronics allows one to combine different materials in the design. Not only conductive or dielectric, but also semi conductive, electroluminescent, resistive, piezoelectric materials, among others, can be used. Even other materials that can be developed in the future could be used, opening the possibility to many other future applications. Regarding the inks, each year new types of inks appear, adding new possibilities. The newest inks are including stretchable and washable characteristics that can give

them other uses and properties. When selecting inks, the printing technique must be considered. Depending on the technology such as inkjet, screen, offset, flexography, jet or gravure, the available inks are different. In other words, not all the inks are available for all the techniques. Thus, the compatibility of the materials must be analysed in each design. In addition, it is important to highlight that the more layers are deposited, the more complex is the fabrication of the circuits. Each deposited layer can affect not only the layer below but also the layer above.

Within the field of 2D touchpad sensors, the major highlight of this thesis was the creation of a touchpad based on projected capacitive (pro-cap) technologies. This touchpad was developed to be used with textile substrates using a low cost, printing technique such as screen-printing. This technology is habitual in textile industry. Two types of architecture with different sizes of electrodes and different types of textiles were developed, and their correct operation was verified. Although the initial design was well known, the adaptation to the printed solution was a challenge. One important aspect to consider was the electrical connectivity. The deposited layers sometimes need to be electrical connected with the next layers and sometimes need to be isolated. Hence, it was necessary to control the printing process in order to avoid short circuits. Another aspect to deal with was the use of connectors that were compatible with the textile substrate giving good connectivity and conductivity to the testing circuit.

The integration of a 2D touchpad sensor with an electroluminescent display (ELD) grid was carried out with successful results. This integration had to consider the fields emitted by the ELD, so an electro-magnetic interference (EMI) shield had to be incorporated into the assembly. This made the fabrication more complex. Another considered aspect was that the application of the ELD on textile reduced considerably the luminosity compared to other well-known configurations using transparent polyethylene terephthalate (PET) substrates based on indium tin oxide (ITO). As a result of this work, two solutions were presented as alternatives to improve the luminosity, the ELD on a transparent substrate based on ITO and the use of polyurethane with poly(3,4-ethylenedioxythiophene):poly(styrene sulfonate) (PEDOT:PSS).

Then, more advanced interfaces were studied. As a result, a 3D gesture sensor based on E-field change technologies was developed to be used with textile substrates using screen-printing. In addition, some solutions were presented to deal with the problematic of controlling the dielectric performance. The most relevant conclusion was that this solution allows one to print the sensor on a larger range of fabrics. Properties such as the geometry, number and position of the electrodes allow the sensor to detect some gestures such as position tracker, approach or swipe.

The final part of this work dealt with a boosted 3D gesture sensor. This sensor allows greater sensing distances with respect to the previous 3D gesture sensor developed. Two designs were presented and validated with respect to the detection of gestures with successful results. In addition, three manufacturing techniques were used: screen

printing using conductive ink, embroidery with conductive thread and heat lamination with conductive fabric. Then, a user validation was carried out, testing several gestures with different subjects. In order to assess their durability and stability, a comparative study of the sensor behaviour under variations of humidity and temperature was performed. Moreover, the resistance against washing cycles was measured.

Finally, it is interesting to remark that this work will contribute to use these gesture sensors on both flat and curved surfaces. Hence, this type of sensors can be used in parts of clothes, such as sleeves, trouser legs or textiles for furniture or automotive such as seats, armchairs, sofas or beds.

6.2. Future research lines

Next, the following topics are proposed to be considered as future research lines:

- Development of miniaturized sensors in order to be used in other applications that could require gesture or movement detection. Making the sensors smaller would allow them to be easily integrated in applications that require smaller surfaces.
- Implementation of a sensor with a higher number of capacitors in order to increase their accuracy, resolution or operational range. This feature is directly linked with both, the printing process and the materials used.
- Application of capacitive sensors in other applications different to touch sensors. As demonstrated, the operation of the sensors depends on the humidity and temperature conditions. Some applications, such as, robotic applications, can be sensitive to these changes. It would be interesting to detect these environmental conditions by means of using smart textiles
- Development of algorithms for adapting the response to the context dynamically. It would avoid the use of a previous calibration before the use of the sensor.
- Development of an application to detect changes due to curvatures on the textile substrate. In each curved position, the context varies, and the capacitance measured is different. The same can be applied to detect movements.

Regarding technology transfer, a deep study about the optimization of the manufacturing process considering the multilayer designs must be carried out. A semiautomatic screen-printing machine was used during this work and the costs of fabrication should be estimated. Some other industrial alternative equipment such as, roll to roll printing solutions, should be considered.